



**The impact of sphingolipids on
Neisseria meningitidis and their role in
meningococcal pathogenicity**

**Einfluss von Sphingolipiden auf *Neisseria meningitidis*
und deren Bedeutung für die Pathogenität**

Dissertation

for a doctoral degree at the Graduate School of Life Sciences,
Julius-Maximilians-Universität Würzburg,
Section Infection and Immunity

submitted by

Simon Peters

from

Cologne

Würzburg 2020





**The impact of sphingolipids on
Neisseria meningitidis and their role in
meningococcal pathogenicity**

**Einfluss von Sphingolipiden auf *Neisseria meningitidis*
und deren Bedeutung für die Pathogenität**

Dissertation

for a doctoral degree at the Graduate School of Life Sciences,
Julius-Maximilians-Universität Würzburg,
Section Infection and Immunity

submitted by

Simon Peters

from

Cologne

Würzburg 2020

Submitted on:

Office stamp

Members of the Thesis Committee

Chairperson: Prof. Dr. J. Seibel

Primary Supervisor: Prof. Dr. A. Schubert-Unkmeir

Supervisor (Second): Prof. Dr. M. Sauer

Supervisor (Third): Dr. Kay Johswich

Date of Public Defence:

Date of Receipt of Certificates:

I. Table of contents

| | |
|---|-----------|
| I. Table of contents | 1 |
| II. Figure Register | 4 |
| III. Table Register | 6 |
| IV. Abbreviation Index | 7 |
| Va. Summary | 8 |
| Vb. Zusammenfassung | 9 |
| 1. Introduction | 11 |
| 1.1 <i>Neisseria meningitidis</i> | 11 |
| 1.2. Interaction with the human host | 12 |
| 1.2.1 Colonization and survival in the nasopharynx | 12 |
| 1.2.2 Virulence factors associated with host cell interaction | 14 |
| 1.2.3 Proliferation in the bloodstream | 16 |
| 1.2.4 Interaction with the blood–cerebrospinal–fluid barrier | 17 |
| 1.3 Sphingolipids | 18 |
| 1.3.1 Physiological role of sphingolipids | 20 |
| 1.3.2 Sphingolipids and infection | 21 |
| 1.3.2.1 Sphingolipids and <i>Neisseria meningitidis</i> | 22 |
| 1.3.3 Sphingolipids as antimicrobial agents | 23 |
| 1.3.4 Functionalized sphingolipids | 24 |
| 1.4 Aim of this study..... | 26 |
| 2. Material and Methods | 27 |
| 2.1 Material..... | 27 |
| 2.1.1 Laboratory equipment..... | 27 |
| 2.1.1.1 Devices | 27 |
| 2.1.1.2 Consumables | 28 |
| 2.1.1.3 Kits..... | 29 |
| 2.1.1.4 Chemicals and reagents | 30 |
| 2.1.1.5 Antibiotics | 32 |
| 2.1.1.6 Lipids | 32 |
| 2.1.1.7 Antibodies and dyes..... | 33 |
| 2.1.1.8 Plasmids | 34 |
| 2.1.1.9 Primer | 35 |
| 2.1.2 Solutions, Buffer and Media..... | 36 |
| 2.1.3 Bacterial strains | 38 |
| 2.1.4 Cell lines..... | 39 |
| 2.1.5 Software | 40 |
| 2.2 Methods..... | 41 |

| | |
|--|-----------|
| 2.2.1 Bacterial culture techniques..... | 41 |
| 2.2.1.1 Solid and liquid growth of <i>N. meningitidis</i> | 41 |
| 2.2.1.2 Stocking of bacteria..... | 41 |
| 2.2.1.3 Bacterial growth curve experiments | 41 |
| 2.2.1.4 Transformation of <i>N. meningitidis</i> | 42 |
| 2.2.1.5 Transformation of chemically competent <i>E. coli</i> TOP10 | 42 |
| 2.2.1.6 Polymerase chain reaction | 42 |
| 2.2.1.7 Visualization and purification of PCR products | 44 |
| 2.2.1.8 Construction of mutant strains in <i>N. meningitidis</i> | 44 |
| 2.2.2 Cell culture methods and infection..... | 45 |
| 2.2.2.1 Quantification of bacterial adherence and invasion into host cells | 45 |
| 2.2.3 Cell cycle synchronization | 46 |
| 2.2.4 Flow Cytometry | 46 |
| 2.2.5 Immunofluorescence microscopy | 47 |
| 2.2.6 ASM activity assay | 47 |
| 2.2.7 Calcium measurement..... | 48 |
| 2.2.8 Preparation of pilus-enriched fractions..... | 48 |
| 2.2.9 Neisserial membrane separation | 49 |
| 2.2.9.1 Western- and Dot blot | 50 |
| 2.2.9.2 Quantification of protein | 50 |
| 2.2.9.3 Mass spectrometry..... | 51 |
| 2.2.10 Statistics | 52 |
| 3. Results | 53 |
| 3.1 Meningococcal induced ceramide platform formation is mediated by T4P and intracellular calcium release..... | 53 |
| 3.1.1 <i>N. meningitidis</i> strain 8013/12 induces T4P dependent ceramide accumulation on human brain microvascular endothelial cells (HBMEC) | 53 |
| 3.1.2 <i>N. meningitidis</i> infection of HBMEC leads to the translocation of lysosomal ASM to the cell surface | 56 |
| 3.1.3 Infection of HBMEC with <i>N. meningitidis</i> induced intracellular calcium release from the ER..... | 58 |
| 3.1.4 Intracellular calcium is important for the translocation of the ASM to the surface .. | 61 |
| 3.1.5 The PilC subunit of the meningococcal T4P is involved in ceramide release | 62 |
| 3.1.6 Inhibition of intracellular calcium release reduced the number of invasive bacteria | 64 |
| 3.1.7 Treatment of HBMEC with pili enriched fractions induced translocation of the lysosomal ASM and ceramide generation on the cell surface..... | 65 |
| 3.1.8 Interaction with the CD147 receptor as putative mediator for calcium release | 69 |
| 3.2 Importance of cell cycle regulated gangliosides for meningococcal infection..... | 72 |
| 3.2.1 Cell cycle dependent surface expression of GM1 and Gb3..... | 72 |
| 3.2.2 Increased number of cells in the G1 phase correlates with increased GM1 surface abundance | 74 |

| | |
|--|---|
| 3.2.3 Interaction between <i>N. meningitidis</i> and GM1 is important for bacterial invasion .. | 76 |
| 3.3 The antimicrobial activity of sphingolipids against <i>N. meningitidis</i> | 77 |
| 3.3.1 CLEM reveals concentration related differences in localization of functionalized sphingolipids | 79 |
| 3.3.2 Mass Spectrometric analysis confirm the primary effect on the outer membrane.. | 81 |
| 4. Discussion | 83 |
| 4.1 Meningococcal-induced ceramide platform formation | 83 |
| 4.2 Cell-cycle-regulated gangliosides and meningococcal infection | 86 |
| 4.3 Antimicrobial activity of sphingolipids against <i>N. meningitidis</i> | 88 |
| Conclusion and future research..... | 92 |
| References..... | 94 |
| Appendix..... | 108 |
| Acknowledgment | 108 |
| Publications and presentations | 109 |
| Curriculum Vitae | Fehler! Textmarke nicht definiert. |
| Affidativ/ Eidesstattliche Erklärung..... | 112 |

II. Figure Register

Figure 1: Schematic representation of the meningococcal type 4 pilus. 15

Figure 2: Host factors involved in bacterial adhesion and stabilization. 16

Figure 3: Sphingolipid de novo synthesis in the endoplasmatic reticulum. 19

Figure 4: Interaction between bacterial pathogens, sphingolipid enzymes and metabolites. 22

Figure 5: Size comparison of various fluorescence probes. 25

Figure 6: Ceramide surface level peaked after 4 h post infection. 53

Figure 7: Highly piliated *N. meningitidis* strain 8013 induce the formation of CRPs on HBMEC. 54

Figure 8: *N. meningitidis* strain 8013 induce CRP formation in a Type 4 pili (T4P) and host ASM dependent manner. 55

Figure 9: Highly piliated *N. meningitidis* strain 8013 induce ASM surface activity on HBMEC. 56

Figure 10: *N. meningitidis* induces the translocation of lysosomal ASM and Lamp1 to the cell surface. 57

Figure 11: ASM surface intensity increases during infection. 58

Figure 12: *N. meningitidis* increased cytosolic Ca²⁺ levels in brain endothelial cells derived from the endoplasmatic reticulum. 60

Figure 13: *N. meningitidis*-induced ASM translocation to the plasma membrane is Ca²⁺ dependent. 61

Figure 14: Depletion of calcium abolished ASM activity on the cell surface. 62

Figure 15: Ceramide release and CRP formation in response to isogenic $\Delta pilC1$ or $\Delta pilC2$ meningococcal mutants. 63

Figure 16: Depletion of the Ca²⁺ level interferes with invasion of *N. meningitidis* strain 8013 into HBMEC. 64

Figure 17: Effect of 2-APB on neisserial growth. 65

Figure 18: Western blot or dot blot analyses of pili enriched fractions of *N. meningitidis* 8013. 66

Figure 19: Effect of pilus-enriched fractions on Ca²⁺ fluxes, ASM translocation and activity, and ceramide release. 67

Figure 20: Treatment of HBMEC with pilus-enriched fractions increased the number of plasma membrane-associated CRPs. 68

Figure 21: CD147 expression on HBMEC and recruitment underneath meningococcal microcolonies. 70

Figure 22: An antibody against the C-terminal domain D2 of CD147 blocks *N. meningitidis* – induced calcium flux (MEM-M6/6). 71

Figure 23: Visualization of sphingolipids GM1 and Gb3 in the plasma membrane of brain endothelial cells. 73

Figure 24: GM1 but not Gb3 accumulates around *N. meningitidis*. 74

Figure 25: Serum starvation led to an increased number of cells in the G1 phase. 75

Figure 26: Serum starvation led to an increase of GM1 surface abundance. 75

Figure 27: Blocking of GM1 strongly reduces meningococcal invasiveness. 76

Figure 28: TEM micrographs show the effect on *N. meningitidis* treated with azido-modified sphingolipids. 78

| | |
|---|----|
| Figure 29: CLEM reveals concentration dependent localization of ω -N ₃ -C ₆ -Ceramid in <i>N. meningitidis</i> | 80 |
| Figure 30: CLEM reveals concentration dependent localization of ω -N ₃ -Sphingosine in <i>N. meningitidis</i> | 80 |
| Figure 31: Quantification of azido-functionalized sphingolipid levels in membrane fractions of <i>N. meningitidis</i> by mass spectrometry. | 82 |

III. Table Register

| | |
|--|----|
| Table 1: Devices used in this study | 27 |
| Table 2: Consumables used in this study | 28 |
| Table 3: Commercial kits used in this study..... | 29 |
| Table 4: Chemicals and reagents used in this study..... | 30 |
| Table 5: Antibiotics used in this study..... | 32 |
| Table 6: Commercial and customized lipids used in this study | 32 |
| Table 7: Antibodies and dyes used in this study | 33 |
| Table 8: Plasmids used in this study..... | 34 |
| Table 9: Primer used in this study | 35 |
| Table 10: Solutions, buffer and media used in this study..... | 36 |
| Table 11: Bacterial strains used in this study..... | 38 |
| Table 12: Cell lines used in this study..... | 39 |
| Table 13: Software used in this study | 40 |
| Table 14: General example for the PCR reaction mixture..... | 43 |
| Table 15: General PCR reaction conditions..... | 43 |

IV. Abbreviation Index

| Abbreviation | Explanation | Abbreviation | Explanation |
|------------------|---|-------------------|--|
| \pm SD | \pm standard deviation | LDH | Lactate dehydrogenase |
| 2-APB | 2- Aminoethoxydiphenyl borate | LOS | Lipooligosaccharide |
| 3Ks | 3-Ketosphingosine | MBC | Minimal bactericidal concentration |
| b-CSF | Brain-Cerebrospinal Fluid | MgCl ₂ | Magnesium chloride |
| BSA | Bovine serum albumin | MIC | Minimal inhibitory concentration |
| Ca ²⁺ | Calcium | min | Minute(s) |
| CD | Cluster of differentiation | MLST | Multi Locus Sequence Typing |
| CD147 | Basigin; extracellular matrix metalloproteinase inducer (EMMPRIN) | MOI | Multiplicity of infection |
| CerS | Ceramide synthase | NaCl ₂ | Sodium chloride |
| CERT | Ceramide Transporter | NADPH | Dihydronicotinamide-adenine dinucleotide phosphate |
| CLEM | Correlative light and electron microscopy | Nm | <i>Neisseria meningitidis</i> |
| CO ₂ | Carbon dioxide | NPD | Niemann Pick disease |
| CRP | Ceramide rich platform | NSM | Neutral sphingomyelinase |
| CTCF | Corrected total cell fluorescence | Opa | Opacity-Associated Protein |
| CtxB | Cholera-toxin B subunit | Opc | Opacity proteins |
| DBCO | Dibenzocyclooctyne | PCR | Polymerase chain reaction |
| DMSO | Dimethyl sulfoxide | PeF | Pilus enriched fraction |
| dSTORM | Direct stochastic optical reconstruction microscopy | PI | Propodium iodid |
| ER | Endoplasmic reticulum | PorB | Porin B |
| EtOH | Ethanol | RPMI | Roswell Park Memorial Institute |
| fHbp | Factor H binding protein | S/L-ASM | Secretory/Lysosomal acid sphingomyelinase |
| Gb3 | Globotriaosylceramide | Sg | Serogroup |
| GFP | Green fluorescent protein | SM | Sphingomyeline |
| GM1 | monosialotetrahexosylganglioside | SMase | Sphingomyelinase |
| h | Hour(s) | SPAAC | Strain promoted azide alkyne cycloaddition |
| HBMEC | Human brain microvascular endothelial cells | ST | Sequence Type |
| HBSS | Hanks balanced salt solution | StxB | Shiga-toxin B subunit |
| HPLC | High-performance liquid chromatography | T4P | Type 4 Pili |
| HS | Human serum | TCO | Trans-cyclooctene |
| IgG | Immunoglobulin G | β 2AR | β -2-Adrenergic Receptor |

Va. Summary

The obligate human pathogen *Neisseria meningitidis* is a major cause of sepsis and meningitis worldwide. It affects mainly toddlers and infants and is responsible for thousands of deaths each year. In this study, different aspects of the importance of sphingolipids in meningococcal pathogenicity were investigated. In a first step, the acid sphingomyelinase (ASM), which degrades membrane sphingomyelin to ceramide, was studied in the context of meningococcal infection. A requirement for ASM surface activity is its translocation from the lysosomal compartment to the cell surface, a process that is currently poorly understood.

This study used various approaches, including classical invasion and adherence assays, flow cytometry, and classical and super resolution immunofluorescence microscopy (*d*STORM). The results showed that the live, highly piliated *N. meningitidis* strain 8013/12 induced calcium-dependent ASM translocation in human brain microvascular endothelial cells (HBMEC). Furthermore, it promoted the formation of ceramide-rich platforms (CRPs). In addition, ASM translocation and CRP formation were observed after treating the cells with pili-enriched fractions derived from the same strain. The importance for *N. meningitidis* to utilize this pathway was shown by the inhibition of the calcium-dependent ASM translocation, which greatly decreased the number of invasive bacteria.

I also investigated the importance of the glycosphingolipids GM1 and Gb3. The results showed that GM1, but not Gb3, plays an important role in the ability of *N. meningitidis* to invade HBMEC. By combining *d*STORM imaging and microbiological approaches, we demonstrated that GM1 accumulated prolifically around bacteria during the infection, and that this interaction seemed essential for meningococcal invasion.

Sphingolipids are not only known for their beneficial effect on pathogens. Sphingoid bases, including sphingosine, are known for their antimicrobial activity. In the last part of this study, a novel correlative light and electron microscopy approach was established in the combination with click chemistry to precisely localize azido-functionalized sphingolipids in *N. meningitidis*. The result showed a distinct concentration-dependent localization in either the outer membrane (low concentration) or accumulated in the cytosol (high concentration). This pattern was confirmed by mass spectrometry on separated membrane fractions. Our data provide a first insight into the underlying mechanism of antimicrobial sphingolipids.

Vb. Zusammenfassung

Der obligate Humanpathogen *Neisseria meningitidis* ist weltweit einer der Hauptursachen für Sepsis und Meningitis. Er befällt vor allem Kleinkinder und Säuglinge und ist jedes Jahr für Tausende von Todesfällen verantwortlich. In dieser Studie wurden verschiedene Aspekte der Bedeutung von Sphingolipiden bei der Pathogenität von Meningokokken untersucht. In einem ersten Schritt wurde die saure Sphingomyelinase (ASM), die Membran-Sphingomyelin zu Ceramid abbaut, im Zusammenhang mit einer Meningokokken-Infektion untersucht. Eine Voraussetzung für die Oberflächenaktivität der ASM ist ihre Translokation vom lysosomalen Kompartiment auf die Zelloberfläche, ein Prozess, der derzeit noch wenig verstanden wird.

In dieser Studie wurden verschiedene Ansätze verwendet, darunter klassische Invasions- und Adhärenztests, Durchflusszytometrie sowie klassische und supraauflösende Immunfluoreszenzmikroskopie (*d*STORM). Die Ergebnisse zeigten, dass der lebende, hochpiliatisierte *N. meningitidis* Stamm 8013/12 eine kalziumabhängige ASM-Translokation in mikrovaskulären Endothelzellen des menschlichen Gehirns (HBMEC) induzierte. Des Weiteren förderte er die Bildung Ceramid-reicher Plattformen (CRPs). Zusätzlich wurden ASM-Translokation und CRP-Bildung beobachtet, nachdem die Zellen mit pili-angereicherten Fraktionen desselben Stammes behandelt worden waren. Die Bedeutung für *N. meningitidis* in der Pathogenese zeigte sich durch die Hemmung der Calcium-abhängigen ASM-Translokation, wodurch die Zahl der invasiven Bakterien stark reduziert wurde.

Ich untersuchte auch die Bedeutung der Glykosphingolipide GM1 und Gb3. Die Ergebnisse zeigten, dass GM1, aber nicht Gb3, eine wichtige Rolle bei der Fähigkeit von *N. meningitidis* spielt, in Gehirndothelzellen einzudringen. Durch die Kombination von *d*STORM-Bildgebung und mikrobiologischen Ansätzen konnten wir zeigen, dass sich GM1 während der Infektion vermehrt um die Bakterien herum anreicherte und dass diese Interaktion für die Invasion von Meningokokken essenziell ist.

Sphingolipide sind nicht nur für ihre positive Wirkung auf Krankheitserreger bekannt. Sphingoidbasen, einschließlich Sphingosin, sind zusätzlich für ihre antimikrobielle Aktivität bekannt. Im letzten Teil dieser Studie wurde ein neuartiger korrelativer licht- und elektronenmikroskopischer Ansatz in der Kombination mit Click-Chemie etabliert, um azidofunktionalisierte Sphingolipide in *N. meningitidis* genau zu lokalisieren. Das

Ergebnis zeigte eine deutliche konzentrationsabhängige Lokalisation entweder in der äußeren Membran (niedrige Konzentration) oder akkumuliert im Zytosol (hohe Konzentration). Dieses Muster konnte durch einen Massenspektrometrischen Ansatz bestätigt werden. Hierfür wurde eine Separation der inneren und äußeren Membran, nach Behandlung mit der niedrigen Konzentration, etabliert. Die verschiedenen Membranfraktionen wurden anschließend auf ihren Gehalt an funktionalisierten Sphingolipiden hin untersucht und bestätigten die Lokalisierung in der äußeren Membran. Unsere Daten geben einen ersten Einblick in den zugrundeliegenden Mechanismus der antimikrobiellen Sphingolipide.

1. Introduction

1.1 *Neisseria meningitidis*

Neisseria meningitidis (*Nm*, the meningococcus) is an obligate human Gram-negative bacterium and a major cause of septicemia and meningitis worldwide. The meningococcus, with its characteristic appearance as diplococcus, was initially described in the cerebrospinal fluid of a lethal case of meningitis by Marchiafava and Celli in 1884. Three years later, it was firstly isolated by Weichselbaum (Weichselbaum, 1887). *N. meningitidis* colonizes – mostly asymptotically – the nasopharyngeal mucosa of approximately 10 % of the general population. The prevalence is relatively low in young infants (4.5 %) and the peak occurs among young adults (19-years old, 23.7 %) (Christensen *et al.*, 2010; Sidorenko *et al.*, 2019).

N. meningitidis can be classified into different serotypes (STs), based on multi locus sequence typing (MLST) of seven housekeeping genes (*abcZ*, *adk*, *aroE*, *fumC*, *gdh*, *pdhC* and *pgm*) (Birtles *et al.*, 2005; Maiden *et al.*, 1998). Another classification method, which is more widely known, is the separation into serogroups (Sg), differing in the expression of various polysaccharide capsules. To date 13 different serogroups have been identified (A, B, C, D, 29E, H, I, K, L, W-135, X, Y and Z), of which only six are connected to infectious diseases (A, B, C, W-135, X, Y) (Odile *et al.*, 2013).

The prevalence of the infectious serogroups differs according to the region. For example serogroups B, C, W-135 and Y are predominant in Europe, America and Australia, whereas serogroup A is predominant in Asia and Africa - especially the sub-Saharan region, dubbed as the meningitis belt (Claus *et al.*, 2005). In addition, serogroup X has become more prevalent in African regions in recent years (Pelton, 2016).

Different vaccines are available, such as quadrivalent polysaccharide or conjugate vaccines against serogroup A, C, W-135, and Y, and monovalent conjugate vaccines against serogroup B and C (CDC, 2017). Nonetheless, the rate of invasive meningococcal infection remains relatively high, with 500.000 to 1.2 million infections per year and a case lethality rate between 10 % and 15 % (CDC, 2017; Chang *et al.*, 2012). The average incubation time is 3 – 4 days (range: 2–10 days); thereafter, the most common early symptoms are fever, headache and a stiff neck. Additional possible symptoms are nausea, vomiting, photophobia and altered mental status or confusion (CDC, 2017).

The most prominent clinical manifestations of invasive meningococcal infections are meningitis and septicemia (purpura fulminans), which can occur separately or together. Less common manifestations are pneumonia, arthritis, otitis media and epiglottitis (CDC, 2017; Stephens, 2012). Importantly, even appropriate treatment of invasive meningococcal infections, using third generation cephalosporine (such as Cefotaxim) or penicillin G, does not alleviate the high risk of lifelong sequelae among 10 to 20 % of patients. These sequelae include deafness, learning disabilities and limb amputations (Edwards and Baker, 1981; Grimwood *et al.*, 2000; Johswich - Homepage: Institute for hygiene and microbiology; Tzeng and Stephens, 2000).

1.2. Interaction with the human host

1.2.1 Colonization and survival in the nasopharynx

After transmission via aerosol, the first step of meningococcal infection is colonization of the nasopharyngeal region, where *N. meningitidis* encounter the epithelial barrier. This specific barrier consists of two different epithelial cell structures: the stratified squamous epithelium and the columnar respiratory epithelium. The stratified squamous epithelium consists of a multilayer structure of flattened epithelial cells with a strong barrier function (Wang *et al.*, 2019). The columnar respiratory epithelium consists of basal, goblet and ciliated cells, which moisten the nasopharyngeal region and provide protection by producing mucus and an accompanying mucociliary clearance mechanism (Crystal *et al.*, 2008; Kia'i N., 2019). The 10 – 15 µm thick mucus layer represents a challenging environment for colonization. It has bacteriostatic properties due to the scarcity of nutrients such as glucose and iron and an abundance of antimicrobial peptides (e.g. β -defensins) as well as components of the complement system and immunoglobulin A (IgA). These substances inhibit bacterial survival and adherence to mucosal components (Baker and Baines, 2018; Coureuil *et al.*, 2019; De Rose *et al.*, 2018; Smith *et al.*, 2013).

For successful colonization of the nasopharynx, *N. meningitidis* is well adapted to the challenges mentioned above. To overcome the nutritional limitations, meningococci use a broad range of carbon sources, including glucose, pyruvate and lactate. They are also equipped with up to four different iron uptake systems: transferrin binding proteins, lactoferrin binding proteins, and two independent heme transport systems)

(Coureuil *et al.*, 2019; Exley *et al.*, 2005; Perkins-Balding *et al.*, 2004). To enhance the success of colonization regarding the various antimicrobial components, *N. meningitidis* improves their initial adherence—mediated by their type 4 pili (T4P)—by secreting an IgA protease and expressing a broad range of defensive molecules and structures against the innate host defense. Most important here are the polysaccharide capsule, the lipooligosaccharide (LOS), the factor H binding protein (fHbp) and the expression of the MtrCDE efflux pump against antimicrobial peptides (Coureuil *et al.*, 2019; Rouquette-Loughlin *et al.*, 2004; Seib *et al.*, 2009).

Despite the nasopharyngeal region being difficult to survive in, a diverse microbiota colonize this niche. This fact further increases the survival pressure with strong competition for newly entering bacteria (Wang *et al.*, 2018). The bacterial community can be separated into four main groups. The first three are dominated by *Moraxella spp.*, *Fusobacterium spp.*, or *Streptococcus spp.*, respectively. The fourth group has greater bacterial diversity with *Corynebacterium spp.*, *Staphylococcus spp.* and *Dolosigranulum spp.* as the main members of the bacterial community (De Boeck *et al.*, 2017). Less abundant bacteria include for example *Neisseria spp.*, *Haemophilus spp.* or *Staphylococcus spp.* (De Boeck *et al.*, 2017).

To compete with other bacteria, *N. meningitidis* expresses two polymorphic toxins (PTs): MafB and CdiA (Arenas *et al.*, 2013; Jamet and Nassif, 2015a). All PTs share common features like the N-terminal signal peptide for secretion, the C-terminal toxin domain and, importantly, an immunity protein encoded directly downstream of the toxin. A specific feature of PTs is that a given N-terminal region can be found fused to distinct toxic domains and vice versa (Jamet and Nassif, 2015b). The MafB toxin has a EndoU ribonuclease activity, cleaving the RNA from competing bacteria only if it contains uridylates (Jamet and Nassif, 2015a). The CdiA is a contact dependent toxin, known for the inhibition of neighboring bacteria by either disruption of the target cell membrane integrity or degradation of cellular nucleic acids (De Gregorio *et al.*, 2019). In addition, recent studies suggest a colonization advantage for *N. meningitidis* mediated by the presence of the meningococcal prophage MDA Φ . It was shown that the MDA Φ phage promotes bacteria-bacteria interactions and with that increase the biomass of bacteria colonizing a monolayer of epithelial cells (Bille *et al.*, 2017; Coureuil *et al.*, 2019; Meyer *et al.*, 2016).

1.2.2 Virulence factors associated with host cell interaction

A broad range of bacterial virulence factors are described in the context of adhesion and interaction with human epithelial and endothelial cells. In addition to the major adhesins, including T4P and the outer membrane proteins OpcA and Opa, the meningococcus also expresses some minor adhesins, such as NadA or App (Capecchi *et al.*, 2005; Serruto *et al.*, 2003; Virji *et al.*, 1993a; Virji *et al.*, 1995; Virji *et al.*, 1993b). Despite the importance of the minor and major adhesins for the late stages of adhesion and interaction with host cells, most are hidden under the capsule of *N. meningitidis* and therefore do not interact directly with the cells. The only major adhesion, which overcomes the capsular barrier, is the T4P. Virji *et al.* demonstrated the importance of T4P for initial adherence in an *in vitro* model; here unpiliated, capsulated meningococci could not adhere to endothelial cells (Virji *et al.*, 1993b).

The pilus fibre is a multimeric structure, up to several microns long, that is composed mainly of the single structural component PilE, also known as major pilin. In addition to PilE, several other structural pilin proteins (including PilC, PilD, PilG and PilF and the minor pilins PilX, PilV and ComP) contribute to T4P functioning (Carbonnelle *et al.*, 2006; Helaine *et al.*, 2005; Nassif *et al.*, 1994; Tonjum *et al.*, 1995) (Figure 1). The meningococcal T4P can be separated into two classes, I and II. Although the two classes share the same structural proteins, as mentioned, they differ in their way of antigenic variation. Class I pili achieve their variation from several silent pilus genes (*pilS*) by gene conversation, transferring DNA from the silent to the expression locus of *pilE*. By contrast, class II pili lack such a mechanism and instead display multiple glycosylation sites rather than the single one found in class I (Gault *et al.*, 2015).

Besides their role in initial adherence, T4P also mediate the natural competence of the meningococcus (mediated by ComP), bacterial movement (known as twitching motility) and initiation of host signal transduction cascades (Fussenegger *et al.*, 1997; Hoffmann *et al.*, 2001; Merz *et al.*, 2000).

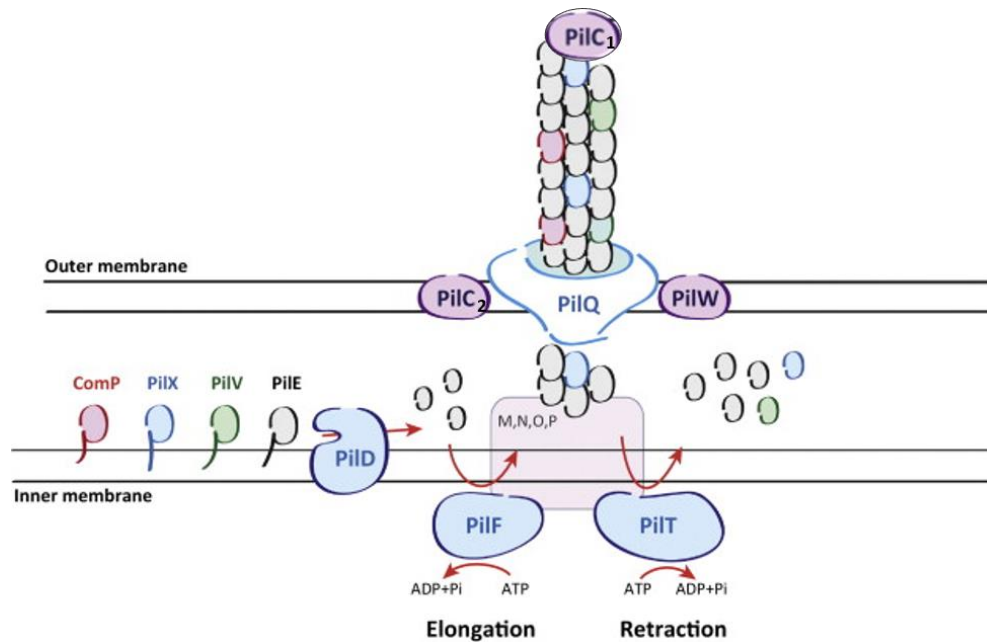


Figure 1: Schematic representation of the meningococcal type 4 pilus.

Components involved in type 4 pili formation. Adapted from Coureuil *et al.* 2014

On the side of the host, various receptors are supposed to interact with T4P; they include CD46, laminin receptors and the platelet activation factor receptor (Coureuil *et al.*, 2019). During the past decade, the CD147 receptor (also called Basigin/EMMPRIN) became a focal point of research. CD147 belongs to the Ig receptor superfamily, with two external Ig and one single transmembrane domain. The external domains are divided into the membrane distal D1 and the membrane proximal D2 domain.

The importance of interaction of the meningococcal T4P and the D2 domain of CD147 has been shown by various approaches, including competition assays and truncated versions of CD147 lacking the D2 domain. The experiments were able to show that the PilE and PilV subunits of the T4P are the key mediators of this interaction (Bernard *et al.*, 2014; Maïssa *et al.*, 2017).

Another important receptor is the G-protein coupled β 2-adrenergic receptor (β 2AR). The β 2AR is not needed for initial attachment of the bacteria, but forms complexes with, and is activated by CD147 (Maïssa *et al.*, 2017). Activation of β 2AR leads to actin rearrangement and polymerization (through e.g. ErbB2 recruitment and Src tyrosine kinase activation) beneath the bacterial colonies. The result is the formation and stabilization of so-called cortical plaques (Figure 2). Many other host factors are also

involved in stabilizing these meningococcal colonies, such as E-selectin, ICAM1 and VCAM1 (dos Santos Souza *et al.*, 2020).

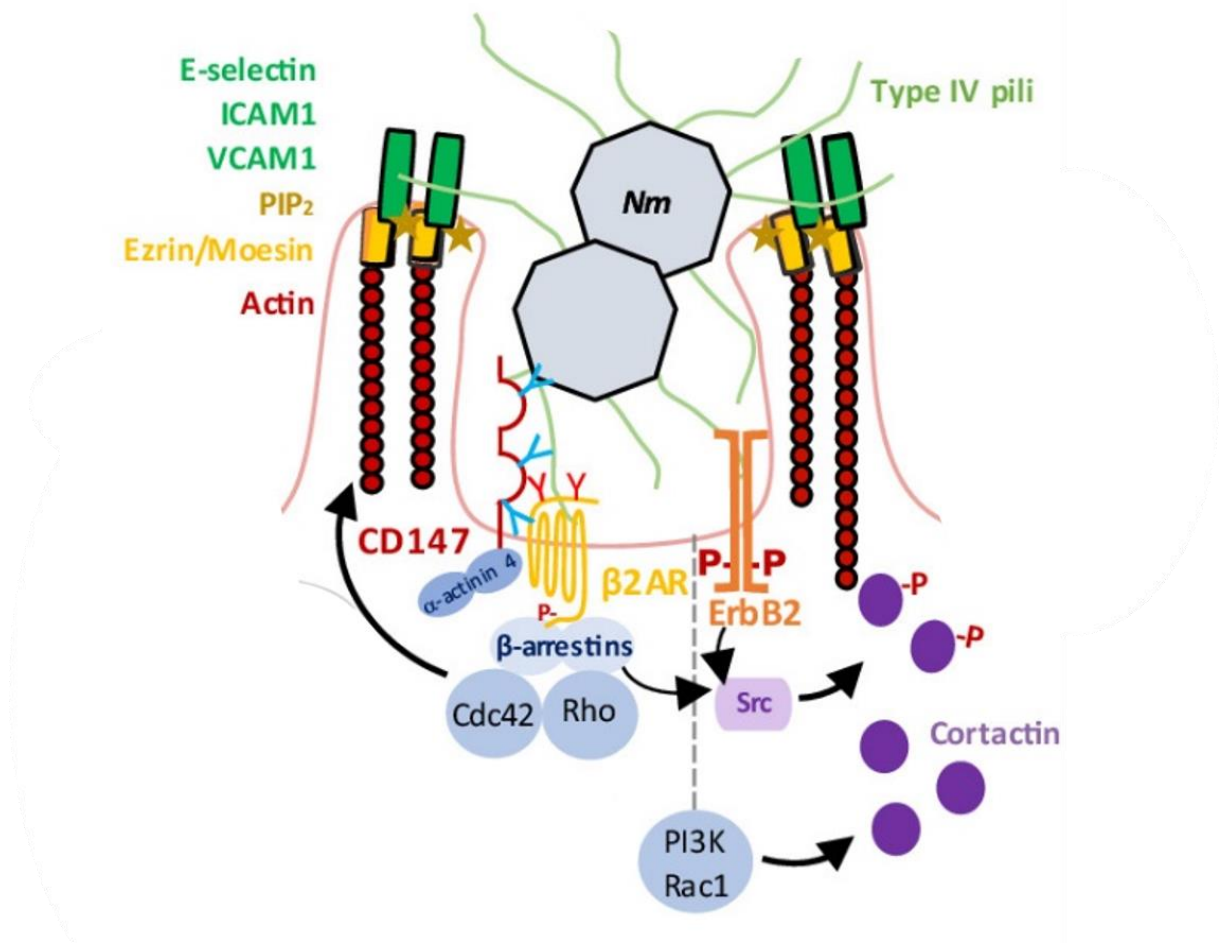


Figure 2: Host factors involved in bacterial adhesion and stabilization.

Schematic drawing of a selection of important host factors in bacterial adhesion and stabilization after initial CD147/T4P interaction. Adapted from Souza *et al.* 2020 (dos Santos Souza *et al.*, 2020)

1.2.3 Proliferation in the bloodstream

After colonizing the nasopharynx, *N. meningitidis* overcomes the epithelial barrier and invades the bloodstream. The main hypothesis for meningococcal transport through the barrier is active translocation by internalization and trafficking within intracellular vacuoles (Coureuil *et al.*, 2019). The trigger for switching from the carrier to the infectious state – that is translocation through the epithelial barrier – is still unknown. It has been suggested that damage to the epithelium, for example by viral co-infections or climatic conditions, favours meningococcal infections (Coureuil *et al.*, 2019; Hubert *et al.*, 1992; Sultan *et al.*, 2005).

In the bloodstream, the meningococcus encounters new and known challenges for survival and proliferation. It benefits from the same set of factors, which are important for colonization of the nasopharyngeal region. These factors include protection against the host immune system (polysaccharide capsule, the LOS, the fHbp and the MtrCDE efflux pump) and the presence of iron acquisition systems (e.g. transferrin and lactoferrin binding proteins, and two independent heme transport systems). Whereas the capsule is the most important factor for bacterial survival in the bloodstream, another important pathogenicity factor during the blood stage are T4P, which provide the possibility for meningococcus to adhere to endothelial cells and resist the laminar flow of the bloodstream (Join-Lambert *et al.*, 2013).

Once adhered to the endothelial cells, *N. meningitidis* starts to replicate. It forms large colonies at the apical surface of the endothelium, leading to thrombus formation, which could manifest throughout the body. The most severe form is known as purpura fulminans (Join-Lambert *et al.*, 2013).

1.2.4 Interaction with the blood–cerebrospinal–fluid barrier

The blood–cerebrospinal–fluid barrier (b–CSFB) is formed by specialized endothelial cells. Compared with typical peripheral endothelial cells, this barrier is characterized by low or no pinocytosis, high mitochondrial content, polarized expression of ion and peptide transporters, lack of fenestration, and an increased number of and exclusively expressed tight junction proteins (e.g. Claudin 5 and Occludin) (Yu *et al.*, 2015).

The interaction of *N. meningitidis* with this endothelial barrier has been the subject of many studies and is probably the best-understood step in meningococcal pathogenesis. As already described regarding the proliferation in the bloodstream, the meningococcus mainly relies on T4P – including the activation of host factors – for its initial attachment. Once adhered, the single diplococcus can start to replicate and protects itself against the shear forces in the bloodstream by inducing membrane protrusion formation towards the bacterial colonies (Mikaty *et al.*, 2009).

1.3 Sphingolipids

Thudichum first described sphingolipids in 1884, and he named them after the sphinx because of their enigmatic function. Initially narrowed down to their role in membrane homeostasis, sphingolipids become more prominent during recent decades. Sphingolipids are known to be important first and second messengers in various signalling pathways and play a vital role in the formation of highly ordered membrane microdomains, the so-called lipid rafts (Futerman and Hannun, 2004).

Like all other membrane lipids, sphingolipids show an amphipathic character. The hydrophobic tail region of sphingolipids shares a common sphingoid base backbone of sphingosine, sphinganine or phytosphingosine. This is coupled by an amide bond, to a fatty-acid side chain of varying length. The negatively charged, hydrophilic head group of sphingolipids displays vast variability of different motives. These range from the simplest head motive, found in the group of ceramides and consisting of just two hydroxyl groups, to more complex sphingolipids – such as sphingomyelin, which has a phosphatidylcholine head motive. Another example is the highly complex sugar-residue motives found in glycosphingolipids (Merrill, 2002).

In the cell, the *de novo* biosynthetic pathway is located in the endoplasmic reticulum (ER). Synthesis starts with the condensation of palmitoyl-CoA and L-serine, catalysed by the serine palmitoyltransferase (SPT) to 3-ketosphinganine (3KS). Further steps include the NADPH-dependent generation of sphinganine; coupling of the fatty-acid side chain, resulting in dihydroceramide; and the introduction of a double bond in the sphinganine backbone to form ceramide (Figure 3) (Wigger *et al.*, 2019).

For further modification of the basic ceramide to more complex sphingolipids, the ceramide must be transported to the Golgi apparatus. Because ceramides are membrane-bound and display low solubility in aqueous solutions, like the cellular environment, ceramide mobilization is achieved either by vesicular transport or is mediated by the ceramide transfer protein (CERT) (Gault *et al.*, 2010). Once in the Golgi, the ceramide is further processed towards the complex sphingolipids, such as sphingomyelin and glycosphingolipids. The sorting and distribution of the lipids to their target membranes is then achieved through specialized vesicle based transport from the trans-Golgi network (Deng *et al.*, 2016).

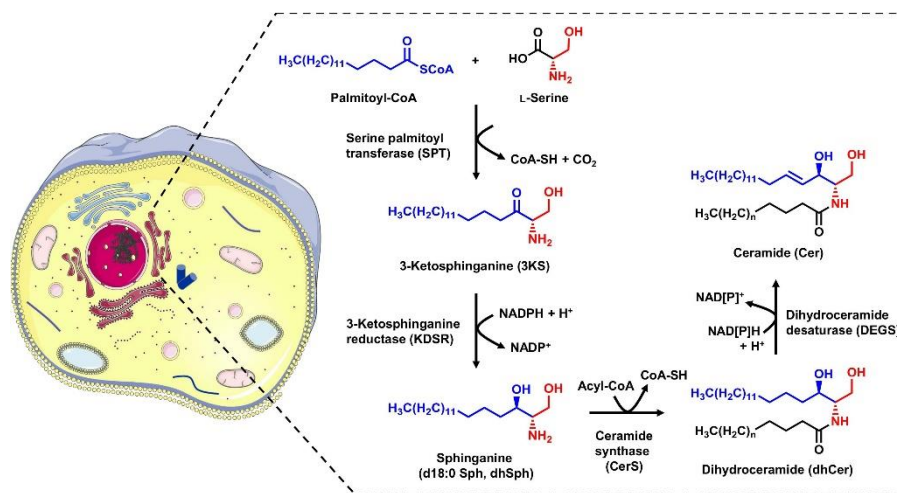


Figure 3: Sphingolipid de novo synthesis in the endoplasmic reticulum.

Overview of the steps of sphingolipid de novo synthesis that occur in the ER. Image taken from Wigger *et al.*, 2019.

Apart from the de novo synthesis, there are various mechanisms for recycling and restructuring specific sphingolipids into other metabolites. One mechanism, the salvage pathway, includes conversion of sphingomyelin to ceramide at the inner and outer leaflet of the plasma membrane. This process alters the membrane curvature as well as the fluidity and distribution of other lipids and receptors (Alonso and Goñi, 2018; Burgert *et al.*, 2017). The hydrolysis of sphingomyelin to ceramide and phosphocholine is mediated by a subset of enzymes called sphingomyelinases (SMases). SMases are differentiated depending on their pH optimum into acid SMases (ASM) or neutral SMases (NSM). For the NSM, three different genes (*Smpd2-4*) encode for different enzymes (NSM 1-3) (Airola and Hannun, 2013; Pavoine and Pecker, 2009). According to their pH optima, the various NSMs act intracellularly at the inner leaflet of the plasma membrane (Andrieu-Abadie and Levade, 2002; Czarny and Schnitzer, 2004).

In contrast, only one gene, *Smpd-1*, encodes for two distinct isoforms of the ASM, the secretory (S-ASM) and the lysosomal (L-ASM) (Schissel *et al.*, 1996). Arising from the same precursor protein, S-ASM and L-ASM are separated during processing in the Golgi by different glycosylation and modification of the N- and C-terminal regions. Whereas S-ASM is constantly released into the extracellular space through the constitutive secretory pathway, L-ASM enters the lysosomal pathway by binding to the manose-6-phosphate receptor (Kornhuber *et al.*, 2015). The acidic environment in the

lysosome offers optimal pH conditions for L-ASM activity. However, and notably L-ASM also shows extracellular activity on the outer leaflet of the cell. The activity in the extracellular space, with its neutral pH, is achieved through an acidic microenvironment created by fusion of the lysosome and outer membrane and the release of V1 H(+)-ATPases (Xu *et al.*, 2012).

1.3.1 Physiological role of sphingolipids

The functions of sphingolipids in the cell are as diverse as their structures and with that, the focus is here on the lipids and enzymes important for this study. Besides their role in maintaining the membrane integrity, sphingolipids are involved in many biological processes. These include cell differentiation, growth and death, as well as senescence and inflammatory responses (Hannun and Obeid, 2018).

Ceramides are generated through de novo synthesis by one of the six ceramide synthases (CerS 1-6) or the salvage pathway (such as the recycling pathway of sphingomyelin). Their functions depend strongly on the length of the fatty acid side chain attached to the sphingoid base. The chain length of ceramides varies from 2 carbons (C2 ceramide) to 36 (C36), but the length is typically between 14 and 36 carbons (C14 – C36; (Merrill, 2011)). Their physiological functions range from cell cycle arrest (exogenous C2 and C6) to pro- and antiapoptotic signalling (C16, C18 or C24, depending on the cell type) and protection against desiccation in the skin (C26-36) (Grösch *et al.*, 2012; Hannun and Obeid, 2018; Sandhoff, 2010).

As already mentioned, either one of the three neutral or the acid sphingomyelinase catalyses the recycling of ceramide. From a healthy physiological perspective, that is their purpose. Mutation in the *Smpd1* gene leads to a marked decrease in ASM activity in the lysosome and results in severe lysosomal lipid-storage disorders, namely Niemann Pick disease (NPD) type A and B. This disease occurs in approximately 1 of 250,000 individuals and, especially type A, is almost always fatal (Bajwa H, 2020).

Glycosphingolipids, with their complex head moieties, have many different functions in the cell. Due to their complexity, the exact physiological role of a large proportion of glycosphingolipid remains elusive. Two well-studied representatives are the monosialotetra-hexosylganglioside GM1 and the globotriaosylceramide Gb3. GM1 is predominantly a brain ganglioside that displays a receptor function. It plays an

important role in maintaining neuronal plasticity by interacting with plasma membrane proteins resulting in signalling platform formations and activation of pathways involved in neuronal differentiation and protection from neurodegeneration (Chiricozzi *et al.*, 2020). Hence alteration of GM1 levels may affect the development of neurodegenerative diseases such as Alzheimers or Parkinsons (Chiricozzi *et al.*, 2020).

Gb3, also called CD77, has different entities depending on the cell type. It is known as an antigen of germinal center B cells that are entering apoptosis, the rare human blood group P^k antigen, as shiga toxin receptor on the intestinal epithelium. It can be found on endothelial cells, among others (Desselle *et al.*, 2012; Mangeney *et al.*, 1991; Obrig *et al.*, 1993).

In addition to their natural physiological function in humans, both glycosphingolipids are known to mediate the interaction between cells and a broad range of pathogens. GM1 can be targeted by the Simian virus T40, *Brucella suis*, *Vibrio cholerae* and *Escherichia coli*. The interaction between Gb3 and the Human Immunodeficiency Virus (HIV) or *Shigella dysenteriae* has similarly been described (Schlegel *et al.*, 2019).

1.3.2 Sphingolipids and infection

In recent decades, much effort was focussed on investigating pathogens' interactions with sphingolipids. Besides the examples of GM1 and Gb3, many other interactions between bacteria and the sphingolipid metabolism have been documented to date, including *Neisseria spp.*, *Legionella*, *Simkania* and *Chlamydia* (Figure 4). In addition to bacteria, the interaction also occurs with different viruses - including rhinovirus, measles and Ebola virus (Kunz and Kozjak-Pavlovic, 2019; Schneider-Schaulies and Schneider-Schaulies, 2015).

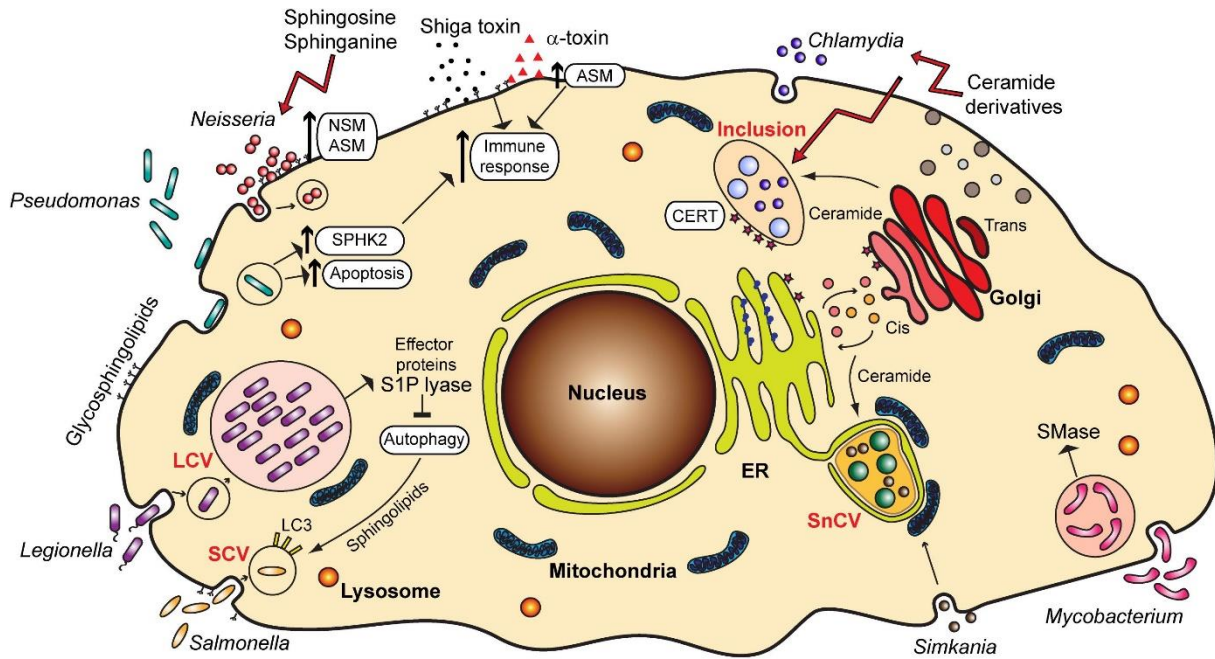


Figure 4: Interaction between bacterial pathogens, sphingolipid enzymes and metabolites.

ER, endoplasmic reticulum; LCV, Legionella-containing vacuole; SCV, Salmonella-containing vacuole; SnCV, Simkania negevensis-containing vacuole; ASM, acid sphingomyelinase; NSM, neutral sphingomyelinase; SPHK2, sphingosine kinase 2; S1P, sphingosine-1-phosphate; SMase, sphingomyelinase; CERT, ceramide transfer protein; LC3, Microtubule-associated protein 1A/1B-light chain 3. Taken from (Kunz and Kozjak-Pavlovic, 2019).

1.3.2.1 Sphingolipids and *Neisseria meningitidis*

Although much is known about the interaction between *N. meningitidis* and the sphingolipid metabolism, certain details remain elusive. Initially, the importance of sphingolipids in meningococcal infection was shown by Simonis *et al.* (2014), who detected increased ASM abundance and activity in human brain microvascular endothelial cells (HBMEC) during the course of infection, in an OpcA-dependent manner (Simonis *et al.*, 2014). Confirmation of the importance for the bacteria was the inhibition of ASM activation by the chemical inhibitor amitriptyline or siRNA, leading to marked decrease of invasive bacteria without effecting their adherence. Additionally, it was shown that the ceramide surface levels increased together with the ASM surface abundance to promote the formation of ceramide-rich platforms (CRPs). In these CRPs, different receptors could cluster, including the ErbB2 receptor, important for meningococcal invasiveness.

In an infection experiment with an *OpcA* deficient mutant, it was shown that the bacteria could still induce ASM translocation and activation. The result show that approximately 80 % of the ASM activity remains compared to the wild type strain. This finding raises the question of what other bacterial factors and host pathways are involved in ASM translocation and CPR formation.

The ambition of ceramides to form such CRPs was further elucidated by super resolution microscopy (here direct stochastic optical reconstruction microscopy (*d*STORM)). The accumulation of receptors in the CRPs, which then serve as signalling platforms, has also been hypothesised (Burgert *et al.*, 2017).

1.3.3 Sphingolipids as antimicrobial agents

Another emerging field of interactions concerns the antimicrobial activity of a subset of sphingolipids. The sphingoid base, sphingosine, is the best-studied example, but also the entire area of antimicrobial (sphingo)-lipids is receiving attention and is intensely studied. The antimicrobial activity of sphingolipid species against a broad range of pathogens has been demonstrated, including Gram-positive and -negative bacteria and fungi (Becker *et al.*, 2017; Bibel *et al.*, 1992; Dongfack *et al.*, 2012; Fischer *et al.*, 2012; Fischer *et al.*, 2013).

Recent studies by our group also showed the antimicrobial activity of natural and functionalized ceramides against *N. meningitidis* (Becam *et al.*, 2017). However, the mechanism of action remains elusive. Recently there were indications for *E. coli* and *P. aeruginosa* that the killing effect of sphingosine relies on interaction between the protonated NH₂ group and the bacterial plasma membrane lipid, cardiolipin (Verhaegh *et al.*, 2020). Although this may explain the antimicrobial activity of sphingosine, the protonated NH₂ group does not exist in antimicrobial ceramides due to the coupled fatty acid side chain.

There are two popular hypotheses. The first involves primarily an effect on the membrane. The second refers to an accumulation of lipids in the bacterial cytosol, where they interfere with the metabolism.

1.3.4 Functionalized sphingolipids

The term functionalised sphingolipids in this study refers to the addition of a chemical group to the sphingolipids, suitable for a “click-chemistry” reaction (Kolb *et al.*, 2001). This group may be either a trans-cyclooctene (TCO) or – as in case of the current work - an azide (N₃) and can be introduced to various positions. The synthesis of a functionalised sphingolipid necessitates a complete multistep synthesis of the lipid of interest (Lang *et al.*, 2020; Walter *et al.*, 2017).

In this study, the azide group was introduced to the ω position of the sphingosine or the C6 ceramide side chain. Afterwards the lipids could then be used for the click-chemistry reaction to couple the lipid with a dibenzocyclooctyne (DBCO)-containing fluorescent dye. This reaction relies on the natural aspiration from the azide to form a complex with an alkyne, via for example the Cu(I)-free strain promoted azide-alkyne cycloaddition (Debets *et al.*, 2011; Jewett and Bertozzi, 2010). This method offers several advantages compared to conventional antibody or fluorescence-tag-based staining methods. Because the azide-alkyne reaction does not occur naturally in living systems, unspecific binding of the alkyne-coupled dye can mostly be excluded. There is evidence that the alkyne-coupled dye could react in an azide-independent manner with cysteine thiol groups (van Geel *et al.*, 2012). Nevertheless, the unspecific side reaction occurs about two orders of magnitude lower and does not change the overall crucial advantage of this method, the unmatched specificity (Dommerholt *et al.*, 2016; Goryunova, 2020).

Another advantage of the click-chemistry reaction is the size of the reaction partners (Figure 5). The alkyne/dye complex is approximately 190 times smaller than an IgG and 34 times smaller than GFP, based on molecular weight. With their small sizes, the click-chemistry reaction partners show the least interference with their target, making them especially suitable for experiments involving living cells or bacteria.

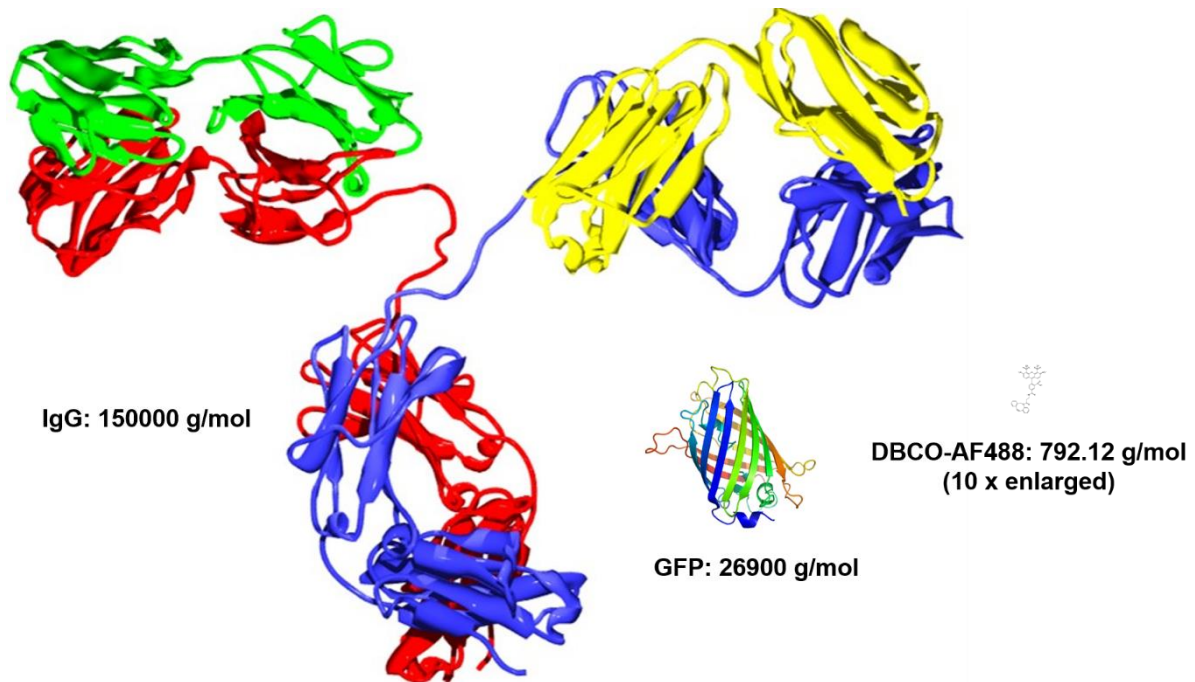


Figure 5: Size comparison of various fluorescence probes.

The figure shows an approximate size comparison between an IgG antibody, the GFP protein and the DBCO-AF488 alkyne/dye complex used for click-chemistry. Image sizes were calculated based on their individual molecular weight. Single images were obtained from the following sources: DBCO-AF488 – www.jenabioscience.com; GFP – www.wikipedia.org; IgG - fcio.at/media/12813/ulrich-wieltsch-thermo-fisher.pdf

1.4 Aim of this study

Based on previous findings of our group, regarding the importance of sphingolipid metabolites and enzymes, the aim of this study was to examine aspects of the interaction between host-derived sphingolipids and *N. meningitidis*.

The focus was therefore on the following topics:

- Involvement of meningococcal type 4 pilus (T4P) in translocating the acid sphingomyelinase (ASM) from lysosome to the cell surface and in the formation of ceramide-enriched platforms (CRPs)
- The role of T4P-induced calcium release from intracellular storages in ASM translocation and CRP formation
- The importance of host gangliosides (glycosphingolipids) GM1 and Gb3 in the context of meningococcal infection of human brain microvascular endothelial cells
- The mechanisms of antimicrobial active sphingolipids against *N. meningitidis*, as revealed by high end localization microscopy and application of mass spectrometry to membrane lipids

To address those topics, the establishment and adaptation of different methods was necessary. This included real time calcium measurements on infected cells, purification of meningococcal type 4 pili, colorimetric based live cell ASM activity analysis and a membrane separation assay

2. Material and Methods

2.1 Material

2.1.1 Laboratory equipment

2.1.1.1 Devices

Table 1: Devices used in this study

| Device | Designation | Manufacturer |
|----------------------------|---|--|
| Balances | PT120 120-5DM | Sartorius Kern |
| Biological Safety cabinets | Safe 2020 NU-437-400E | Thermo Scientific Nuair |
| Blot Chamber | Mini Trans-Blot Cell | Bio-Rad |
| Centrifuges | CT15E CT15RE 1.0R Megafuge 1.0 Megafuge RC 5B Plus WX+ Ultracentrifuge | Hitachi Koki Hitachi Koki Heraeus Heraeus Sorvall Sorvall |
| CO ₂ Incubators | B 5060 DHD Autoflow | Heraeus Instruments Nuair |
| Crimper | Crimper | Sorvall |
| Electrophoresis Chamber | Compact XS/S/M | Biometra |
| Freezer (-20°) | Freezer | Liebherr |
| Fridge (4°C) | Profi Line | Liebherr |
| Gas Burner | Flammy S | Schütt |
| Heater | 2099-DA | Liebisch |
| Magnetic stirrer | MR Hei Standard | Heidolph |
| Microplate Photometer | Infinite F200 Pro Reader | Tecan |
| Microscope | Eclipse Ti Wilovert | Nikon Will Wetzlar |
| pH Meter | Lab 850 | Schott Instruments |
| Phero-Shaker | PH-SH II | Biotec-Fischer |

2. Material and Methods

| Device | Designation | Manufacturer |
|-------------------|---|-----------------------------|
| Photometer | Photometer | WPA |
| Pipet Boy | Accu-jet® pro | Brand |
| Pipettes | Reference 10/100/1000 µl Transferpette S 2.5 µl Transferpette 12 100 µl | Eppendorf Brand Brand |
| Power Supplies | Standard Power Pack P25 Power Pac 300 | Biometra Bio-Rad |
| See-Saw | Duomax 1030 | Heidolph |
| Shaking incubator | Certomat H | B. Braun Biotech |
| Thermocycler | T3000 | Biometra |
| Thermo-Shaker | T21 | Biometra |
| Vortex Mixer | 7-2020 | neoLab |

2.1.1.2 Consumables

Table 2: Consumables used in this study

| Designation | Supplier |
|---|--|
| Cell Culture Flasks (T25, T75) | Sarstedt |
| Columbia Blood Agar Plate | Bio Mérieux |
| Cotton swab | Heinz Herenz Hamburg |
| Cover glass (12 mm) | A. Hartenstein |
| FACS Tube (5 ml) | Falcon |
| Microscopy slides: <ul style="list-style-type: none"> - 8 chambered coverglass system #1.5 high performance - Lab-Tek II Chambered Coverglass W/Cover #1.5 Borosilicate Sterile - ibidi 1.5 µ-Slide 8 Well uncoated - ibidi 1.5 µ-Slide 8 Well ibiTreat | Cellvis Thermo scientific ibidi ibidi |
| Neubauer Improved Disposable Counting Chamber Typ C-Chip™ | A. Hartenstein |

| Designation | Supplier |
|---|--|
| Nitrocellulose Blotting Membrane | GE Healthcare |
| Pipette tips (10, 100, 1000 µl) | Eppendorf |
| Reaction tubes: <ul style="list-style-type: none"> - Safe Seal (0.5, 1.5, 2 ml) - Cellstar tubes (15, 50 ml) | Sarstedt Greiner Bio-One GmbH |
| Serological pipets (5, 10, 25 ml) | Sarstedt |
| Sterile filter Filtropur S 0.2 (0.2 µm pore size) | Sarstedt AG & Co. KG |
| Ultracentrifuge Tubes: <ul style="list-style-type: none"> - 11.5 ml PA Ultra crimp tube - 12 ml PA | Thermo scientific Thermo scientific |
| Vivaspin 20 (10000 MWCO PES) Vivaspin 6 (5000 MWCO PES) | Sartorius |
| Well Plates: <ul style="list-style-type: none"> - 6/24/96-well Standard F Plate - 96-well plate black wall clear bottom - 96-well plate black wall, black bottom | Sarstedt AG & Co. KG Thermo scientific Thermo scientific |
| Whatman Paper | GE Healthcare |

2.1.1.3 Kits

Table 3: Commercial kits used in this study

| Designation | Manufacturer |
|---|---------------------|
| ASM activity assay | Echelon |
| Clarity™ Western ECL Substrate | Bio-Rad |
| Fluo-8 no wash Calcium assay Kit | abcam |
| Lactate Dehydrogenase Activity Assay Kit | Sigma Aldrich |
| Pierce™ BCA Protein Assay Kit | Thermo scientific |
| QIAamp® DNA Mini Kit | QIAGEN |
| QIAGEN® Plasmid Midi Kit | QIAGEN |
| QIAprep® Spin Miniprep Kit | QIAGEN |

| Designation | Manufacturer |
|---------------------------------------|---------------------|
| QIAquick® Gel Extraction Kit | QIAGEN |
| QIAquick® PCR Purification Kit | QIAGEN |

2.1.1.4 Chemicals and reagents

Table 4: Chemicals and reagents used in this study

| Designation | Manufacturer |
|---|---------------------|
| 2-Aminoethoxydiphenyl borate (2-APB) | Tocris |
| Acetic acid (100 %) | Carl Roth |
| Acrylamid Solution (30 %) | Carl Roth |
| Ammonium persulfate (APS) | AppliChem |
| Aqua dest. | Braun |
| Coomassie Brilliant Blue G-250 | Serva |
| DMSO (Dimethylsufoxid) | Carl Roth |
| ECGS | CellSystems |
| EDTA | AppliChem |
| Ethanol (96, 100 %) | Carl Roth |
| Ethanolamine | Sigma Aldrich |
| Fe(NO₃)₃ | Sigma Aldrich |
| Fetal calf serum (FCS) | Gibco |
| Gelantine | Sigma Aldrich |
| Hanks Balance Salt Solution (HBSS) | Sigma Aldrich |
| Heparin | Biochrom |
| HEPES | Sigma Aldrich |

2. Material and Methods

| Designation | Manufacturer |
|-------------------------------------|---------------------|
| Human serum | TCS Bioscience |
| Ionomycin | Abcam |
| Isopropanol (100 %) | Carl Roth |
| K₂HPO₄ | Merck Chemicals |
| KH₂PO₄ | Merck Chemicals |
| LB broth base | Invitrogen |
| L-glutamine | Gibco |
| Lysozyme | Sigma Aldrich |
| MgCl₂ | Carl Roth |
| NaCl | Carl Roth |
| NaHCO₃ | Merck Chemicals |
| Non-essential amino acids | Gibco |
| NU-serum | Corning |
| Paraformaldehyde (PFA) | Carl Roth |
| Poly-L-lysine | Sigma Aldrich |
| Propodium iodid | Thermo Fisher |
| Proteose peptone | BD Biosciences |
| RPMI 1640 | Gibco |
| Saponin | Serva |
| Skim milk | AppliChem |
| Sodium pyruvate | Sigma Aldrich |
| Sucrose | Merck Chemicals |

| Designation | Manufacturer |
|------------------------|---------------|
| TEMED | Carl Roth |
| Thiamine pyrophosphate | Sigma Aldrich |
| Tris-HCl | Carl Roth |
| Triton X-100 | Carl Roth |
| Trypsin-EDTA | Gibco |
| Tween 20 | Carl Roth |

2.1.1.5 Antibiotics

Table 5: Antibiotics used in this study

| Designation | Solvent | Concentration* | Supplier |
|---------------|---------------|----------------|---------------|
| Gentamicin | A. dest | 200 µg/ml | Biochrom |
| Erythromycin | 100 % Ethanol | 7 µg/ml | Sigma Aldrich |
| Spectinomycin | A. dest | 75 µg/ml | Sigma Aldrich |

*= Concentration used for *Neisseria meningitidis*

2.1.1.6 Lipids

Table 6: Commercial and customized lipids used in this study

| Designation | Solvent | Source/Reference |
|--|---------------|--|
| D-erythro-sphingosine | 100 % ethanol | Santa Cruz Biotechnology |
| ω-N ₃ -C ₆ -ceramide (d18:1/6:0-ω-N ₃) | 100 % ethanol | Tim Walter (Walter <i>et al.</i> , 2017) |
| ω-N ₃ -sphingosine | 100 % ethanol | Julian Fink (Lang <i>et al.</i> , 2020) |

2.1.1.7 Antibodies and dyes

Table 7: Antibodies and dyes used in this study

| Designation | Host | Isotype | Manufacturer / Identifier |
|--|--------|---------|---------------------------------------|
| Primary Antibodies | | | |
| Anti-Ceramide | mouse | IgM | Enzo / MID15B4 |
| Anti-C16/24 Ceramide | rabbit | IgG | Erhard Bieberich |
| Anti-LAMP-1-PE | mouse | IgG | Santa Cruz / H4A3 |
| Anti-ASM | mouse | IgG2a | Abcam / mAbcam74281 |
| Anti-ASM | rabbit | IgG | Santa Cruz / H181 |
| Anti-PilE | mouse | IgG | SM1 / (Virji and Heckels, 1983) |
| Anti-PorB | rabbit | IgG | Genosys Biotechnologies / Heike Klaus |
| Anti-CD147 | mouse | IgG1 | BioRad / M6/1 and M6/6 |
| Mouse-IgG-Isotype | mouse | IgG | Thermo Fisher / PPV06 |
| Mouse-IgM-Isotype | mouse | IgM | Immunostep / ICIGMPU |
| Rabbit-IgG-Isotype | rabbit | IgG | Santa Cruz / sc-2027 |
| Anti-OpcA | mouse | IgG | mAb306 / M. Achtman |
| Secondary Antibodies | | | |
| Anti-mouse-IgM-Cy5 | goat | IgG | Jackson Immunoresearch |
| Anti-rabbit-IgG-Cy5 | goat | IgG | Jackson Immunoresearch |
| Anti-rabbit-IgG-Cy3 | mouse | | Jackson Immunoresearch |
| Anti-rabbit-IgG-Alexa Fluor 647 | goat | IgG | Jackson Immunoresearch |
| Anti-mouse-IgG-HRP | goat | IgG | Jackson Immunoresearch |
| Anti-rabbit-IgG-HRP | goat | IgG | Jackson Immunoresearch |

| Designation | Host | Isotype | Manufacturer / Identifier |
|---|------|---------|---------------------------|
| Clickable Dyes | | | |
| DBCO-AF 488 | - | - | Jena Bioscience |
| Toxins for Labeling | | | |
| CtxB (custom conjugated to Alexa Fluor 647/555) | - | - | Sigma-Aldrich |
| StxB custom conjugated to Alexa Fluor 647/555) | - | - | Sigma-Aldrich |
| Indicator Dyes | | | |
| Fluo 8 | - | - | Abcam |
| Hoechst 33342 | - | - | Invitrogen |

2.1.1.8 Plasmids

Table 8: Plasmids used in this study

| Designation | Background | Resistance | Source/Reference |
|-------------------------|-------------|------------------------------|--|
| pTL1 | pBluescript | Ampicillin | (Unkmeir <i>et al.</i> , 2002) |
| pTL1- <i>pilE</i> | pBluescript | Ampicillin | This study |
| pTL1- <i>pilC1</i> | pBluescript | Ampicillin | This study |
| pTL1- <i>pilC2</i> | pBluescript | Ampicillin | This study |
| pTL1- <i>pilE</i> -SmR | pBluescript | Ampicillin/ Spectinomycin | This study |
| pTL1- <i>pilC1</i> -SmR | pBluescript | Ampicillin/ Spectinomycin | This study |
| pTL1- <i>pilC2</i> -SmR | pBluescript | Ampicillin/ Spectinomycin | This study |
| pEG2-GFP | pEG2 | Erythromycin | (Christodoulides <i>et al.</i> , 2000) |

2.1.1.9 Primer

Table 9: Primer used in this study

| AGSU ID | Oligonucleotides | Sequence ^a (5'-3') | Localization ^b | Restriction site |
|---------|------------------------|---|---------------------------|------------------|
| #750 | <i>pilC1_EcoRI_F</i> | CCG <u>gaattc</u> CAGTAAA TACGCTATTATC | 1952796 - 1952814 | <i>EcoRI</i> |
| #758 | <i>pilC1_exp_F</i> | ACTTGTCTATAAAA CCCG | 1953150 - 1953167 | |
| #759 | <i>pilC1_exp_in_R</i> | CCCAAGGAAATATC GCGG | 1953419 - 1953402 | |
| #760 | <i>pilC1_exp_out_R</i> | GGTGATATCTTTAA TCCC | 1953507 - 1953490 | |
| #752 | <i>pilC1_invF</i> | CGG <u>cctagg</u> CGCCAA ACTGCACCTGC | 1953462 - 1953478 | <i>AvrII</i> |
| #753 | <i>pilC1_invR</i> | CGG <u>cctagg</u> CCCGCA TTTTTTACCAAG | 1953206 - 1953189 | <i>AvrII</i> |
| #751 | <i>pilC1_XbaI_R</i> | CCG <u>tctaga</u> TTTCAAT ATCCGACTTAT | 1953907 - 1953890 | <i>XbaI</i> |
| #754 | <i>pilC2_EcoRI_F</i> | CGG <u>gaattc</u> CCTATCC ATACGTTATTG | 44683 - 44700 | <i>EcoRI</i> |
| #761 | <i>pilC2_exp_F</i> | AACCCAATTTACCT TCGG | 45056 - 45073 | |
| #762 | <i>pilC2_exp_in_R</i> | GTATGGGCTTTGCG CACC | 45290 - 45273 | |
| #763 | <i>pilC2_exp_out_R</i> | ACTGTTATGCCTTG CGCG | 45445 - 45428 | |
| #756 | <i>pilC2_invF</i> | CGG <u>cctagg</u> GTCTTTT ATCTGAACGCC | 45372 - 45389 | <i>AvrII</i> |
| #757 | <i>pilC2_invR</i> | CGG <u>cctagg</u> TATATAT CCAGCTTGCCG | 45118 - 45101 | <i>AvrII</i> |
| #755 | <i>pilC2_XbaI_R</i> | CGG <u>tctaga</u> TTTTAAT CTGCGTATCAC | 45831 - 45814 | <i>XbaI</i> |
| #591 | <i>pilE_exp_F</i> | GGTTTTACCCTTAT CGAGCT | 17477 - 17458 | |
| #592 | <i>pilE_exp_R</i> | GGATGGCTTCGGA AACTTG | 17363 - 17381 | |
| #545 | <i>pilE_inv_F</i> | CTGTGG <u>cctagg</u> CGT CAAACGGTTCGGT C | 17144 - 17127 | <i>AvrII</i> |
| #546 | <i>pilE_inv_R</i> | ACGGCT <u>cctagg</u> TGA CCTTCAGCCAAAAG G | 17347 - 17364 | <i>AvrII</i> |
| #544 | <i>pilE_XbaI_R</i> | GCGCGC <u>tctaga</u> TTAG CTGGCAGATGAATC | 16989 - 17006 | <i>XbaI</i> |
| #543 | <i>pilE_XhoI_F</i> | GCGCGC <u>cctcga</u> ATG AACACCCTTCAAAA AGG | 17495 - 17476 | <i>XhoI</i> |

^arestriction sites are in small letters and underlined, ^bcoordinates according to genome annotation from NeMeSys (Rusniok *et al.*, 2009)

2.1.2 Solutions, Buffer and Media

Table 10: Solutions, buffer and media used in this study

| Designation | Components | Mixture | Comments |
|--------------------------------------|--|---|---|
| Cell culture medium | | | |
| HBMEC Medium | <ul style="list-style-type: none"> - RPMI 1640 - FCS - NU-Serum - L-Glutamine (2 mM) - Sodium Pyruvate (1mM) - MEM NEAA - ECGS - Heparin | <ul style="list-style-type: none"> 10 % 10 % 1 % 1 % 1 % 30 µg/ml 5 U/ml | Store at 4°C |
| Infection Medium | <ul style="list-style-type: none"> - RPMI 1640 - HS | <ul style="list-style-type: none"> 90 % 10 % | Prepare fresh for each experiment |
| Bacterial culture | | | |
| Kellog´s Supplement I | <ul style="list-style-type: none"> - Glucose - Glutamine - Thiamine pyrophosphate | <ul style="list-style-type: none"> 40 g 1 g 2 mg | Add to 100 ml with Aqua dest. |
| Kellog´s Supplement II | <ul style="list-style-type: none"> - Fe(NO₃)₃ | 50 mg | Add to 100 ml with Aqua dest. |
| Kellog´s Supplement for PPM + | <ul style="list-style-type: none"> - Kellog´s Supplement I - Kellog´s Supplement II | <ul style="list-style-type: none"> 100 ml 10 ml | Filter sterile with a 0.2 µm filter |
| Buffer Solution for PPM | <ul style="list-style-type: none"> - KH₂PO₄ - K₂HPO₄ | <ul style="list-style-type: none"> 200 g 50 g | Add to 1 L with Aqua dest., adjust pH to 7.25 – 7.5 and autoclave |
| PPM | <ul style="list-style-type: none"> - Proteose peptone - NaCl - Starch - Buffer solution | <ul style="list-style-type: none"> 7.5 g 2.5 g 0.25 g 10 ml | Add to 500 ml with Aqua dest., adjust pH to 7.2 and autoclave |
| PPM + | <ul style="list-style-type: none"> - PPM - Kellog´s Supplement - MgCl₂ (2 M) - NaHCO₃ (8.4 %) | <ul style="list-style-type: none"> 50 ml 500 µl 250 µl 250 µl | Prepare fresh for each experiment, For mutant strains: add appropriate antibiotic |

2. Material and Methods

| Designation | Components | Mixture | Comments |
|---------------------------------------|---|---|--|
| SOB medium | - Yeast extract - Tryptone - NaCl - KCl (250mM) | 0.5 g 2 g 0.05 g 1 ml | Add to 100 ml with Aqua dest., adjust pH to 7 and autoclave |
| SOC medium | - SOB medium - MgCl ₂ (2 M) - MgSO ₄ (1 M) - Glucose (1 M) | 5 ml 25 µl 50 µl 100 µl | Filter sterile, aliquot and store at - 20°C |
| Freezing medium | - Tryptic Soy Broth - Glycerin (86 %) - Aqua dest. | 30 g 465 ml 535 ml | Warm slightly to dissolve and autoclave |
| Buffers and solutions | | | |
| FACS Buffer | - PBS - FCS | 95 % 5 % | |
| 2X Stop Mix | - 0.5 M Tris-HCl pH = 6.8 - Glycerin 100 % - 20 % SDS - Aqua dest. - β-Mercaptoethanol | 14 ml 11.2 ml 11.2 ml 9.8 ml 3.43 ml | Handle β-Mercaptoethanol only under a fume hood |
| Stacking gel | - 0.5 M Tris-HCl pH = 6.8 - 20 % SDS - 16 % APS - TEMED - Rotiphorese® Gel 30 - Aqua dest. | 1.25 ml 25 µl 30 µl 5 µl 0.7 ml 3 ml | |
| Separating gel | - 1.5 M Tris-HCl pH = 8.8 - 20 % SDS - 16 % APS - TEMED - Rotiphorese® Gel 30 - Aqua dest. | 2.5 ml 50 µl 60 µl 10 µl x ml x ml | Rotiphorese® Gel 30 and aqua dest. ratio varied depending on the gel % |
| PBS-T | - 1 X PBS - Tween 20 | 500 ml 0.5 ml | |
| Blocking Buffer (Western Blot) | - Skim milk - PBS-T | 5 % 95 % | |
| 10 x SDS | - Glycine - Tris-HCl - SDS | 144 g 30 g 10 g | Add Aqua dest. To 1 L |
| 1 X SDS | - 10 X SDS - PBS | 10 % 90 % | |

2. Material and Methods

| Designation | Components | Mixture | Comments |
|---|--|------------------------------------|---|
| Transfer Buffer | - Glycine - Tris-HCl - Methanol | 14.4 g 3 g 20 % | Add Aqua dest. to 1 L |
| Blocking Buffer (Immunofluorescence) | - PBS - BSA | 95 % 5 % | Prepare fresh for each experiment |
| Calcium Measurement Buffer | - HBSS - FCS - HEPES | 46.25 ml 2.5 ml 1.25 ml | Prepare fresh for each experiment |
| Calcium Measurement Loading Solution | - Calcium measurement Buffer - Fluo 8 | 1 ml 0.5 µl | Prepare fresh for each experiment |
| Fixation solution | - PFA - PBS | 4 g 100 ml | Further diluted for different applications (final concentration 2 – 3.7 % PFA) |
| Bradford Reagent | - Coomassie Brilliant Blue G-250 - Methanol - 85 % phosphoric acid (H ₃ PO ₄) - Aqua dest. | 50 mg 50 ml 100 ml 850 ml | Dissolve Coomassie in methanol and add the H ₃ PO ₄ , add acid solution to Aqua dest., filter and store dark at 4°C |

2.1.3 Bacterial strains

Table 11: Bacterial strains used in this study

| WUE ID | Designation | Characteristics | Plasmid | Resistance | Source/Reference |
|--------------|--------------------------|---|---------|------------|--|
| #2135 | <i>Nm MC58</i> | <i>Nm MC58 wild type</i> Sg B strain of the ST-74 (ST-32 cc) | - | - | E.R. Moxon (McGuinness <i>et al.</i> , 1991) |
| #2832 | <i>Nm 8013 (clone12)</i> | <i>Nm 8013 (clone12) wild type</i> Sg C strain of the ST-177 (ST-18cc) | - | - | M. Taha (Nassif <i>et al.</i> , 1994) |

| WUE ID | Designation | Characteristics | Plasmid | Resistance | Source/Reference |
|--------|------------------------------|--|------------------------------------|---------------|------------------|
| #5128 | <i>Nm</i> 8013 GFP | GFP expressing mutant of <i>Nm</i> 8013 | pEG2-GFP-Erm ^R | Erythromycin | This study |
| #4985 | <i>Nm</i> 8013Δ <i>pilE</i> | PilE deficient mutant of <i>Nm</i> 8013 | <i>pTL1-pilE-Spec^R</i> | Spectinomycin | This study |
| #5521 | <i>Nm</i> 8013Δ <i>pilC1</i> | PilC1 deficient mutant of <i>Nm</i> 8013 | <i>pTL1-pilC1-Spec^R</i> | Spectinomycin | This study |
| #5524 | <i>Nm</i> 8013Δ <i>pilC2</i> | PilC2 deficient mutant of <i>Nm</i> 8013 | <i>pTL1-pilC2-Spec^R</i> | Spectinomycin | This study |

**Nm* = *Neisseria meningitidis*; *Sg* = Serogroup; *ST* = Sequencetype; *cc* = clonal complex

2.1.4 Cell lines

Table 12: Cell lines used in this study

| Designation | Description | Source/Reference |
|-------------|--|--|
| HBMEC | Immortalized human brain microvascular endothelial cells | K. S. Kim (Stins <i>et al.</i> , 1997) |

Human brain microvascular endothelial cells (HBMEC) were isolated from children between 4 and 7 years. The cells were tested regarding to their brain endothelial characteristics and were positive for e.g. factor VIII-Rag, carbonic anhydrase IV, uptake of fluorescently labeled acetylated low-density lipoprotein and expressed gamma glutamyl transpeptidase. In addition, VCAM and ICAM, but only little ELAM expression could be induced by TNF α treatment. The selective expression of cell adhesion molecules, distinguish them from macrovascular endothelial cells (Stins *et al.*, 1997). Immortalization of the cells were achieved by the transformation with the simian virus 40 large T antigen.

2.1.5 Software**Table 13: Software used in this study**

| Designation | Company / Source |
|--------------------------|---|
| FlowJo v10 | FlowJo, LLC. |
| ImageJ (Fiji) | https://fiji.sc/ |
| Microsoft Office | Microsoft Cooperation |
| NIS-Elements AR | Nikon |
| Graph Pad Prism 6 | GraphPad Software |

2.2 Methods

2.2.1 Bacterial culture techniques

2.2.1.1 Solid and liquid growth of *N. meningitidis*

N. meningitidis wildtype strains from frozen stocks (-80°C) were plated and grown overnight on Columbia blood agar plates at 37°C and 5% CO₂ in a humidity incubator. For each experiment, bacteria were transferred directly from the agar plate into 50 ml falcon tubes with a cotton swab and cultured in PPM + medium (proteose-peptone medium supplemented with 1× Kellogg's supplement, 0.01 M MgCl₂ and 0.005 M NaHCO₃) for 90 min in an orbital shaker at 37°C and 200 rpm. Meningococcal mutant strains were grown overnight on GC agar plates (37°C, 5% CO₂) supplemented with the appropriate antibiotic. The bacteria were further handled in the same way like the wild type strains with the addition of appropriate antibiotics in the liquid culture medium.

2.2.1.2 Stocking of bacteria

For stocking, bacteria were plated and grown over night on an appropriate growth plate at 37°C and 5 % CO₂. On the next day, the content of the plate was harvested with a sterile cotton swab and inoculated into 1 ml freezing media added in a cryo-tube. The bacteria were then stored at -80°C.

2.2.1.3 Bacterial growth curve experiments

For growth curve experiments, bacteria from a plate pre-culture were transferred to 10 ml of fresh PPM+ medium. After 90 min incubation at 200 rpm and 37°C, the OD₆₀₀ was estimated and a calculated amount of bacteria, resulting in a final OD₆₀₀ of 0.1, was transferred into fresh medium containing either a final concentration of 50 µM 2-APB or an equivalent amount of DMSO as solvent control. Bacterial growth was then monitored every 30 min for 3 h by measuring the OD₆₀₀.

2.2.1.4 Transformation of *N. meningitidis*

For the transformation of natural competent *N. meningitidis* with plasmid DNA, bacteria from an overnight plate culture were inoculated into 5 ml PPM+. The OD₆₀₀ then measured and adjusted to 0.1 with fresh PPM+. For the transformation, 1 ml of the bacterial suspension was then transferred to an Eppendorf-tube and 100 – 200 ng plasmid DNA was added. The transformation mixture was afterwards incubated for 5 – 6 h at 37°C and 200 rpm in an orbital shaker. Control of growth was carried out by the addition of a control tube without the addition of the plasmid to measure the OD₆₀₀. Afterwards, the bacteria were washed twice and re-suspended in 100 µl PPM+. Success of the transformation was controlled by plating the bacteria on appropriate antibiotics and colony PCR on the next day.

2.2.1.5 Transformation of chemically competent *E. coli* TOP10

For transformation of the commercially available *E. coli* TOP10, the bacteria were slowly thaw on ice and the transformation mixture (100 – 200 ng plasmid DNA) was added directly to the 100 µl of bacteria. The bacteria were then incubated for 1 h on ice and afterwards heat-shocked for 1 min at 42°C. After 2 min cooling on ice, 125 µl of SOC medium was added followed by 1 h of incubation at 37°C and 200 rpm on an orbital shaker. Success of the transformation was controlled by plating the bacteria on appropriate antibiotics and colony PCR on the next day.

2.2.1.6 Polymerase chain reaction

The polymerase chain reaction (PCR) is a method to multiply specific DNA regions between two known short sequences. Those two regions are the binding part for the primers, defining the start and the end of the resulting product. The reaction by itself mimics the DNA replication of a living cell. A DNA polymerase synthesized the complementary strand of the single stranded DNA between the primer pair. The optimal reaction conditions depends on the template DNA and primer design. A general example for the reaction mixture is given in Table 14.

Table 14: General example for the PCR reaction mixture

| Component | Amount |
|------------------------------------|--------------|
| Template DNA | 1 μ l |
| Forward Primer (100 pmol/ μ l) | 0.5 μ l |
| Reverse Primer (100 pmol/ μ l) | 0.5 μ l |
| dNTP (4 mM) | 2.5 μ l |
| 10 x Reaction buffer | 5 μ l |
| MgCl ₂ (25 mM) | 3.25 μ l |
| Aqua dest. | 37.2 μ l |
| Taq-Polymerase (5 U/ μ l) | 0.5 μ l |

The reaction itself based on three different steps, each with their distinct temperature, time and repeat optimum. The different steps with their specific conditions are shown in Table 15.

Table 15: General PCR reaction conditions

| Step | Duration | Temperature | Cycles* |
|-----------------------------|------------------------|--------------------------------|---------|
| Initial denaturation | 5 – 10 min | 94 – 99°C | 1 |
| Denaturation | 1 min | 94°C | 30 |
| Annealing | 1 min | xx°C (depending on the primer) | 30 |
| Elongation | ~ 1 min per 1000 bases | 72°C | 30 |
| Stop | ∞ | 4°C | 1 |

*After the elongation step, the reaction starts again with the denaturation step

2.2.1.7 Visualization and purification of PCR products

Separation of the PCR production was achieved by gel electrophoresis. This method based on the different movement behaviors of the PCR products, through the porous structure of the agarose gel, in an electric field. The agarose act as a molecular sieve in which smaller PCR fragments can move faster compared to bigger fragments. Visualization was obtained by the addition of GelRed into the agarose gel, intercalating into the DNA. The DNA bound GelRed was then imaged with the ChemiDoc and fragment sizes were compared to a standardized marker.

For further downstream application, e.g. cloning, the PCR fragment was purified using the PCR purification kit from Qiagen. The purification based on the binding ability of DNA to a silica membrane in the presence of chaotropic salts. Other, unwanted PCR reaction compounds (e.g. primer, dNTPs) are then washed away and the clean PCR fragment of interest can be eluted afterwards.

2.2.1.8 Construction of mutant strains in *N. meningitidis*

Meningococcal mutants lacking different pilus and or pilus-related genes were constructed together with Jérôme Becam. The respective sequences were downloaded from MicroScope web site using the genome browser MaGe (Magnifying Genome). The “A plasmid Editor (ApE)” version 2.0.47 was used to design primers and select the fitting restriction enzyme.

The construction of an isogenic *pilE* mutant in *N. meningitidis* strain 8013/clone12 is described as an example: to construct an insertional mutation in the *pilE* gene, *pilE* was amplified using oligonucleotides *pilE*_XhoI_F and *pilE*_XbaI_R, (Table 9), cleaved with *XhoI* and *XbaI*, respectively, and cloned into the pTL1 vector, a derivative of the pBluescript vector containing the Neisseria uptake sequence (Unkmeir *et al.*, 2002). The resulting plasmid pTL1::*pilE*, harboring the *pilE* gene fragment was then transformed into chemically competent *E. coli* TOP 10 cells. After confirmation of positive clones by nucleotide sequencing, an inverse PCR was performed using oligonucleotides *pilE*_inv_F and *pilE*_inv_R harboring an *AvrII* restriction site, the resulting construct was digested with *AvrII* and a spectinomycin-resistance cassette was inserted via the *AvrII* sites by replacing about 400 bp of the coding sequence. The resulting vector pTL1::*pilE*::*SmR* was amplified in *E. coli* TOP10 before transformation of the plasmid into *N. meningitidis* strain 8013/clone 12. The construction of further

mutant strains used in this study were generated using the same strategy and appropriate oligonucleotides (Table 9). All mutant strains were confirmed by PCR, sequencing, and Western blot analysis for the presence of Opa, Opc and pili.

2.2.2 Cell culture methods and infection

Immortalized human brain microvascular endothelial cells (HBMEC) were routinely cultured in T75 cell culture flasks, or appropriate multiwell cell culture plates (or slides), coated with 0.2 % gelatin. Cell culture medium consisted of RPMI 1640 medium supplemented with 1% sodium pyruvate (1 mM), 1% l-glutamine (2 mM), and 1% nonessential amino acids plus 5 U/ml heparin and 30 µg/ml endothelial cell growth supplement (ECGS). Cells were incubated at 37°C in 5% CO₂ in a humidified atmosphere.

2.2.2.1 Quantification of bacterial adherence and invasion into host cells

Adhesion and invasion was determined by using the gentamicin protection assay. Cells between the 10th and 25th passages were used for infection assays at a density of 4×10^5 cells/well. Cell culture medium was changed to infection medium [RPMI 1640 + 10% human serum (HS)] and cells were infected with the meningococcal strain of interest at a defined multiplicity of infection (MOI) for 2 to 4 h. If indicated, cells were pre-incubated with compounds (2-APB, CtxB) to be tested in RPMI 1640 for 30 min prior to the medium change. To determine the number of adherent bacteria, cells were washed three times with phosphate buffered saline (PBS), to remove unbound bacteria, and afterward incubated with 1% saponin in RPMI 1640 to lyse the cells. Then, the cell-lysates were collected, diluted and plated on blood agar plates. To quantify invasive bacteria, cells were treated with gentamicin (200 µg/ml) in RPMI 1640 for 2 h at 37°C and 5% CO₂ to kill all extracellular bacteria, prior to lysis by 1% saponin treatment and plating. Experiments were conducted in duplicate.

2.2.3 Cell cycle synchronization

G1 synchronization was performed using the method of serum starvation. 24 h prior to the experiment, HBMEC cell culture medium was removed and cells were washed once with PBS. Afterward, RPMI was added and the cells were further incubated as mentioned before. The cell population shift was controlled by propidium iodid (PI) staining. For that, cells were washed once with PBS and harvested in Eppendorf tubes. Afterward cells were washed three times with PBS, fixed in 3.7% formaldehyde for 30 min on ice and permeabilized with 0.25% Triton X-100 in PBS on ice. Cells were then stained with 10 µg/ml PI + 25 µg/ml RNase and incubated for 30 min at room temperature in the dark and immediately analyzed afterward. 10,000 cells were analyzed using the FACSCalibur™ flow cytometer (BD Bioscience) and data were analyzed and visualized using FlowJo v10 (FlowJo, LLC).

2.2.4 Flow Cytometry

Ceramide staining

3 days prior to the experiment, 1.25×10^5 cells/ml were seeded in a 24-well plate and were grown to approximately 1×10^6 cells/ml. On the day of the infection experiment, cell medium was replaced by RPMI 1640 medium plus 10% human serum and, if indicated, preincubated for 30 min with different concentrations of 2-APB. Cells were infected with the bacteria for 4 h. After infection, the cells were washed once with PBS, trypsinized, and harvested in an Eppendorf tube. After washing with ice-cold fluorescence-activated cell sorting (FACS) buffer (5% fetal calf serum [FCS] in PBS), the cells were incubated with either mouse IgM anti-ceramide (1:30 in FACS buffer), mouse IgG PE-conjugated anti-Lamp1 (1:20 in FACS buffer), mouse IgG2a anti-ASM (1:250 in FACS buffer), or the corresponding isotype control antibodies (1:100 in FACS buffer) for 1.5 h at 4°C in the dark. After incubation, the cells were washed three times with FACS buffer and incubated with the appropriate secondary antibodies (1:500 in FACS buffer) for 30 min. Then, the cells were washed three times with FACS buffer and were fixed in 3.7% paraformaldehyde (FA; in PBS) for 30 min at 4°C. Afterwards, the cells were washed 3 times with FACS buffer and 500 µl was transferred into a FACS tube for measurement. Ten thousand cells were analyzed using a

FACSCalibur™ flow cytometer (BD Bioscience), and the data were analyzed and graphed using FlowJo (v10) software (FlowJo, LLC).

2.2.5 Immunofluorescence microscopy

Ceramide staining

One day prior to the experiment 2.5×10^4 cells/well were seeded in 8-well chamber μ -slides (Ibidi) and grown overnight. Cells were infected with bacteria for 4 h, washed with PBS, and fixed for 20 min with 3.7% paraformaldehyde. For the indicated experiments, cells were infected with GFP-expressing *N. meningitidis* strain 8013, a derivative of *N. meningitidis* 8013 expressing GFP from the plasmid pEG2-Ery (Christodoulides *et al.*, 2000). After fixation, cells were washed two times with PBS and blocked for 5 min in blocking buffer (1% FCS, 2% BSA in PBS). Then, the cells were washed and incubated with the primary antibody (1:200 dilution in blocking buffer) for 45 min at room temperature (RT), followed by treatment with the appropriate Cy fluorescent dye-labeled secondary antibody (1:200 in blocking buffer) for 45 min. (For ASM and LAMP1, cells were stained live on ice before fixation). The samples were covered with PBS, and images were taken using a Nikon Eclipse Ti-E inverted microscope equipped with an Okolab incubator set to 37°C. Images were taken at a $\times 40$ magnification and processed and analyzed using ImageJ software.

2.2.6 ASM activity assay

For determination of ASM surface activity, a commercially available acid sphingomyelinase activity assay kit from Echelon was used with some adaptations to the manufacturer's protocol. One day prior to the infection experiment, 0.75×10^4 cells were seeded into a black-walled, black-bottom 96-well plate. On the day of infection, the growth medium was replaced with RPMI 1640 medium plus 10% human serum, and infection assays were carried out for 2 h at 37°C in 5% CO₂. When indicated, cells were pretreated with 50 μ M 2-APB for 30 min prior to infection. After infection, cells were washed once with PBS and the ASM substrate was added directly to the cells. For pilus-treated samples, 1 μ g of the preparation was added to the cells right after the

substrate was added. The activity of ASM was then detected in the Infinite F200 Pro Reader spectrophotometer at a 360-nm excitation wavelength and a 460-nm emission wavelength every 20 min for 5 h.

2.2.7 Calcium measurement

Intracellular calcium levels were estimated using a Fluo-8 no-wash calcium assay (Abcam). The assay was performed according to the manufacturer's protocol with minor modifications. Briefly, 1.5×10^5 cells/well were seeded in 24-well plates and allowed to plate down overnight. Prior to infection, cell culture medium was removed and the cells were washed twice with Hanks' balanced salt solution (HBSS; calcium free). Cells were incubated with 4 μ M Fluo-8 in HBSS for 30 min at 37°C in 5% CO₂. After incubation, the cells were washed three times with HBSS and covered with 300 μ l HBSS. Fluo-8-loaded cells were then infected with bacteria in the presence or absence of 50 μ M 2-APB or were left uninfected. Changes in intracellular calcium levels were observed over a 20-min period using a Nikon Eclipse Ti-E inverted microscope and evaluated with the time measurement option of Nikon NIS-Elements AR software. For analysis, individual cells were selected for single-cell analysis and tracking of calcium level changes.

2.2.8 Preparation of pilus-enriched fractions

For preparation of pilus-enriched fractions, the bacterial content of 50 blood agar plates was harvested in 40 ml of 0.15 M ethanolamine (in PBS) with a pH of 10.5. Pili were sheared off by intensive vortexing for 2 min, followed by centrifugation at 12,000 \times g for 10 min at RT to remove the cellular debris. The supernatant was used for an additional centrifugation step at 21,000 \times g for 90 min to remove smaller debris. Then, the supernatant was transferred to an Erlenmeyer flask, ammonium sulfate-saturated in 0.15 M ethanolamine was added to a concentration of 10%, and the mixture was incubated under continuous shaking for 30 min at RT. The protein-ammonium sulfate precipitate was then harvested by centrifugation at 21,000 \times g for 15 min. The supernatant was then discarded and the pellet was resuspended in 0.05 M Tris-buffered saline (TBS), pH 7.5. Protein solutions were then applied to a 6-ml Viva Spin

column with a 7,000-dalton-molecular-weight-cut off (MWCO) and were centrifuged at $4,000 \times g$ at RT until the volume reached 1 ml. To clean the sample, TBS was added again to 6 ml, followed by centrifugation as mentioned above. Success of the preparation was carried out by western- and dot blot with a specific antibody against the pili subunit Pile. For the dot blot, the PorB antibody was used as a control for outer membrane residues in the pili enriched fraction.

2.2.9 Neisserial membrane separation

Membrane separation of the meningococcal outer and inner membrane (OM/IM) was performed with minor changes, as previously described (Steeghs *et al.*, 2001). Either ω -N₃-C₆-ceramide, ω -N₃-sphingosine or a corresponding amount of Ethanol were added to a final concentration of 0.1 X the MBC to 100 ml cultures of *N. meningitidis* strain MC58 with an OD₆₀₀ of 0.1. After 3 h of incubation at 37°C in an orbital shaker, bacteria were harvested and washed three times with PBS and in the end resuspended in 50 mM Tris-HCl (pH 8). Afterwards, lysozyme (100 µg / ml) and EDTA (pH 8, 5 mM) were added and the bacteria were incubated for 1 h at RT while shaking. This step was followed by one freeze thaw cycle (-80°C – 37°C) and sonication (10 sec pulses with 5 sec breaks, at 100 % magnitude for a total of 5 min). Unbroken bacteria were removed by centrifugation at 1,200 g and 4°C for 10 min. Then, the supernatant was loaded on top of a sucrose gradient, consisting of a 3 ml 15 % top layer over a 2 ml 55 % cushion (both with 5 mM EDTA pH 8), and centrifuged at 280 000 g and 4°C for 2 h. The crude membrane fraction was then collected, the sucrose concentration estimated with a refractometer and lowered to 30 % by dilution with dH₂O (with 5 mM EDTA, pH 8). Afterwards, the sample was loaded onto a sucrose gradient consisting of 1.3 ml 50 % cushion and 45, 40, 35 % layer on top (2.4 ml each). The gradient was then centrifuged for 41 h at 268,000 g and 4°C and afterwards 800 µl samples were collected from top to bottom.

Then, the purity of the isolated OM and IM fraction was analyzed. Lactate dehydrogenase (LDH) was chosen as inner membrane marker (Osborn *et al.*, 1972) and the presence of the meningococcal OpcA protein as outer membrane marker. LDH was determined with a commercial LDH activity assay and used according to the manufacturer's instructions (Sigma Aldrich). Activity was calculated as LDH activity / µg protein (determined by Bradford assay, see 2.2.12.1). To visualize the relative

amount of OpcA in the samples, the protein amounts were adjusted and utilized in a dot blot assay with a monoclonal mouse anti-OpcA antibody (clone B306) and further processed as described in 2.2.8.1.

2.2.9.1 Western- and Dot blot

Bacterial pilus preparations (500ng) were loaded on 12 % sodium dodecyl sulfate (SDS) polyacrylamide gel electrophoresis was carried out for approximately 1 h at 150 V. The gel was then blotted to a nitrocellulose membrane (1 h / 350mA), blocked for 1 h on an orbital shaker with 5 % skim milk in PBST and incubated O/N with the mouse-anti PilE (SM1) antibody (1:4000 in skim milk) at 4°C on an orbital shaker. On the next day, the membrane was washed 3 times with PBST for 10 min. and after incubated with an anti-mouse HRP second antibody for 1 h at room temperature on an orbital shaker. After washing 3 times with PBST for 10 min. the membrane was incubated with the Clarity Western ECL Substrate (BioRad) for 1 minutes. Protein bands were then visualized with the ChemiDoc.

The dot blot assay was carried out by spotting 4 µl of each sample onto a nitrocellulose membrane. After drying, nonspecific binding sites were blocked with 5 % skim milk in PBS supplemented with 0.05 % Tween 20 (PBS-T) for 1 h at RT on an orbital shaker. Afterwards, primary antibody incubation was performed with a 1:10000 dilution of the antibody for 30 min followed by three washing steps with PBS-T (5 min each). For secondary antibody incubation, an anti-mouse IgG antibody, conjugated to horseradish peroxidase (HRP), was used with a 1:1000 dilution in 5 % skim milk in PBS-T. After 30 min incubation at RT, the membrane was washed again three times with PBS-T and once with PBS for 5 min each. Finally, ECL substrate (BioRad) was added for 1 min and the protein was visualized using the ChemiDoc™ MP Gel and Blot Imaging System (BioRad).

2.2.9.2 Quantification of protein

Protein concentration of the membrane separation samples were estimated using the colometric Bradford assay. 10 µl of each sample and BSA standards (0, 25, 125, 250, 500, 750, 1000, 1500 µg/µl) were transferred to a 96 well plate and covered with 200

μ l Bradford reagent. Then, the plate was incubated for 30 min at 37°C and the absorbance was measured at 595 nm. Sample protein concentrations were then carried out by mathematical calculation based on a regression line through the BSA standards data.

2.2.9.3 Mass spectrometry

Mass spectrometric analysis of the membrane fraction was performed in cooperation with Fabian Schumacher and Burkhard Kleuser (Institute of Nutritional Science, University of Potsdam).

Samples of neisserial membrane fractionation (600 μ l) were filled up with water to 1 ml followed by addition of 110 μ l 10x Baker buffer (300 mM citric acid, 400 mM disodium hydrogen phosphate, pH 3.0). For lipid extraction, 2 ml 1-butanol and 1 ml water-saturated 1-butanol were added. The extraction solvent contained sphingosine-d7 (Sph-d7), sphingosine 1-phosphate-d7 (S1P-d7), C17 ceramide (C17 Cer) and C16 sphingomyelin-d31 (C16 SM-d31) (all Avanti Polar Lipids, Alabaster, USA) as internal standards. Extraction was facilitated by intensive vortexing (1500 rpm) for 10 min at RT. Afterwards, samples were centrifuged for 5 min at 2200 x g (4 °C). The upper organic phase was dried under reduced pressure using a Savant SpeedVac concentrator (Thermo Fisher Scientific, Dreieich, Germany). Dried residues were reconstituted in 200 μ l acetonitrile/methanol/water (47.5:47.5:5 (v:v:v), 0.1% formic acid) and subjected to HPLC-MS/MS sphingolipid quantification. Chromatographic separation was achieved on a 1260 Infinity HPLC (Agilent Technologies, Waldbronn, Germany) equipped with a Poroshell 120 EC-C8 column (3.0 x 150 mm, 2.7 μ m; Agilent Technologies) guarded by a pre-column of identical material. MS/MS analysis was carried out using a 6490 triple-quadrupole mass spectrometer (Agilent Technologies) operating in the positive electrospray ionization mode (ESI+). Long-chain bases (dihydro-Sph, Sph, S1P), Cer and SM species (C16, C18, C20, C22, C24 and C24:1) were analyzed by selected reaction monitoring (SRM) as described recently¹¹. Additionally, the following mass transitions were recorded for quantification of functionalized sphingolipids (collision energies (CE) in parentheses): m/z 341.3 \rightarrow 323.3 for ω -N3-Sph (8 eV) and m/z 439.4 \rightarrow 421.4 (15 eV), m/z 439.4 \rightarrow 282.3 (25 eV), m/z 421.4 \rightarrow 264.3 (25 eV, quantifier) for ω -N3-C6 Cer (d18:1/6:0- ω -N3). Sph-d7 and C17 Cer served as internal standards for quantification of ω -N3-Sphingosine and

ω -N3-C6 Ceramide, respectively. Moreover, quantities of azido-functionalized sphingolipid derivatives were normalized to the C16 SM (SM d18:1/16:0) content of each membrane fraction analyzed. Data processing was performed with MassHunter Software (Agilent Technologies).

2.2.10 Statistics

Statistical analysis was performed with GraphPad Prism (v6) software (GraphPad Software Inc.) by an unpaired two-tailed Student's *t* test or analysis of variance (ANOVA) followed by a *post hoc* test. Significance values are indicated in the individual figure legends.

3. Results

3.1 Meningococcal induced ceramide platform formation is mediated by T4P and intracellular calcium release

3.1.1 *N. meningitidis* strain 8013/12 induces T4P dependent ceramide accumulation on human brain microvascular endothelial cells (HBMEC)

Recent studies in our group revealed the ability of *N. meningitidis* strain MC58 to induce rapid ASM translocation and ceramide platform (CRP) formation (Simonis *et al.*, 2014). This study showed the importance of the interaction between the meningococcal outer membrane protein OpcA and heparan sulfate proteoglycans on the host cell. Using an *opcA* deficient mutant, the ceramide surface amount was reduced by 20 % during infection, suggesting that other factors might contribute to ASM translocation and CRP formation.

To test the hypothesis if the neisserial T4P, as initial adherence mediator, may contribute to CRP formation, the highly piliated, Opa-negative and *opcA* deficient meningococcal strain 8013/12 was used. To analyze the ability of this strain to induce CRPs, HBMEC were infected for 2, 3 or 4 h and surface ceramide levels were measured using flow cytometry (Figure 6).

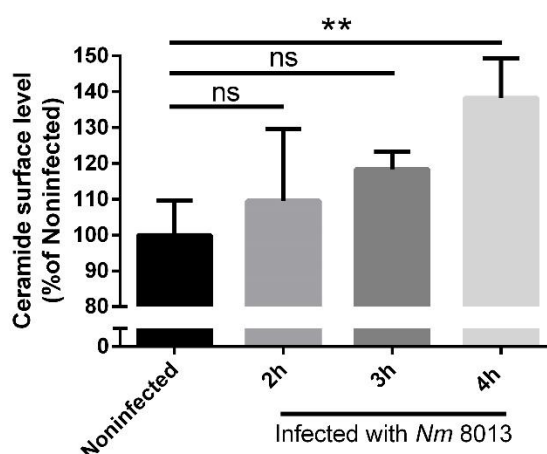


Figure 6: Ceramide surface level peaked after 4 h post infection.

HBMEC were seeded on IBIDI treated IBIDI slides and allowed to grow until the next day. Cells were infected with *Nm* 8013 for 2, 3 or 4 h with an MOI of 100. Afterwards cells were washed, fixed in paraformaldehyde (FA) and stained with an anti-ceramide antibody and secondary Cy5-conjugated goat anti-mouse IgM. Surface ceramide levels were determined by flow cytometry and data are represented as relative levels of ceramides on the host cell surface. Error bars represent mean \pm SD. One-way ANOVA with Dunnett's *post hoc* test was used to determine significance. ** $P < 0.01$; ns = not significant.

The kinetic showed the highest ceramide level after 4 h and was used for all following experiments. Next, to confirm the initial flow experiments, ceramide was visualized on either infected or non-infected HBMEC by immunofluorescence imaging. The result confirmed the ceramide increase on the surface. Additionally, the images showed a strong accumulation of ceramide underneath the bacterial colonies compared to the non-infected control cells (Figure 7).

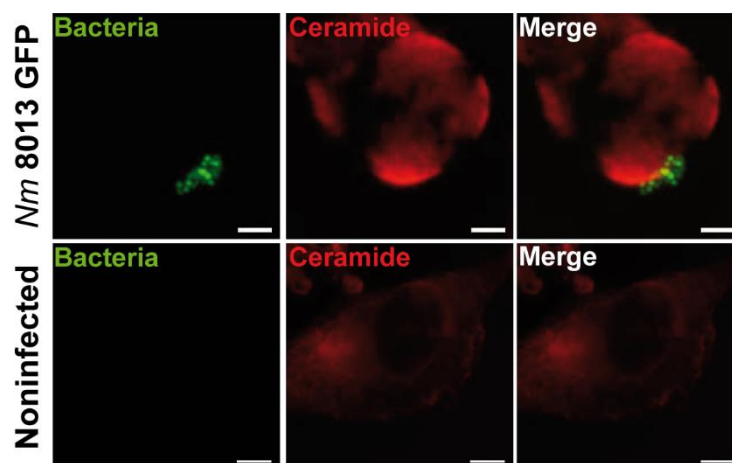


Figure 7: Highly piliated *N. meningitidis* strain 8013 induce the formation of CRPs on HBMEC.

HBMEC were grown to confluence in 8-well Ibidi μ -slides and were infected with a GFP-expressing variant of *N. meningitidis* strain 8013 for 4 h or were left noninfected. Cells were washed, fixed in paraformaldehyde (FA), and stained with an anti-ceramide antibody and secondary Cy5-conjugated goat anti-mouse IgM (red). Images were captured using a Nikon Eclipse Ti-E inverted microscope with a 40 \times objective lens. Bars, 10 μ m.

To test if the T4P played a role in CRPs formation, HBMEC were infected with a *pilE*-deficient mutant (Δ *pilE*) of the 8013/12 strain and compared to the wildtype (WT) and the noninfected control cells. After 4 h of infection, flow cytometry analyses of the ceramide surface amount showed a significant increase in WT infected cells compared to noninfected control cells, which was almost completely abolished on cells infected with the mutant strain (Figure 8A).

To analyze whether the surface ceramide detected in the experiments relied on the ASM activity on the host cell surface, cells were pre-incubated with the ASM inhibitor amitriptyline and afterwards infected with the 8013/12 WT strain. Amitriptyline is a selective inhibitor of the ASM and was previously used to investigate the effect of ASM

inhibition during OpcA-mediated uptake of *N. meningitidis* in HBMEC (Simonis *et al.*, 2014). ASM inhibitor treatment showed a significant decrease of surface ceramide, comparable with the non-infected control cells (Figure 8B).

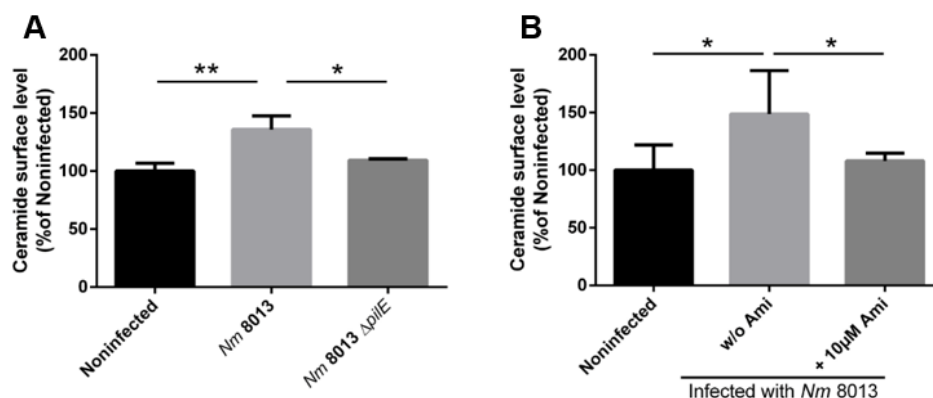


Figure 8: *N. meningitidis* strain 8013 induce CRP formation in a Type 4 pili (T4P) and host ASM dependent manner.

(A) HBMEC were infected with wild-type strain *N. meningitidis* 8013 or an isogenic, pilus-deficient mutant (*N. meningitidis* 8013 $\Delta pilE$) or were left noninfected for 4 h. Surface ceramide levels were determined by flow cytometry, and data are represented as the relative levels of ceramides on the host cell surface. (B) HBMEC were infected with *N. meningitidis* 8013 for 4 h in the presence or absence of the ASM inhibitor amitriptyline (+10 μ M Ami and w/o [without] Ami, respectively) or were left noninfected. Surface ceramide levels were determined by flow cytometry, and data are represented as the relative levels of ceramides on the host cell surface compared to that on noninfected cells. Values are expressed as a percentage of the level for noninfected cells. (B+C) Error bars represent the mean \pm SD. One-way ANOVA with Dunnett's *post hoc* test was used to determine significance. *, $P < 0.05$; **, $P < 0.01$. All experiments were performed at least three times in duplicate.

Earlier studies performed in our group showed that the meningococcal outer membrane protein OpcA contribute to ASM activation and further ceramide enrichment on the surface. Importantly, infection of HBMEC with an OpcA deficient mutant strain only reduced the ceramide surface level by approximately 20 %, suggesting that other meningococcal components also contributed to ASM induction (Simonis *et al.*, 2014). To test the impact of the meningococcal T4P on the ASM activity, a customized ASM activity assay, based on the direct hydrolysis of a fluorogenic substrate by the ASM, was adapted to our cell culture conditions and performed on living HBMEC. For that, HBMEC were infected with either the WT strain or the *pilE*-deficient mutant of 8013/12 (Figure 9) and both isolates were analyzed for their ability to activate the ASM. The

results were normalized to the ASM activity levels in control cells. The data showed, that the WT strain strongly increased ASM activity compared to the noninfected control cells with a peak activity between 130 and 210 min post infection, whereas the pilus deficient mutant was unable to induce ASM activity on the cell surface.

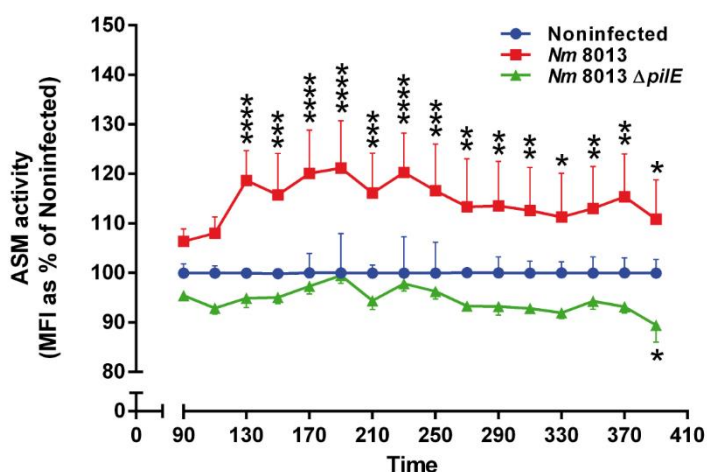


Figure 9: Highly piliated *N. meningitidis* strain 8013 induce ASM surface activity on HBMEC.

ASM activity was determined on HBMEC by measuring sphingomyelin hydrolysis to phosphorylcholine. Cells were seeded in black 96-well plates to confluence and infected with *N. meningitidis* 8013, pilus-deficient strain 8013 $\Delta pilE$ or left noninfected (basal activity). Reported is the activity of ASM after infection with bacteria. Values show the mean \pm SD from three independent experiments. MFI, mean fluorescence intensity. Two-way ANOVA was used to determine significance. *, $P < 0.05$; **, $P < 0.01$; ***, $P < 0.001$; ****, $P < 0.0001$.

3.1.2 *N. meningitidis* infection of HBMEC leads to the translocation of lysosomal ASM to the cell surface

Since ASM activity in HBMEC increased in response to the highly piliated isolate *N. meningitidis* 8013/12 the next step was to visualize and quantify ASM on the cell surface. For that, HBMEC were again infected with a GFP-expressing variant of 8013/12, stained for surface ASM and Lamp1, as marker for their lysosomal origin, and analyzed by immunofluorescence and flow cytometry (Figure 10A+B).

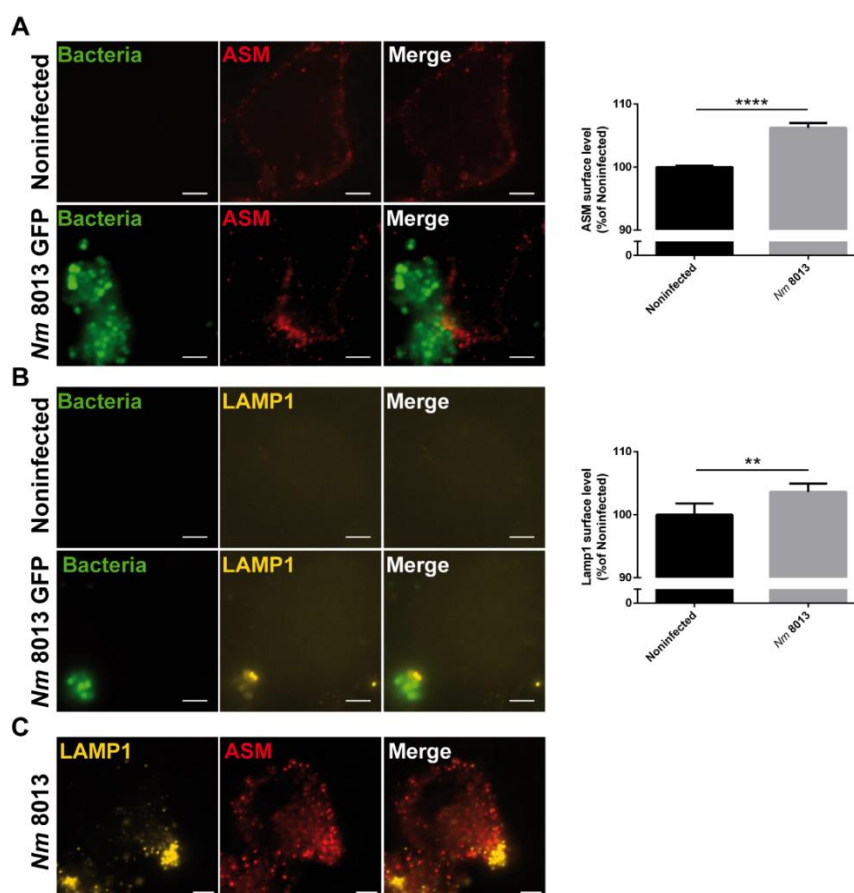


Figure 10: *N. meningitidis* induces the translocation of lysosomal ASM and Lamp1 to the cell surface.

HBMEC were grown to confluence in 8-well Ibidi μ -slides and infected with the GFP-expressing *N. meningitidis* 8013 strain for 4 h or were left noninfected, and then ASM translocation as well as Lamp1 exposure on the host cell surface was evaluated. (A) (Left) Cells were washed, stained live on ice with a rabbit IgG anti-ASM antibody and secondary Cy5-conjugated anti-rabbit IgG F(ab')₂, and then fixed in FA (red). Bars, 5 μ m. (Right) ASM exposure on the plasma membrane was determined by flow cytometry of nonpermeabilized cells. Data show the mean \pm SD from three independent experiments performed in duplicate. ****, $P < 0.0001$ by an unpaired, two-tailed Student's *t* test. (B) (Left) Cells were washed, stained live on ice with a mouse IgG PE-conjugated anti-Lamp1 antibody, and then fixed in FA (yellow). Bars, 5 μ m. (Right) Lamp1 exposure to the plasma membrane was determined by flow cytometry of nonpermeabilized cells. Data show the mean \pm SD from three independent experiments performed in duplicate. **, $P < 0.01$ by an unpaired, two-tailed Student's *t* test. (C) Cells were infected with the *N. meningitidis* 8013 strain for 4 h, washed, fixed in FA, and stained with a mouse IgG PE-conjugated anti-Lamp1 antibody (yellow), as well as rabbit IgG anti-ASM antibody and secondary Cy5-conjugated anti-rabbit IgG F(ab')₂ (red). Bars, 5 μ m.

The results showed a strong increase for surface ASM and Lamp1 after infection in the flow cytometry as well as in immunofluorescence experiments. In addition, ASM and Lamp1 displays a strong co-localization in a double staining experiment (Figure 10C). To add another level of quantification for the ASM surface level, the intensity of the ASM signal on the cell surface was measured and compared using the ImageJ

software (Figure 11). The result underlined the strong increase in ASM surface abundance.

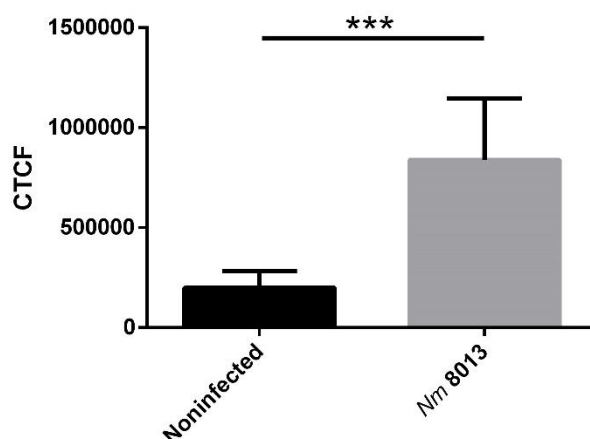


Figure 11: ASM surface intensity increases during infection.

HBMEC were grown to confluence and infected with GFP expressing *Nm* 8013 strain for 4 h or were left noninfected. Cells were washed, fixed and stained with a rabbit IgG anti-ASM antibody and secondary Cy3-conjugated anti-rabbit IgG F(ab')₂. Images were taken using a Nikon Eclipse Ti-E inverted microscope with a 60x oil emersion objective and single cells were further analyzed for their fluorescence. Intensities were measured with ImageJ and the corrected total cell fluorescence (CTCF) was calculated as followed:

CTCF= Integrated Density - (Area of selected cell/Mean of fluorescence background readings)

Result show the mean ±SD of 12 cells for both conditions. ***, P < 0.001 by an unpaired, two-tailed Student's t test.

3.1.3 Infection of HBMEC with *N. meningitidis* induced intracellular calcium release from the ER

A prerequisite for the lysosomal fusion with the outer membrane, and with that the translocation of the ASM to the surface, is an alteration of the intracellular calcium level. Previous studies had shown that different bacteria, including *N. meningitidis* and *N. gonorrhoeae*, are able to induce an elevation of intracellular calcium in epithelial and endothelial cells (Asmat et al., 2014; Kallstrom et al., 1998). To test if the used *N. meningitidis* strain 8013/12 is also capable to induce alterations in the cellular calcium homoeostasis, the calcium indicator dye Fluo 8 was used. This cell permeable indicator dye relies on intracellular esterases to disclose the negatively charged groups and with that, allowing the interaction with calcium only intracellularly. Earlier studies, regarding

the calcium transients in meningococcal infected cells, showed intracellular calcium level at distinct time points (Asmat et al., 2014). But importantly to note, calcium transients occur fast and infection is a dynamic process and with that, the establishment of a live cell infection model was a prerequisite to reveal the individual calcium kinetics in infected cells (Mumtaz et al., 2011). Because time was the most important factor, the assay was performed with a Nikon Eclipse Ti-E microscope with an excellent temporal resolution. Furthermore, the cells were incubated during the whole experiment at 37°C in an Okolab incubation cage.

For the experiment, Fluo 8 loaded HBMEC were infected and the fluorescence signal was measured in real time over 20 min with a 20 x objective to track a large cell population at the same time. The fluorescence images clearly showed that the infected cells responded to the bacteria with an increase in intracellular free calcium (Figure 12A). This was also confirmed by the quantitative analysis of single cells applied to the data shown in Figure 12A (Figure 12B). In eukaryotic cells, cytosolic free calcium could derive from either intra-, or extracellular sources. Intracellularly, calcium is stored in organelles like mitochondria and the endoplasmic reticulum (ER). To reveal the source of the calcium, leading to the intracellular increase, the next step was to test the hypothesis that the calcium is released from the ER, which is the known as the main calcium storage within the cell.

To test this, cells were pretreated with 50 μ M 2-aminoethoxydiphenyl borate (2-APB), a potent inhibitor of the inositol 1, 3, 5- triphosphate (IP_3) receptor, responsible for calcium release from the ER, and transient receptor potential channels. Treatment with 2-APB completely abolished the intracellular calcium changes after infection (Figure 12A and B right). To proof that only infected cells show an increase in intracellular calcium level, the results from above were confirmed by “real”-single cell measurements of infected HBMEC linking the calcium elevation exclusively to infected cells (Figure 12C).

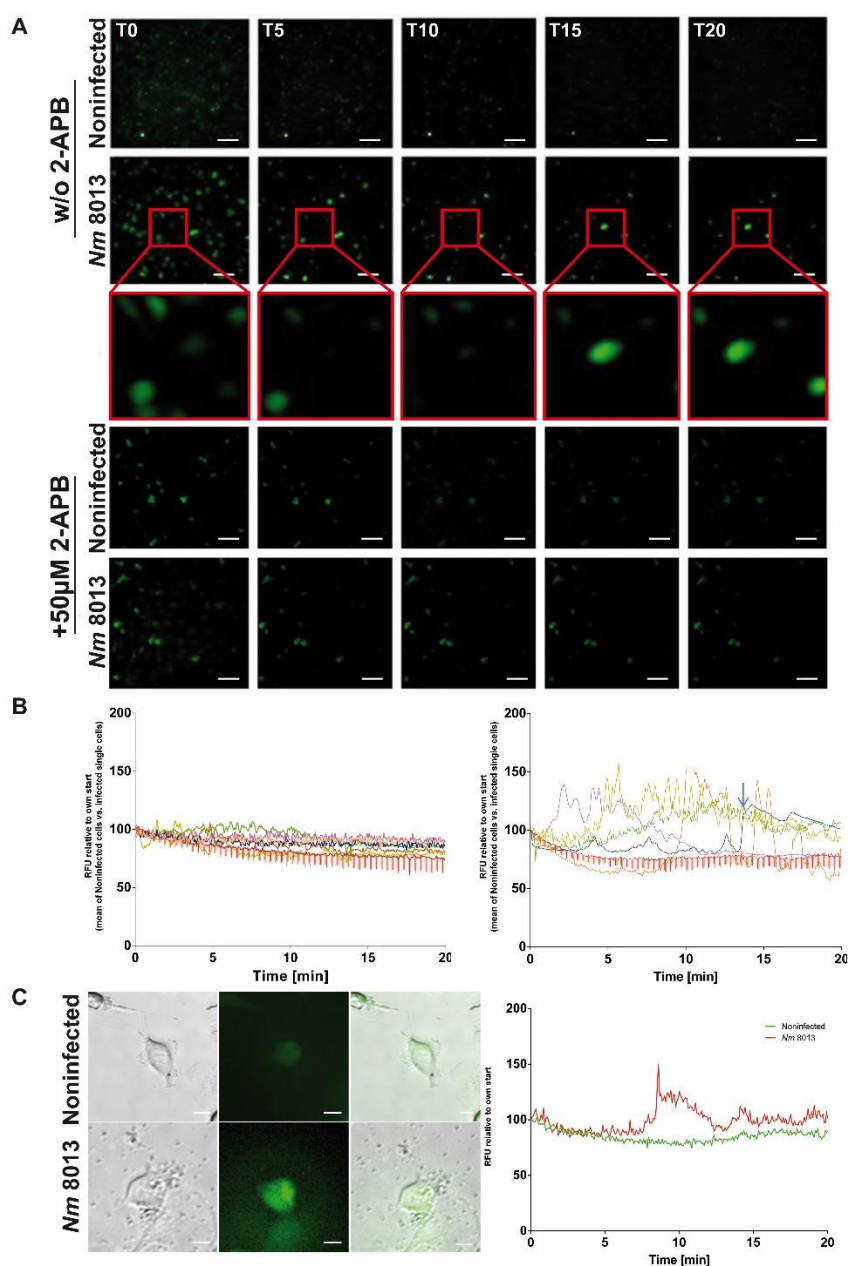


Figure 12: *N. meningitidis* increased cytosolic Ca^{2+} levels in brain endothelial cells derived from the endoplasmic reticulum.

Fluo-8-loaded HBMEC were infected with *N. meningitidis* 8013 in the presence or absence of 50 μM 2-APB or were left noninfected, and cytosolic Ca^{2+} concentrations were monitored over 20 min. Images were captured using a Nikon Eclipse Ti-E inverted microscope and analyzed using NIS Elements AR software (Nikon). (A) Representative fluorescence images taken at the indicated time points (0, 5, 10, 15, and 20 min [T0, T5, T10, T15, and T20, respectively]) are shown. Images were taken at a $\times 20$ magnification. Bars, 100 μm . (B) Fluorescence data from representative cells were exported and are shown as the number of relative fluorescence units (RFU) relative to the start fluorescence intensity value. Images show the results for infected single cells (left) or 2-APB-treated cells (right) versus the mean for noninfected cells. The arrow indicates the results for a single cell that appears at 15 min in the inset in panel A. 2-APB, 2-aminoethoxydiphenyl borate. (C) Representative single-cell analysis results. Pictures (left) show single cells which were analyzed for their fluorescence intensity (right). Bars, 10 μm .

3.1.4 Intracellular calcium is important for the translocation of the ASM to the surface

Because calcium is important for the translocation of the lysosomal ASM to the surface, and thus formation of CRPs, the next step was to test the effect of calcium inhibition with 2-APB on ASM translocation, surface activity and ceramide generation. For that, flow cytometry analyses were carried out after pretreatment of the cells with different concentrations of the IP₃ receptor inhibitor 2-APB. HBMEC were then infected for 4 h with the *N. meningitidis* strain 8013/12 and the surface amount of ASM, Lamp1 and ceramide was estimated. Again, results showed an increase of all stained marker in the infected cells compared to the noninfected cells (Figure 13A-C). However, pretreatment with the inhibitor completely abolished the increased surface abundance during infection already at a low concentration of 10 μM. Importantly, the addition of 2-APB to the noninfected cells did not alter the levels of ceramide amount on the cell surface.

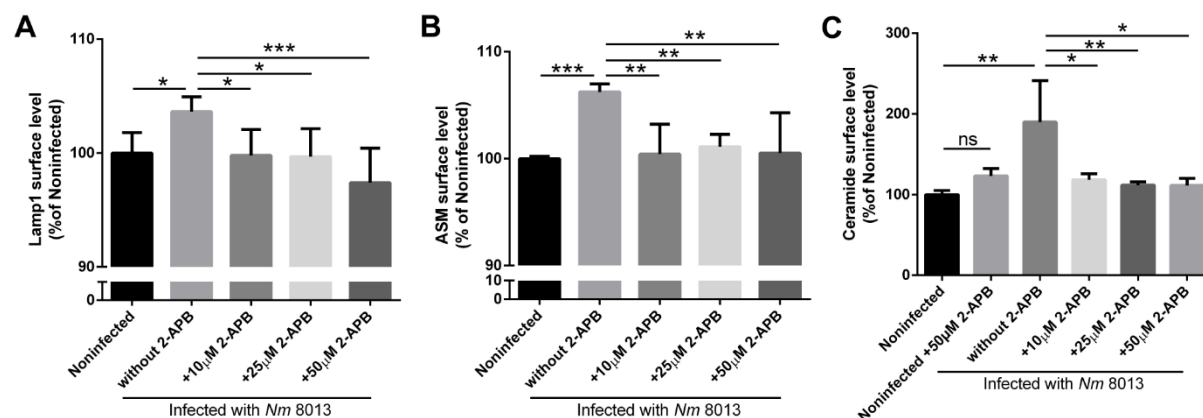


Figure 13: *N. meningitidis*-induced ASM translocation to the plasma membrane is Ca²⁺ dependent.

HBMEC were treated with different concentrations of 2-APB (10, 25, 50 μM) for 30 min prior to infection with *N. meningitidis* 8013. *N. meningitidis*-induced Lamp1 exocytosis, ASM translocation, and ceramide surface levels were detected by flow cytometry analysis using a mouse IgG PE-conjugated anti-Lamp1 antibody (A), a mouse IgG2a anti-ASM antibody and secondary Cy3-conjugated anti-mouse IgG F(ab')₂ (B), or an anti-ceramide antibody and secondary Cy5-conjugated goat anti-mouse IgM (C). Data show the mean ± SD levels as a percentage of those for noninfected cells from three independent experiments performed in duplicate. One-way ANOVA with Dunnett's *post hoc* test was performed to determine significance. *, $P < 0.05$; **, $P < 0.01$; ***, $P < 0.001$.

In addition to the flow cytometric analysis, the activity of the ASM was measured on living cells. HBMECs were either pretreated with 50 μM 2-APB, or left untreated. Afterwards, the cells infected with the *N. meningitidis* strain 8013/12 and the activity was measured over 5 h. The results, normalized to the ASM activity levels in control cells, showed a strong impact of the 2-APB treatment and a strong decrease of the ASM activity during infection was observed compared to the nontreated, infected cells (Figure 14).

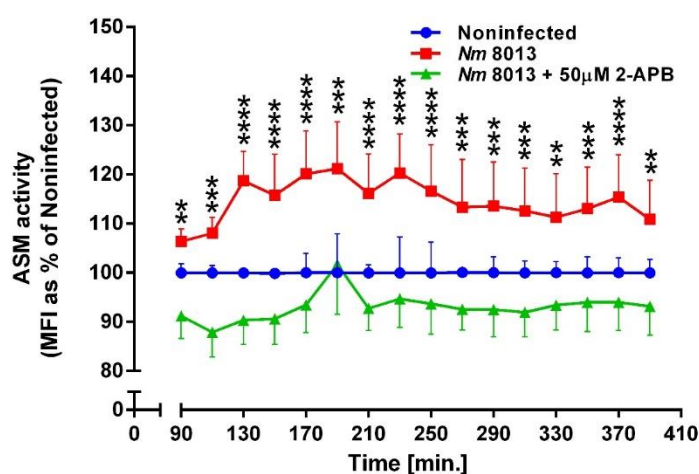


Figure 14: Depletion of calcium abolished ASM activity on the cell surface.

ASM activity after infection with bacteria in the presence (50 μM) or absence of 2-APB. Values show the mean \pm SD from three independent experiments. Two-way ANOVA was used to determine significance. *, $P < 0.05$; **, $P < 0.01$; ***, $P < 0.001$; ****, $P < 0.0001$.

3.1.5 The PilC subunit of the meningococcal T4P is involved in ceramide release

N. meningitidis expresses two paralogous PilC proteins, named PilC1 and PilC2. PilC2 is a membrane bound protein located on the outer leaflet and involved in adhesion to some cell types, not including endothelial cells, and promotes pilus retraction (Morand et al., 2009; Nassif et al., 1994). Compared to this, the PilC1 protein is localized on the tip of the T4P and is described as important mediator of T4P dependent adhesion to endothelial cells (Nassif et al., 1994). To identify the role of these two alleles in CRP formation, $\Delta pilC1$ and $\Delta pilC2$ mutant strains of *N. meningitidis* 8013/12 were constructed and tested for their ability to induce CRP formation. HBMEC were infected with either the WT strain, *pilC1*, *pilC2* or *pilE* mutant and analyzed by

immunofluorescence and flow cytometry for their surface ceramide amount. The data showed that the *pilE* as well as the *pilC1* mutant failed to induce a significant increase in surface ceramide compared to the non-infected control cells, whereas the *pilC2* mutant induced an even stronger increase as the WT (Figure 15A+B). To test if this finding was connected to alterations in the ability of the bacteria to adhere to the cells, the number of bound bacteria was estimated after infection with the WT or the respective mutants. The result showed a correlation between the ability to induce CRPs and the number of adherent bacteria. While the *pilE* and *pilC1* mutants were barely able to adhere to the cells, the *pilC2* mutant showed a hyper-adherent phenotype (Figure 15B).

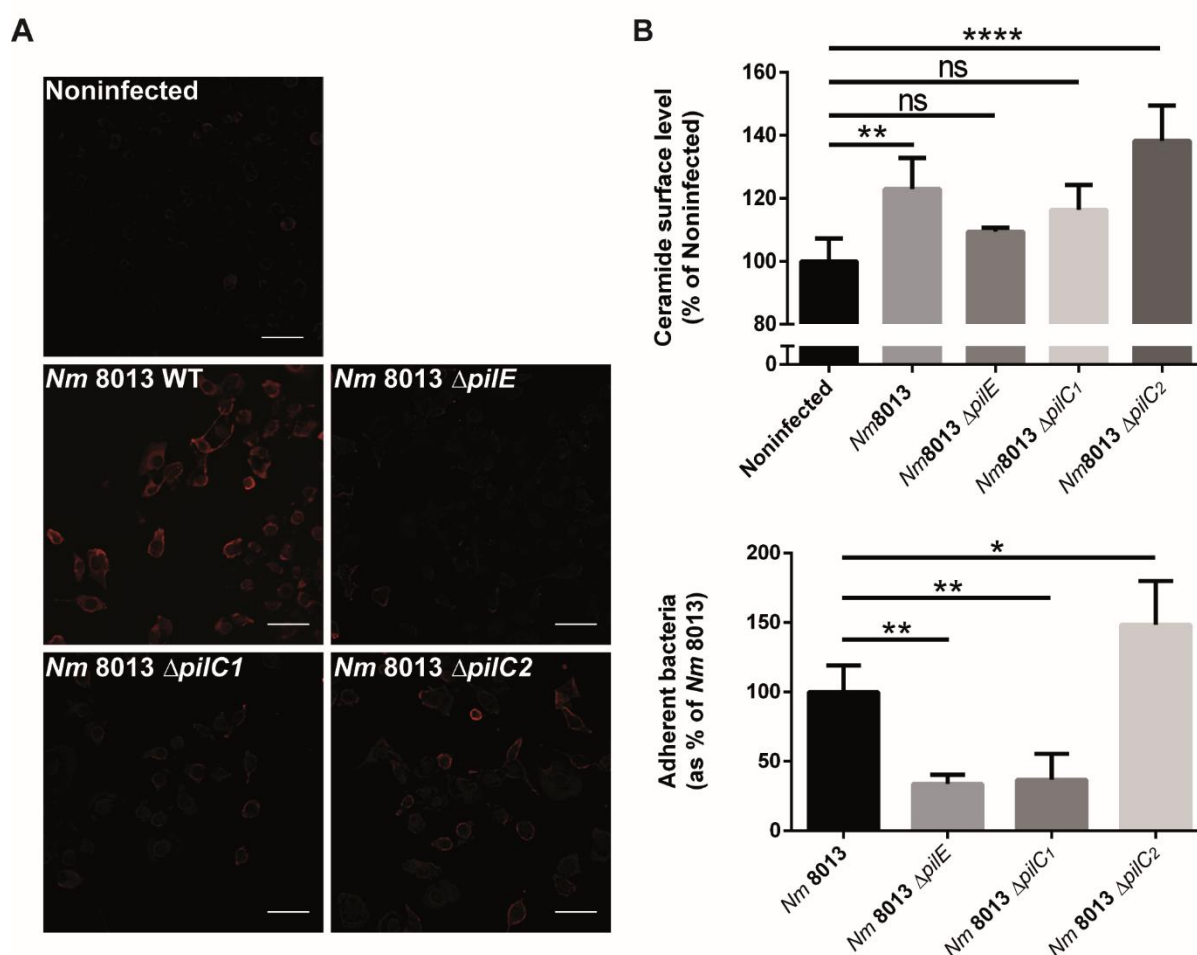


Figure 15: Ceramide release and CRP formation in response to isogenic Δ *pilC1* or Δ *pilC2* meningococcal mutants.

(A) HBMEC were grown to confluence in 8-well Ibidi μ -slides and were infected with wild-type (WT) strain *N. meningitidis* 8013 or isogenic meningococcal mutant *N. meningitidis* 8013 Δ *pilE*, *N. meningitidis* 8013 Δ *pilC1*, or *N. meningitidis* 8013 Δ *pilC2* for 4 h or were left noninfected. (continued next page)

Figure 15: Ceramide release and CRP formation in response to isogenic $\Delta pilC1$ or $\Delta pilC2$ meningococcal mutants. (continued)

Cells were washed, fixed in FA, and stained with an anti-ceramide antibody and secondary Cy5-conjugated goat anti-mouse IgM (red). Images were captured using a Nikon Eclipse Ti-E inverted microscope with a 20 \times objective lens. Bars, 100 μ m. The results of one of three reproducible experiments are shown. (B) HBMEC were infected with wild-type strain *N. meningitidis* 8013 or isogenic mutant *N. meningitidis* 8013 $\Delta pilE$, *N. meningitidis* 8013 $\Delta pilC1$, or *N. meningitidis* 8013 $\Delta pilC2$ or were left noninfected for 4 h. Surface ceramide levels were determined by flow cytometry, and data are represented as the relative levels of ceramides on the host cell surface. (C) HBMEC were infected with the *N. meningitidis* 8013 wild-type strain or the indicated mutants (the $\Delta pilE$, $\Delta pilC1$, or $\Delta pilC2$ mutant) for 4 h at an MOI of 100. Adhesion was determined by a gentamicin protection assay. Error bars represent the mean \pm SD. One-way ANOVA with Dunnett's *post hoc* test was used to determine significance. *, $P < 0.05$; **, $P < 0.01$; ****, $P < 0.0001$; ns, not significant.

3.1.6 Inhibition of intracellular calcium release reduced the number of invasive bacteria

To investigate the impact of calcium depletion on adhesion and invasion properties of *N. meningitidis*, gentamicin protection assays were performed. 2-APB treated (30 min prior to the infection), or non-treated HBMEC were infected for 4 h and the number of adherent and invasive bacteria was determined. Indeed, the inhibition of calcium release from the ER strongly reduced the ability of *N. meningitidis* to invade the host cells in a concentration dependent manner, whereas the number of adherent bacteria was not altered (Figure 16).

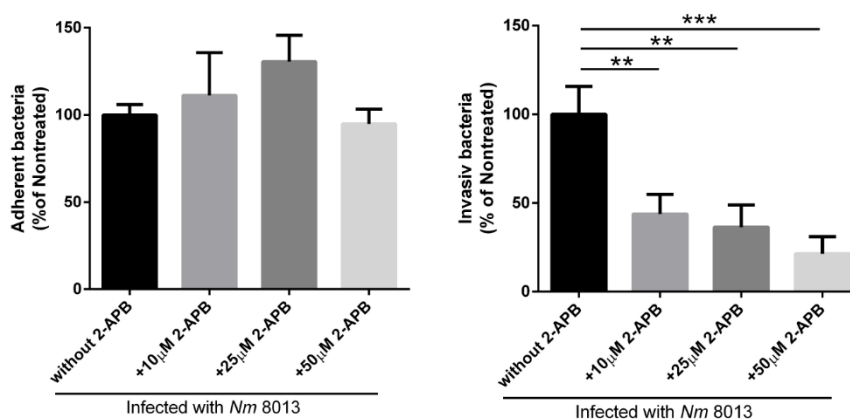


Figure 16: Depletion of the Ca^{2+} level interferes with invasion of *N. meningitidis* strain 8013 into HBMEC.

HBMEC were pretreated with different concentrations (10, 25, 50 μ M) of the 1,4,5-trisphosphate receptor inhibitor 2-APB. Afterwards, cells were infected for 4 h at an MOI of 100, and adhesion (left) and invasion (right) were determined by a gentamicin protection assay. All results show the mean \pm SD levels as a percentage of the levels for untreated control cells from three independent experiments performed in duplicate. P values are relative to the values for untreated control cells and were determined by an ordinary one-way ANOVA with Dunnett's *post hoc* test. **, $P < 0.01$, ***, $P < 0.001$.

Importantly, 2-APB did not show any effects on survival or fitness of the bacteria as demonstrated by growth analysis of the *N. meningitidis* under the same conditions as their encountered during the infection experiments (Figure 17).

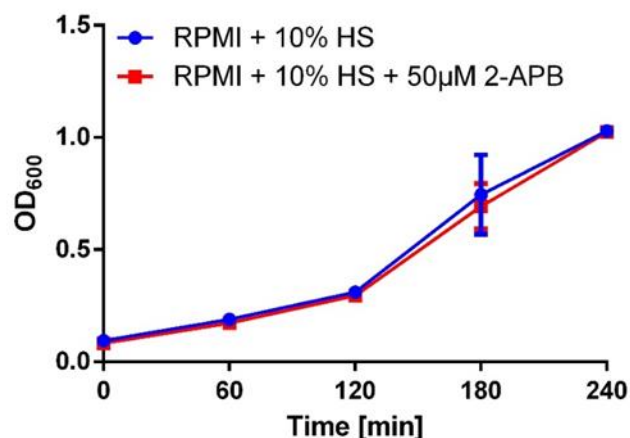


Figure 17: Effect of 2-APB on neisserial growth.

N. meningitidis strain 8013 was inoculated to a final OD₆₀₀ of 0.1 in 10 ml of RPMI (+10 % HS), in the presence or absence of 50 µM 2-APB. Growth was monitored every 30 min over a time course of 3 h. The results show the mean \pm SD of three independent experiments performed in duplicate.

3.1.7 Treatment of HBMEC with pili enriched fractions induced translocation of the lysosomal ASM and ceramide generation on the cell surface.

Because all experiments to this point were performed using living and intact bacteria, the next step was to exclude the possibility of other interactions between bacteria and the host cell beside those mediated by their T4P. For that, the highly piliated *N. meningitidis* strain 8013/12 was used for pilus purification. The, so called, pilus enriched fraction (PeF), was tested for its purity and contamination of membrane fractions by western- and dot blot analysis, carried out with either an PorB antibody as membrane marker and the PilE SM1 antibody. The western blot clearly showed the appearance of the PilE subunit in the PeF, mostly as monomer (Figure 18A). The control of membrane contaminations by the dot blot revealed that the PeF did not contain any detectable membrane constituent (Figure 18B). Importantly, PorB is a major pathogenicity factor involved in calcium influx into the cells. With the proof of PorB absence, the measurement-disturbing factor of calcium influx could also be excluded.

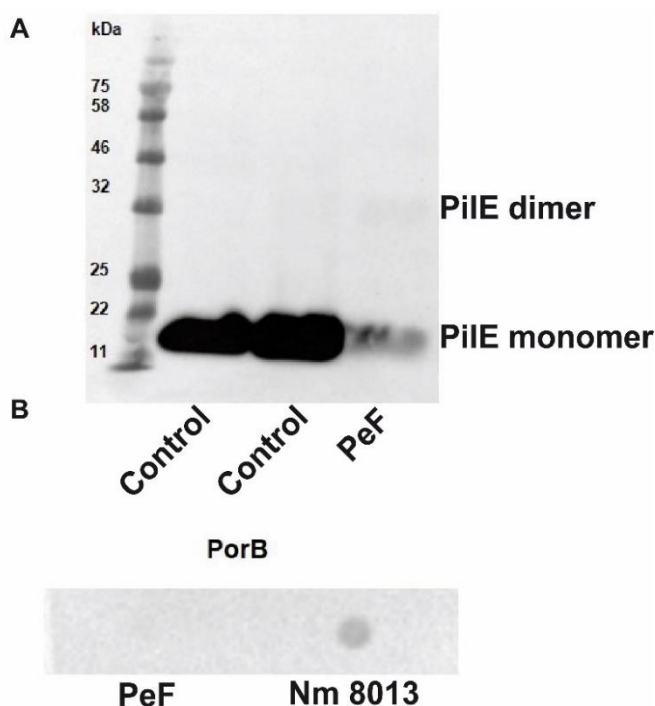


Figure 18: Western blot or dot blot analyses of pili enriched fractions of *N. meningitidis* 8013.

Pili enriched fractions (PeF) were purified from the pilated wildtype strain *N. meningitidis* 8013 and routinely analyzed by (A) immunoblotting with antibody SM1 (anti-PilE mouse monoclonal antibody; generously provided by M. Virji) after SDS-PAGE of whole-cell bacteria (control) or PeF. (B) Dot blot assay using a primary mouse anti-PorB antibody to confirm absence of PorB in PeFs from *N. meningitidis* 8013. Bacterial lysates of *N. meningitidis* 8013 (8013) were used as a positive control.

Treatment of HBMECs with PeF was analyzed by flow cytometry, ASM activity assays and immunofluorescence approaches, similar to the infection experiments. The cells were treated with 2.5 μ g of the PeF and the calcium response was measured in Fluo 8 loaded cells. The result showed a strong and fast response within 2 to 5 min after adding the PeF (Figure 19A). Because the calcium response occurred much faster compared to the response of infected cells with whole bacteria, the detection of surface ASM and ceramide was performed after only 2 h of PeF exposure (4 h with living bacteria). The flow cytometry results showed a slight but significant increase of surface abundance for both markers (Figure 19B). Another approach was used for determination of lysosomal fusion with the membrane by using LysoTracker loaded HBMEC. Treatment of those cells with PeF led to a strong decrease of lysosomal signal in observed cells, indicating the lysosomal fusion with the membrane and release of the LysoTracker into the extracellular space (Figure 19C). Additional confirmation of the quantitative results for the outcome of ASM translocation was given by immunofluorescence imaging, visualizing the increase in surface ceramide after PeF treatment (Figure 19D). Estimation of the ASM surface activity also confirmed that the PeF treatment led to a strong increase of ASM activity in a calcium dependent manner (Figure 19E).

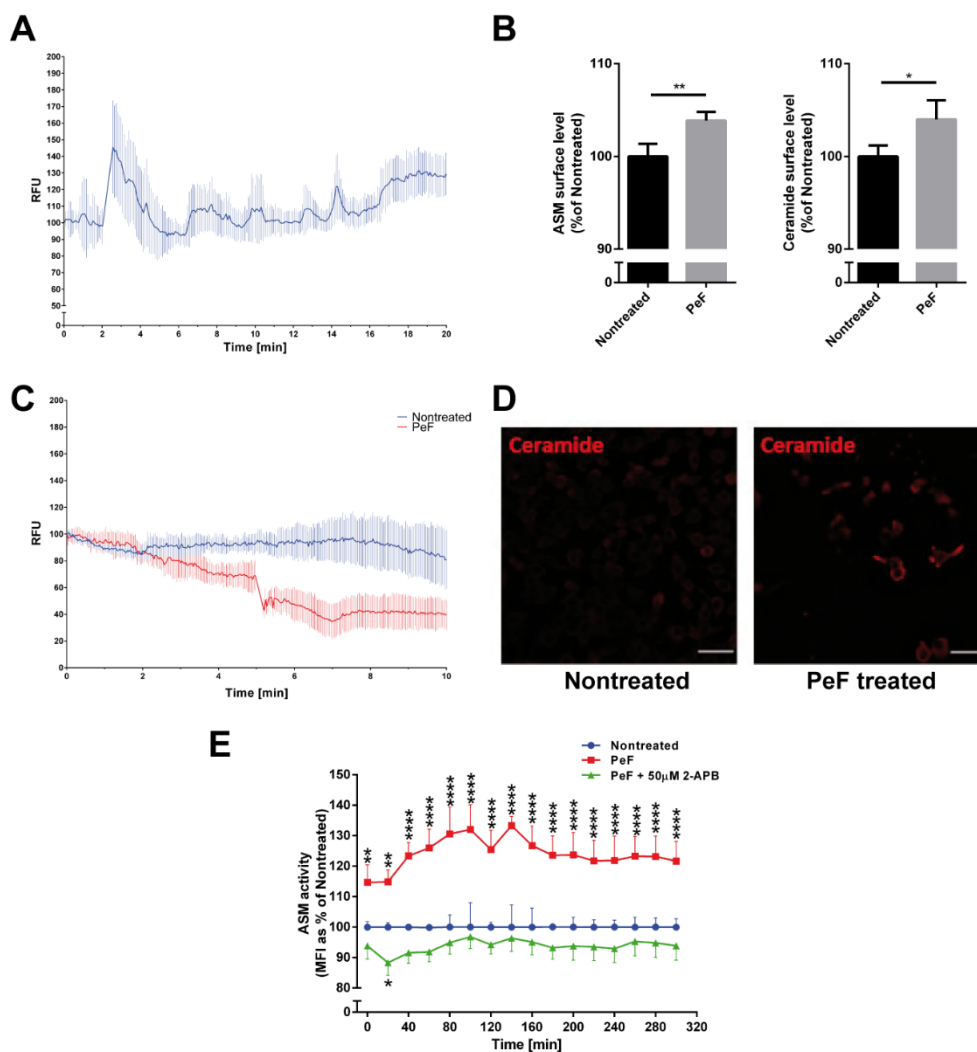


Figure 19: Effect of pilus-enriched fractions on Ca^{2+} fluxes, ASM translocation and activity, and ceramide release.

(A) HBMEC were loaded with Fluo-8 and treated with 2.5 μg pilus-enriched fraction (PeF) from *N. meningitidis* 8013 in Ca^{2+} -free medium. Cytosolic Ca^{2+} concentrations were monitored over 10 min using a Nikon Eclipse Ti-E inverted microscope and analyzed using NIS Elements AR software (Nikon). Fluorescence data from representative cells were exported and are shown as the mean \pm SD number of relative fluorescence units relative to the starting fluorescence intensity value. (B) Cells were maintained in infection medium and incubated with PeF (2.5 μg) from *N. meningitidis* 8013. The pilus-induced translocation of ASM and ceramide surface levels were detected by flow cytometry analysis. Data show the mean \pm SD from three independent experiments performed in duplicate. *P* values were determined by an unpaired, two-tailed Student's *t* test. *, *P* < 0.05; **, *P* < 0.01. (C) HBMEC were loaded with LysoTracker green (80 nM) and treated with PeF (2.5 μg) in Ca^{2+} -free medium. Fluorescence signals were monitored over 10 min. Fluorescence data from representative cells were exported and are shown as the mean \pm SD number of relative fluorescence units relative to the starting fluorescence intensity value. Note the disappearance of the LysoTracker green signal after addition of PeF, indicative of lysosomal exocytosis. (D) Cells were grown to confluence in Ibidi μ -slides and were incubated with PeF (2.5 μg) from *N. meningitidis* 8013 or were left nontreated. Cells were washed, fixed in FA, and stained with an anti-ceramide antibody and secondary Cy5-conjugated goat anti-mouse IgM (red). Bars, 10 μm . (E) Cells were incubated with PeF or left nontreated, and ASM activity was determined. Reported is the activity of ASM after incubation of the cells with PeF (1 μg) from *N. meningitidis* 8013. Values show the mean \pm SD from three independent experiments. A two-way ANOVA was used to determine significance. *, *P* < 0.05; **, *P* < 0.01; ****, *P* < 0.0001.

Additionally, direct stochastic optical reconstruction microscopy (dSTORM), a super resolution technique, was performed on HBMEC treated with PeF. The technical realization, as well as the statistical analysis, was done by Jan Schlegel (Biophysics Department, Hubland). The overall number of CRPs with a size of ~ 80 nm in the plasma membrane was slightly increased after treatment with $2.5 \mu\text{g}$ PeF, but significantly elevated on HBMEC after 2 h of exposure to $5 \mu\text{g}$ pilus-enriched fractions. The formation of CRPs could be prevented by treatment with 2-APB (Figure 20). To point out the advantage of this method, conventional immunofluorescence was performed on the same samples (Figure 20D).

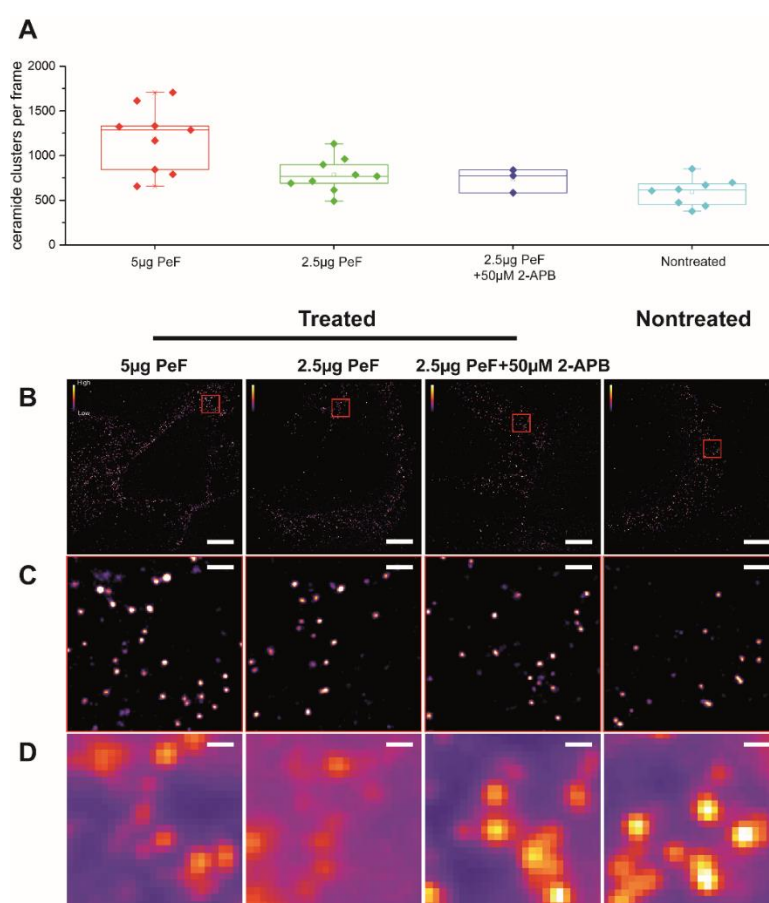


Figure 20: Treatment of HBMEC with pilus-enriched fractions increased the number of plasma membrane-associated CRPs.

(A) Quantification of subdiffraction-sized CRPs within the plasma membrane of HBMEC pretreated with different concentrations of the pilus-enriched fraction (PeF) at $5 \mu\text{g}$, $2.5 \mu\text{g}$, or $2.5 \mu\text{g}$ or with $50 \mu\text{M}$ 2-APB or not treated. The superresolution images show a dose-dependent enrichment of sphingolipid nanodomains upon pilus treatment. (B) Representative dSTORM images of HBMEC treated with the indicated concentrations of PeF (as shown in panel A). (C) Images of the corresponding dSTORM insets (red squares) from panel B, illustrating the increase in the number of CRPs induced by the addition of PeF. (D) Conventional diffraction-limited microscopy of the sections shown in panel C. Bars, $5 \mu\text{m}$ (B) and 500 nm (C and D).

3.1.8 Interaction with the CD147 receptor as putative mediator for calcium release

As recently described, the CD147 receptor (also called Basigin or EMMPRIN) has shown to be a critical host receptor for the interaction of meningococcal T4P subunits (Bernard *et al.*, 2014). Besides its importance for *N. meningitidis*, the CD147 receptor is well described as important host cell factor for other pathogens such as the human immunodeficiency virus (HIV), hepatitis B (HBV) and the bacterial pathogen *Listeria monocytogenes* (Till *et al.*, 2008; Xiong *et al.*, 2014).

To test the involvement of CD147 upstream of calcium release in our infection model, the first step was to confirm expression of CD147 on the surface of the HBMEC. Expression of CD147 was evaluated by flow cytometry analyses using a monoclonal antibody directed against the D2 domain of the receptor (MEM-M6/6). Flow cytometry data verified the presence of the receptor on HBMEC (Figure 21A). To confirm the role of CD147 in the interaction of *N. meningitidis* with HBMEC as recently shown for the immortalized cell line hBMEC/D3 (Bernard *et al.*, 2014), HBMEC were infected and afterwards stained with an CD147 antibody, recognizing the membrane proximal D1 domain (MEM-M6/1), which is known to not compete with the meningococcal binding. LSM imaging were performed by Jan Schlegel (Biozentrum) and showed an accumulation of the receptor underneath the bacteria colonies, forming so called 'honeycomb-like' structures (Figure 21B). The importance of the T4P in CD147 mediated adherence was analyzed by binding experiments of *N. meningitidis* strain 8013/12, or its isogenic Pile deficient mutant $\Delta pilE$, to purified and immobilized CD147-Fc. The estimation of bound bacteria showed that the lack of the pilus drastically reduced the ability of *N. meningitidis* to bind to the receptor (Figure 21C).

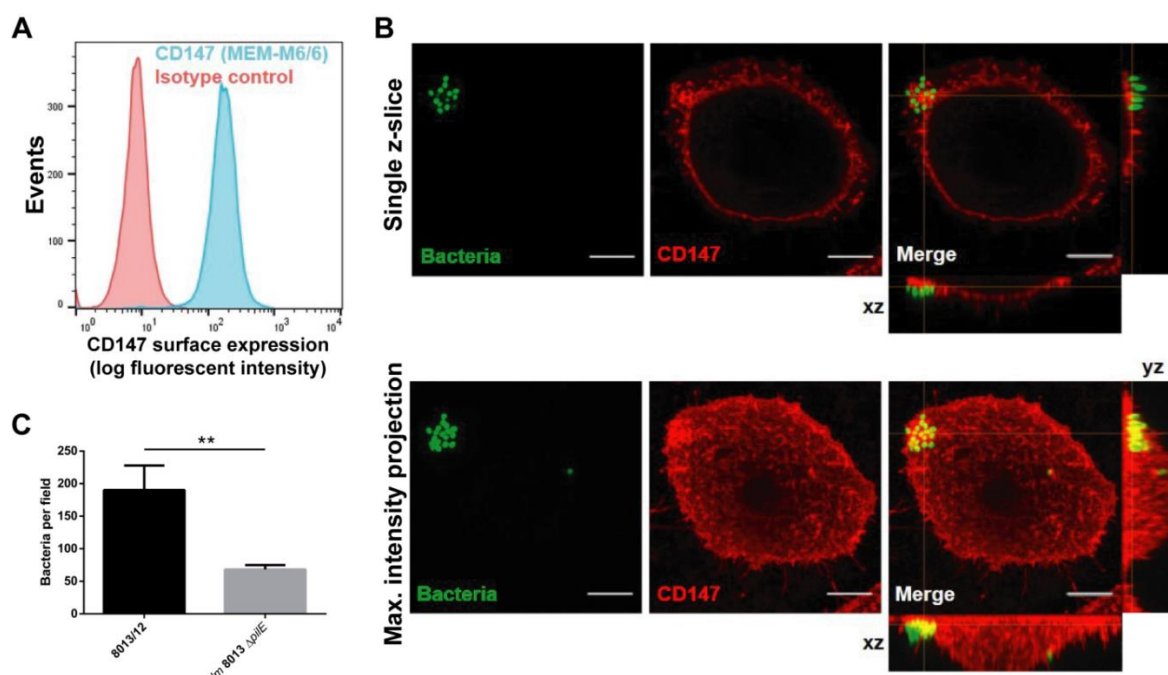


Figure 21: CD147 expression on HBMEC and recruitment underneath meningococcal microcolonies.

(A) Surface expression of CD147 on HBMEC was quantified by flow cytometry. Red: Isotype control, blue: monoclonal antibody MEM-M6/6, that recognized the C-terminal D2 domain of CD147. (B) Infection of HBMEC with *N. meningitidis* strain 8013 for 4 h results in recruitment of CD147 underneath meningococcal microcolonies as demonstrated for hCMEC/D3 cells (Bernard *et al.*, 2014). Staining was performed using MEM-M6/1 antibody. (C) Adhesion of wildtype strain *Nm* 8013 and pilus-deficient mutant *Nm* 8013 Δ *pilE* to immobilized CD147-Fc quantified after 2 h incubation. Mean \pm SD of three independent experiments performed in duplicate is shown. ** $P < 0.01$, in unpaired, two-tailed Student's *t* test.

The next step was to test whether antibodies directed against CD147 could block the release of calcium transients. HBMEC were therefore treated with the MEM-M6/6 antibody, competing with the pilus for the same D2 domain of the receptor. Indeed, pre-incubation of HBMEC with the CD147 specific MEM-M6/6 antibody, abolished calcium mobilization in HBMEC that were treated with of PeF (Figure 22A+B). Afterwards, it was investigated whether activation of the receptor by binding of the MEM-M6/6 antibody to the C-terminal D2 domain might trigger calcium release in HBMEC. Indeed, a significant calcium response in HBMEC was observed at about 8 min after addition (Figure 22C).

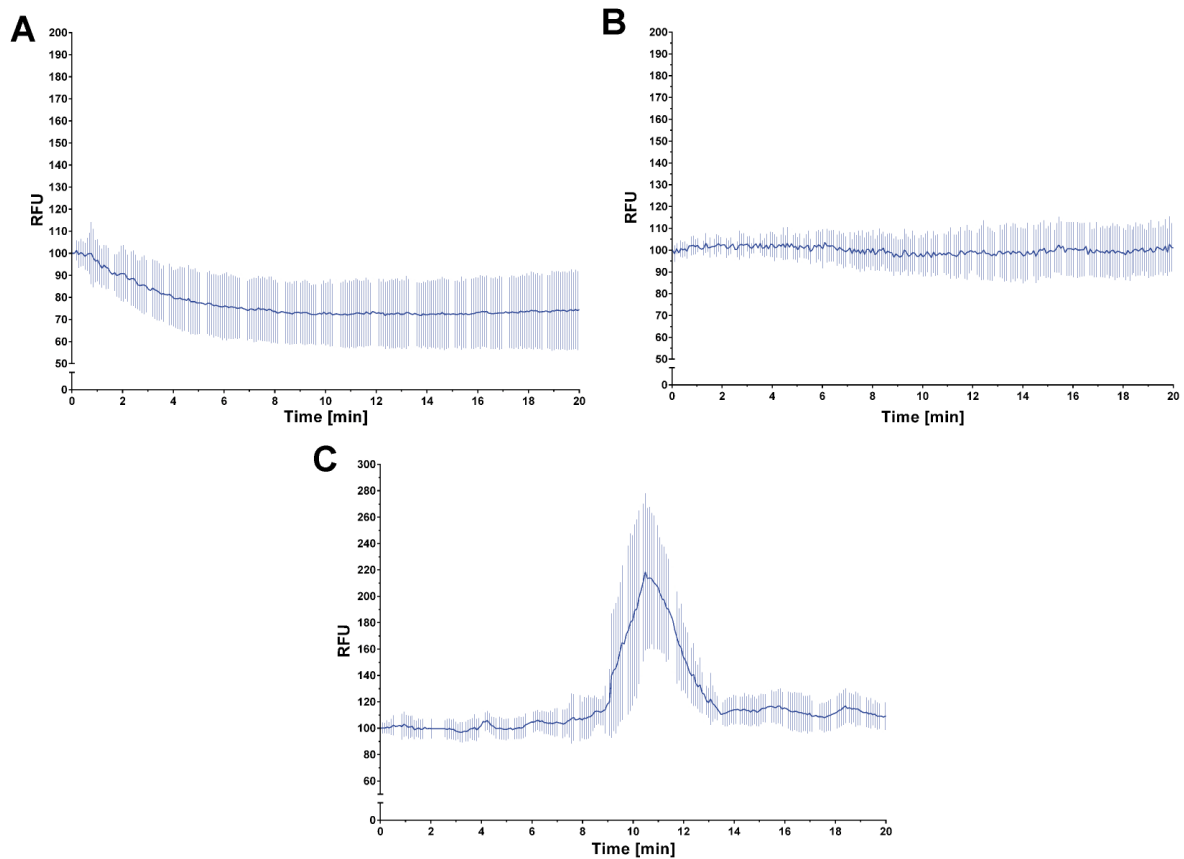


Figure 22: An antibody against the C-terminal domain D2 of CD147 blocks *N. meningitidis* –induced calcium flux (MEM-M6/6).

(A) Fluo-8 loaded HBMEC were pre-incubated for 60 min with monoclonal CD147 IgG (10 μ g/ml) antibody (MEM-M6/6; recognizes the C-terminal domain D2 of CD147) before addition of crude pili (2.5 μ g) from *Nm* 8013 in calcium-free medium or left untreated (B). (C) Fluo-8 loaded HBMEC stimulated with MEM-M6/6 antibody (10 μ g/ml) in calcium-free medium. The gap indicates the addition of the antibody. Cytosolic calcium concentrations were monitored over 20 min in single cells. Fluorescence data from representative cells were exported and are shown as mean \pm SD RFU relative to the start fluorescence intensity value. Experiments were repeated three times and a representative experiment is shown.

The results of this section are also published in *Infection and Immunity* (Peters et al., 2019).

3.2 Importance of cell cycle regulated gangliosides for meningococcal infection

Besides ceramide, a broad range of sphingolipids and enzymes involved in the synthesis play an important role in host pathogen interactions (Kunz and Kozjak-Pavlovic, 2019). The group of gangliosides (a class of glycosphingolipids) seems to be especially important in the context of meningococcal pathogenicity, because interaction with the essential T4P receptor CD147 relies on the membrane lipid composition. It was shown that the CD147 receptor, together with others, preferentially localize in lipid rafts, consisting mainly of the ganglioside GM1 and cholesterol which may promote bacterial invasion (Li et al., 2013; Wu et al., 2017). In addition, a recent study indicates a broad range of direct interactions between the meningococcal T4P and host cell derived glycosylation structures, including the ganglioside head motives (Mubaiwa et al., 2017). Interactions between pathogens and membrane gangliosides are well described and seems to be a widely used port of entry for diverse pathogens. Two major players, named GM1 and Gb3, are known to interact with e.g. the Simian virus 40, *Brucella suis*, *Vibrio cholera* for GM1 and the Human Immunodeficiency Virus and *Shigella dysenteriae* for Gb3 (Schlegel et al., 2019). Moreover, GM1 is also in the focus of research, due to its ability to induce clathrin-dependent (and independent) endocytosis after binding to the cholera toxin B subunit and maybe promoting pathogen entrance into the cell in a similar way (Torgersen et al., 2001)

3.2.1 Cell cycle dependent surface expression of GM1 and Gb3

Because GM1 and Gb3 are known for their cell cycle dependent surface expression, the distribution of those two gangliosides on HBMEC were addressed using immunofluorescence. For that, cells were incubated with either cholera toxin B subunit (CtxB, against GM1) or shiga toxin B subunit (StxB, against Gb3) and analyzed by LSM (Figure 23, performed by Jan Schlegel (Schlegel *et al.*, 2019)). Indeed, as described in the literature, the majority of the cells was either GM1 or Gb3 positive.

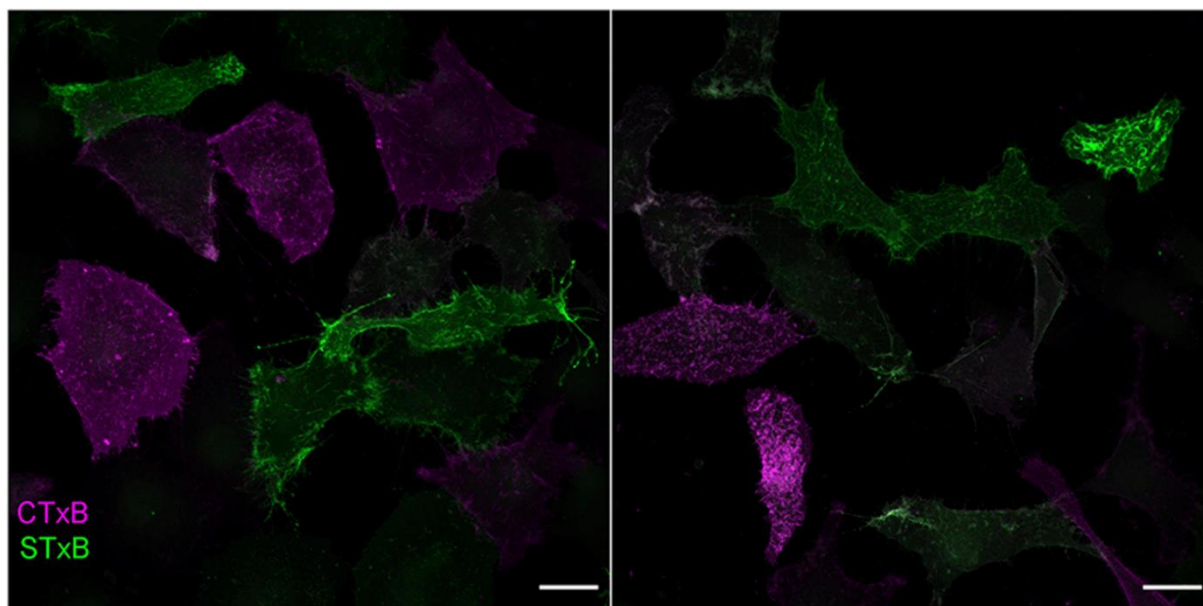


Figure 23: Visualization of sphingolipids GM1 and Gb3 in the plasma membrane of brain endothelial cells.

Two exemplary confocal laser scanning microscopy images of GM1 (magenta), labeled with CtxB and Gb3 (green), labeled with STxB. Scale bar, 20 μm . Adapted from Schlegel et al. 2019.

To test if one (or both) of the gangliosides play a role in the context of meningococcal interaction with the host cell, super resolution microscopy (dSTORM) was applied to HBMECs infected with a GFP expressing *N. meningitidis* strain MC58. The cells were infected for 2.5 h, fixed and stained with either CtxB or StxB (staining and image acquisition was performed by Jan Schlegel). Whereas the results showed that Gb3 (stained with StxB) surface distribution does not alter during the infection, the GM1 staining instead displayed a strong accumulation of the ganglioside surrounding the bacteria colonies (Figure 24 A+B)

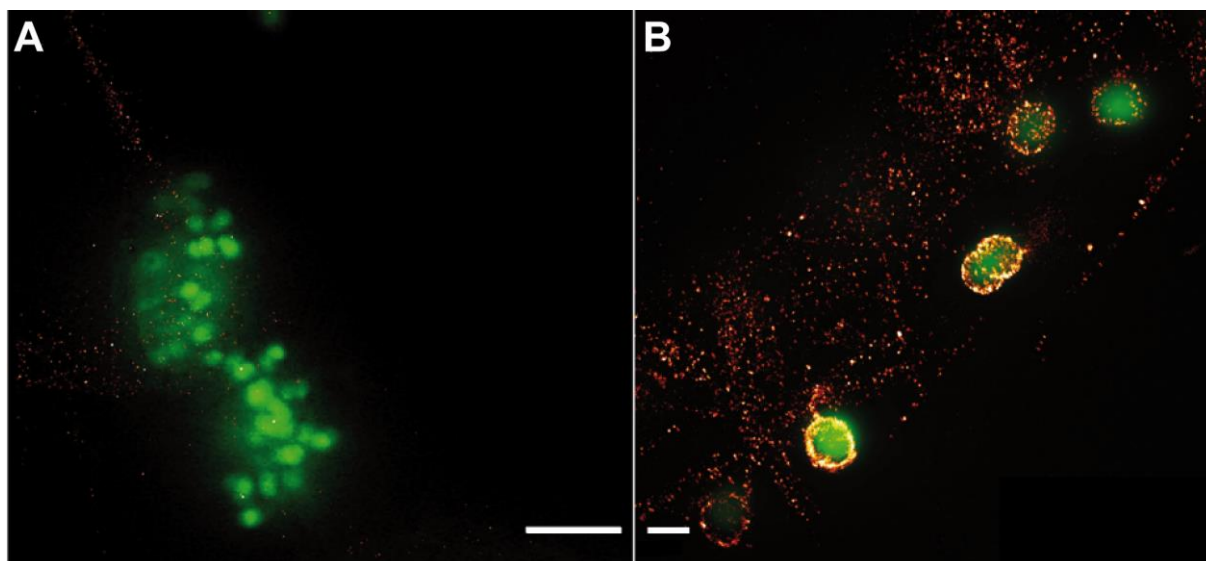


Figure 24: GM1 but not Gb3 accumulates around *N. meningitidis*.

Representative *d*STORM images of HBMECs infected with GFP expressing *Nm* MC58. (A) Staining with StxB against Gb3. Scale bar 5 μ m. (B) Staining with CtxB against GM1. Scale bar 1 μ m. Adapted from Schlegel *et al.* 2019.

3.2.2 Increased number of cells in the G1 phase correlates with increased GM1 surface abundance

Due to the previous results, the role of GM1 was further elucidated. For that, the first step was to increase the number of cells in the G1 phase (in which the cells display the highest expression of GM1). To shift the population towards the G1 phase, serum starvation was used to deprive the cells of energy for the transition to the S phase. The effect was then estimated by propidium iodid (PI) staining followed by flow cytometry (Figure 25). The histogram shows a representative result and indicates the gating strategy. The shift towards an increased number of cells in the G1 phase was obtained and further proofed by statistical analysis (Figure 25). Moreover, non- and G1 synchronized cells were tested for their GM1 surface levels by flow cytometry (Figure 26). The result showed an increased GM1 signal in the serum-starved cells, comparable to the increased number of cells in the G1 phase (Figure 25). Additionally, the impact of infection of either non- or G1 synchronized cells was tested. The results indicated an even stronger increase in GM1 surface abundance on the infected cells compared to the noninfected cells.

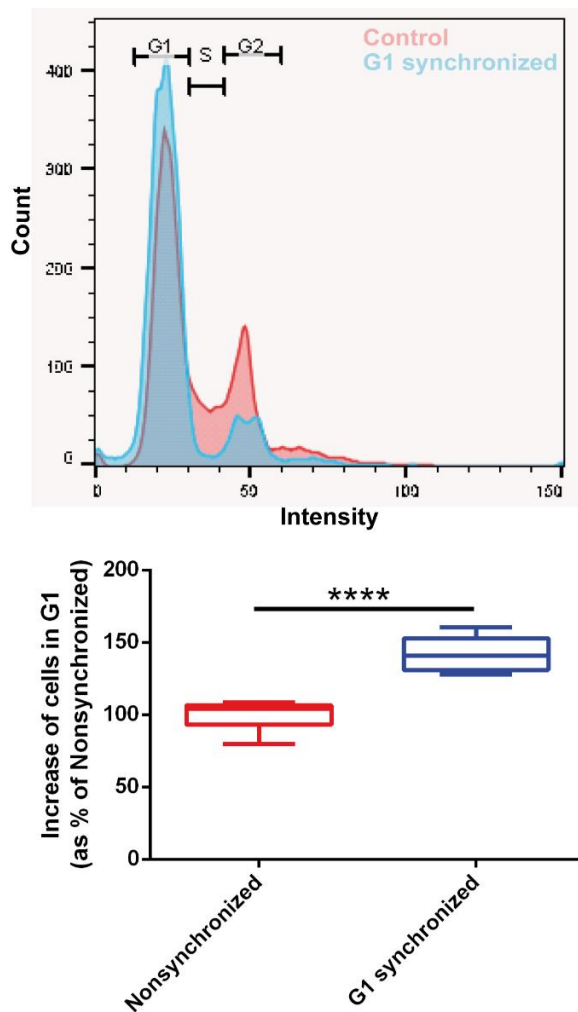


Figure 25: Serum starvation led to an increased number of cells in the G1 phase.

Results of serum starvation on the phase distribution in the cell population, estimated by PI staining. (Top) Representative histogram of 10,000 cells stained with PI showing the population shift and indicates the gating strategy applied to all experiments. (Bottom) Statistical analysis from the flow cytometric experiments. Box plots showing the interquartile range (IQR) of 3 experiments performed in duplicates with median as line. The whiskers represent the lowest and highest value within 1.5 IQR of the lower and upper quartile, respectively. ****, $P < 0.0001$ in unpaired, two-tailed Student's t test.

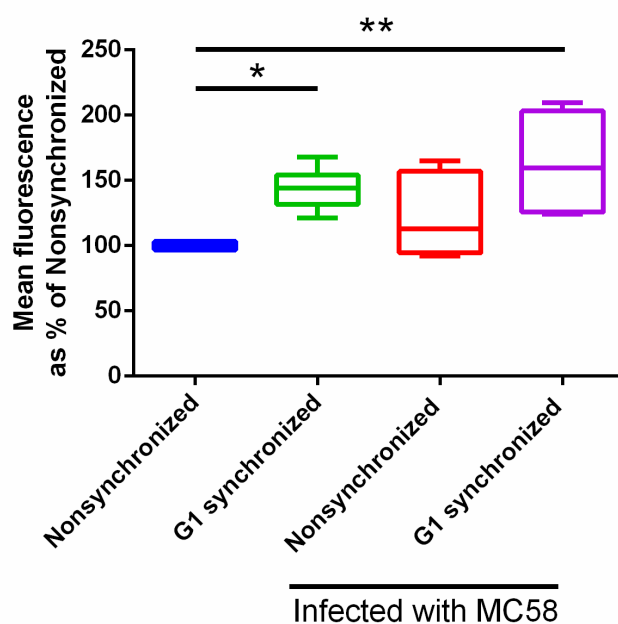


Figure 26: Serum starvation led to an increase of GM1 surface abundance.

Estimation of GM1 surface levels on non- or G1 synchronized HBMECs. If indicated, cells were infected with the *N. meningitidis* strain MC58 for 4 h. For the analysis of cell surface GM1, cells were stained with Alexa Fluor 647-conjugated CtxB for 30 minutes at room temperature in the dark. Then, cells were fixed for 30 min at 4°C, washed three times with FACS buffer and analyzed by flow cytometry. Box plots showing the interquartile range (IQR) of 3 experiments performed in duplicates with median as line. The whiskers represent the lowest and highest value within 1.5 IQR of the lower and upper quartile, respectively. *, $P < 0.05$; **, $P < 0.01$ in an Ordinary one-way ANOVA with Dunnett's *post hoc* test.

3.2.3 Interaction between *N. meningitidis* and GM1 is important for bacterial invasion

To determine the importance of GM1 for meningococcal pathogenicity, gentamicin protection assays were performed. HBMEC, either G1 or non-synchronized, were infected with *N. meningitidis* strain MC58 and the number of adherent and invasive bacteria was determined. The shift of HBMEC towards the G1 phase significantly enhanced bacterial uptake into the cell (Figure 27 A). To test if this results was based on the increased GM1 surface abundance, HBMEC were incubated with CtxB 30 min prior to the infection to block a possible meningococcal – GM1 interaction. Indeed, pre-incubation with CtxB led to a strong decrease of invasive bacteria in the non-synchronized cell and even stronger in the G1 synchronized (Figure 27 A). Importantly, the changes in invasiveness were not based on an altered adherence of the bacteria (Figure 27 B).

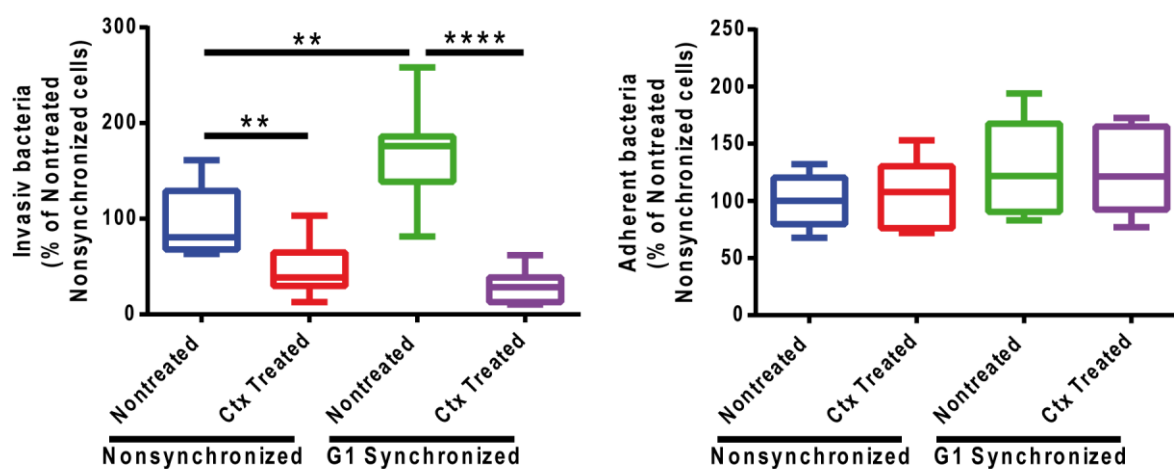


Figure 27: Blocking of GM1 strongly reduces meningococcal invasiveness.

G1 or non-synchronized HBMEC were treated with 6.6 $\mu\text{g/ml}$ CtxB for 30 min (if indicated). Afterwards, cells were infected for 4 h at an MOI of 100, and invasion (A) and adhesion (B) were determined by a gentamicin protection assay. Box plots showing the interquartile range (IQR) of 3 experiments performed in duplicates with median as line. The whiskers represent the lowest and highest value within 1.5 IQR of the lower and upper quartile, respectively. Ordinary one-way ANOVA with Dunnett's *post hoc* test was applied to the data. **, $P < 0.01$, ****, $P < 0.0001$

The results of this section are also published in *Frontiers in Cell and Developmental Biology* (Schlegel et al., 2019).

3.3 The antimicrobial activity of sphingolipids against *N. meningitidis*

Beside the important function of sphingolipids in maintaining the membrane integrity and their involvement in the regulation of e.g. cell growth and proliferation, several studies indicate a role of sphingoid bases and fatty acids in the defense against pathogenic microorganisms (Becker et al., 2017; Bibel et al., 1992; Fischer et al., 2012). Sphingoid bases are active against Gram-positive and Gram-negative bacteria (Fischer et al., 2012). Whereas a recent study identified the mechanism of the bactericidal effect of sphingosine, by interaction with the bacterial membrane lipid cardiolipin leading to membrane permeabilization (Verhaegh et al., 2020), the antimicrobial mechanism of azido-modified sphingolipids however is still unknown so far. Previously, our group showed the antimicrobial activity of sphingolipids, including natural and functionalized sphingolipids, against *N. meningitidis*. (Becam et al., 2017). It was shown that the addition of a functional azido group to the omega position of the fatty acid chain side of a synthetic short chain ceramide (ω -azido-C₆-ceramide) led to efficient killing of *N. meningitidis* (Becam et al., 2017; Walter et al., 2017). Importantly, the compound showed no cytotoxic effects on eukaryotic cells (Becam et al., 2017). These initial results were recently confirmed and extended, including a novel azido modified sphingosine, ω -azido-sphingosine, by Lena Kaiser. She compared MIC/MBC values for the unmodified sphingosine and the functionalized forms, ω -N₃-sphingosine and ω -N₃-C₆-ceramide, and showed a comparable microbial activity of the modified sphingolipids and the natural compound against *N. meningitidis*. Transmission and scanning electron microscopy (TEM/SEM) based studies by Lena Kaiser also revealed a strong impact on the bacterial morphology after treatment with a concentration of the lipids corresponding to 0.1 X, or 1 X the MBC (Figure 28).

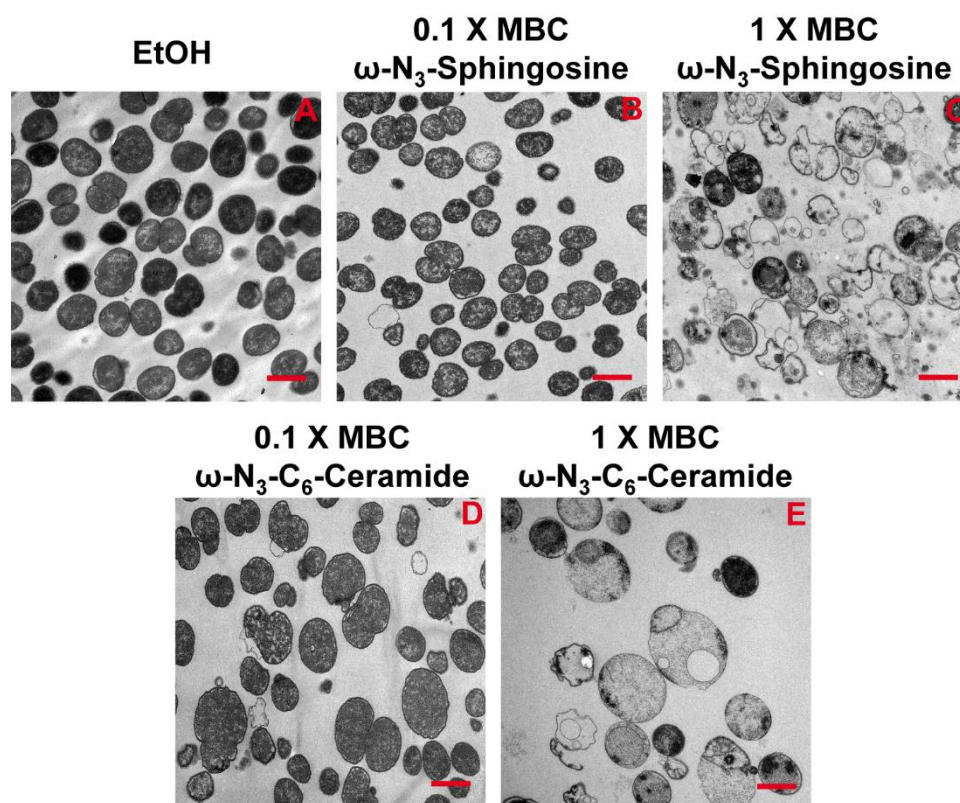


Figure 28: TEM micrographs show the effect on *N. meningitidis* treated with azido-modified sphingolipids.

Representative TEM of *N. meningitidis* treated with either ethanol (EtOH) (A), 0.1 / 1 X MBC of ω -N₃-sphingosine (B+C) or 0.1 / 1 X MBC of ω -N₃-C₆-ceramide (D+E). *N. meningitidis* treated with 0.1 X MBC of ω -N₃-sphingosine or ω -N₃-C₆-ceramide showed a slight alteration of their surfaces and shape (B+D) and intact intracellular content. However, some bacteria displayed a strong elongation of the outer membrane. *N. meningitidis* treated with 1 X MBC of ω -N₃-sphingosine or ω -N₃-C₆-ceramide were distorted to various degrees and their surfaces were wrinkled (C+E). Many bacteria appeared in various stages of lysis with compromise of the cell wall and plasma membrane. Bacteria showed intracellular inclusion bodies appearing in high electron density in electron micrographs and additional vesicles that filled the intracellular content. Scale bars: 1 μ m.

Treatment of *N. meningitidis* with low concentrations, of either functionalized ceramide or sphingosine, did not affect the majority of the bacteria, compared to the ethanol treated control group. Whereas the majority of the bacteria still displayed their normal “coffee-bean shape” like morphology, a subset of the bacteria showed morphological changes like outer membrane elongation and a loss intracellular content, indicated by a reduction of electron density (Figure 28 B+D). In contrast, high concentration treatment of both compounds resulted in a massive alteration in morphology and effected the whole population. Most bacteria lost large parts of their outer membrane

and their cellular content. In addition, treatment led to intracellular vacuole formation and an accumulation of membranous like structures in the cytosol (Figure 28 C+E).

3.3.1 CLEM reveals concentration related differences in localization of functionalized sphingolipids

Fluorescence microscopy is a powerful tool for locating and identifying specific molecules, but is limited by the lack of information about the cellular context and resolution limits. On the other hand, electron microscopy has the highest possible resolution but is restricted to grey scale images, making the identification of molecules partially impossible. These limitations are overcome by the combination of both techniques, called correlative light and electron microscopy (CLEM) (de Boer et al., 2015). To achieve a more functional picture of the antimicrobial effect shown before, a novel CLEM approach was established in cooperation with Lena Kaiser und Christian Stigloher (Microscopy Core Unit, Würzburg). For that, the functional azide group of the lipids were, direct after treatment, coupled to a DBCO-dye and further processed in the adapted, established CLEM workflow (Markert *et al.*, 2017).

Treatment of *N. meningitidis* with 0.1 X the MBC of ω -N₃-C₆-Ceramide showed a similar morphological pattern as shown in Figure 27, effecting only a subset of the bacteria (Figure 29 left panel/ SEM). The CLEM approach revealed that the compound integrates primarily into the membrane and could be found in the elongated outer membrane. In contrast, no membrane signal was obtained in the sample treated with 1 X the MBC. In contrast, a strong accumulation in electron dense regions inside the bacteria was observed (Figure 29 right panel). Since the bacteria mostly lost their outer membrane during high concentration treatment, this result indicated an effect primarily on the outer membrane. In the case of functionalized sphingosine, the low concentration treatment showed an even stronger signal exclusively in membrane elongations whereas high concentration displayed a similar picture compared to the functionalized ceramide (Figure 30).

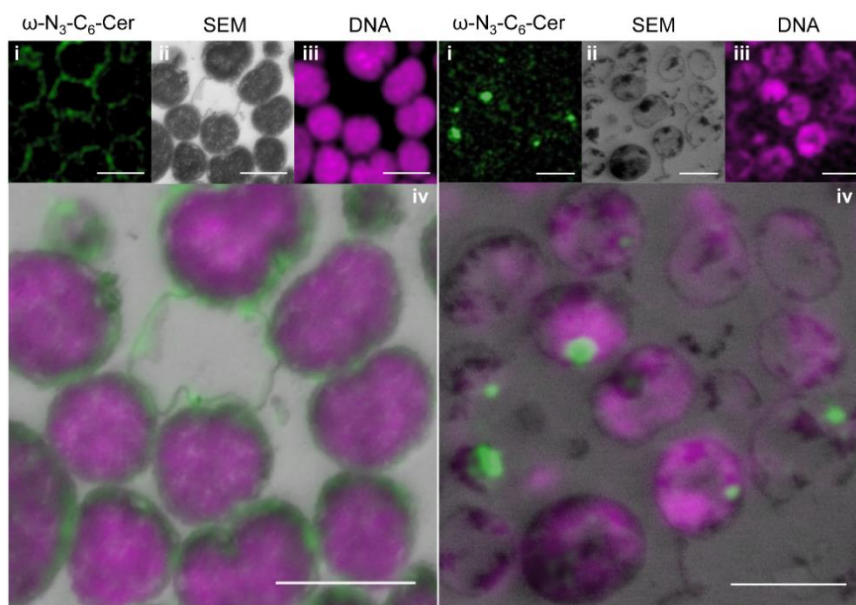


Figure 29: CLEM reveals concentration dependent localization of ω -N₃-C₆-Ceramide in *N. meningitidis*.

Representative CLEM images of *N. meningitidis* treated with 0.1 X MBC (left) or 1 X MBC (right) of ω -N₃-C₆-ceramide. Upper rows show representative single images of the ω -N₃-C₆-ceramide (ω -N₃-C₆-Cer (green)) and DNA signal (magenta) taken with SIM (i and iii) and *N. meningitidis* image taken with SEM (ii). Final images after unbiased correlation are shown in iv. Scale bars: 1 μ m. Experimental procedure, image acquisition and correlation were performed by Lena Kaiser.

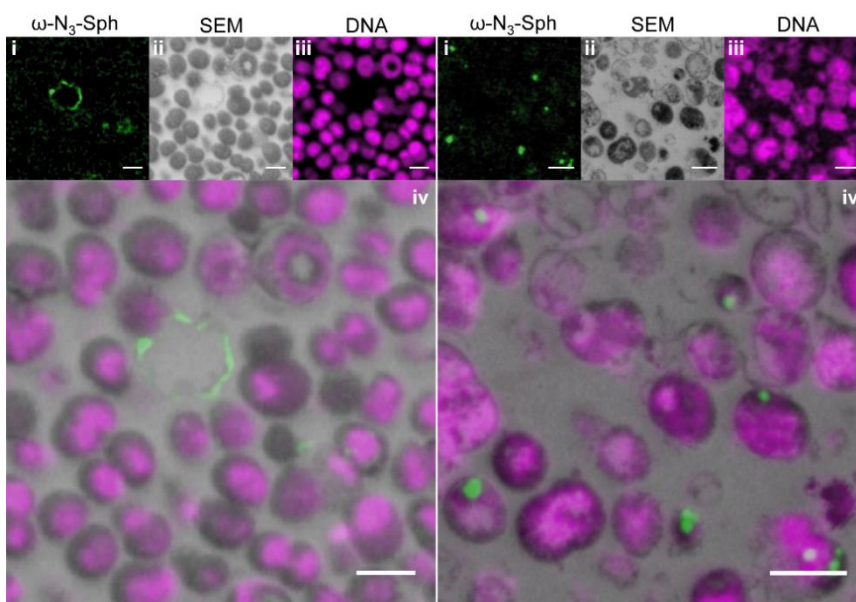


Figure 30: CLEM reveals concentration dependent localization of ω -N₃-Sphingosine in *N. meningitidis*.

Representative CLEM images of *N. meningitidis* treated with 0.1 X MBC (left) or 1 X MBC (right) of ω -N₃-sphingosine. Upper rows show representative single images of the ω -N₃-sphingosine (ω -N₃-Sph (green)) and DNA signal (magenta) taken with SIM (i and iii) and *N. meningitidis* image taken with SEM (ii). Final images after unbiased correlation are shown in iv. Scale bars: 1 μ m. Experimental procedure, image acquisition and correlation were performed by Lena Kaiser.

3.3.2 Mass Spectrometric analysis confirm the primary effect on the outer membrane

Due to the low resolution of the fluorescence imaging, compared to the electron microscopy, the next aim was to confirm the indicated localization in the outer membrane, after low concentration treatment, by HPLC-MS/MS. For that, a membrane separation assay was established to separate the inner and outer membrane of the bacteria after incubation with 0.1 X the MBC of either ω -N₃-sphingosine or ω -N₃-C₆-ceramide. Afterwards, the amount of functionalized lipids in the different membrane fractions (1 to 12) was quantified. Both treatments showed a similar picture regarding the lactate dehydrogenase (LDH) activity, a marker for the inner membrane. Whereas the LDH activity was the highest in fraction 1 - 4 and decreased with every further fractions, the amount of the outer membrane protein OpcA showed a reverse appearance with the highest intensities in the fractions with the lowest LDH activity (Figure 31 A and B). The amount of ω -N₃-sphingosine (Figure 31 A) or ω -N₃-C₆-ceramide (Figure 31 B), measured in the same fractions that have been used for the fraction characterization, showed a negative correlation with the LDH activity and a positive correlation with the OpcA amount. Importantly, classification of the fractions into inner membrane, intermediate and outer membrane was done with the ethanol treated control group, based on the LDH activity, and transferred to the treated samples (Figure 31 C and D).

For ω -N₃-sphingosine and ω -N₃-C₆-ceramide, fraction number 9 appeared as the cleanest outer membrane fraction with the lowest LDH activity and the strongest OpcA signal. In this specific fraction, the amount of functionalized lipids was strongly increased, especially compared to the inner membrane fractions. Of note, functionalized sphingolipids were quantified in relation to the canonical sphingolipid C16 sphingomyelin (C16 SM), a typical membrane lipid whose occurrence in *N. meningitidis* most likely derived from the bacterial growth medium.

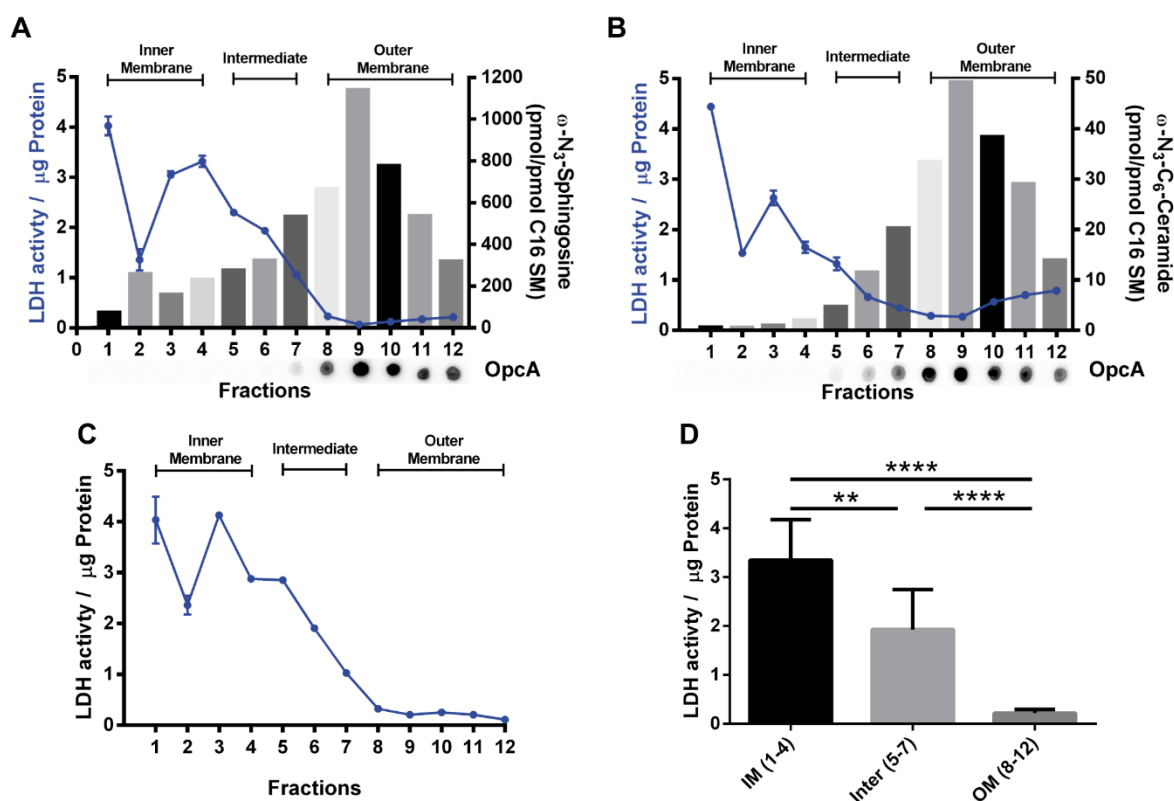


Figure 31: Quantification of azido-functionalized sphingolipid levels in membrane fractions of *N. meningitidis* by mass spectrometry.

Characterization of membrane fractions (1 – 12) of *N. meningitidis* after treatment of bacteria with either ω -N₃-sphingosine (A), ω -N₃-C₆-ceramide (B) or ethanol (C). Each fraction was tested for LDH activity per μg protein (blue line), as inner membrane marker and OpcA (only for A and B) abundance by dot blot (below X-axis) as outer membrane marker. (A+B) Bars represent the amount of azido-functionalized sphingosine or ceramide, as determined by HPLC-MS/MS, normalized to the amount of C16 sphingomyelin (SM) found in the samples. LDH data show the mean \pm SD of a representative experiment performed in duplicate. (D) Statistical comparison of the LDH activity between the pooled groups (Inner Membrane (IM) fractions 1 to 4, Intermediate (Inter) fractions 5 to 7 and Outer Membrane (OM) fractions 8 to 12). The graph shows the mean \pm SD. One-way ANOVA with Dunnett's *post hoc* test was used to determine significance. **, $P < 0.01$; ****, $P < 0.0001$.

4. Discussion

4.1 Meningococcal-induced ceramide platform formation

Host cell derived sphingolipids and enzymes involved in their metabolism have been shown to be a major contributor to host-pathogen interaction for many bacteria and viruses (Kunz and Kozjak-Pavlovic, 2019; Schneider-Schaulies and Schneider-Schaulies, 2015). The activity and localization of the ASM, as a key enzyme of the sphingolipid recycling pathway, is thus a crucial target for various pathogens. Through its ability to alter ceramide abundance at the surface - and hence also membrane microdomain compositions, the ASM indirectly alters cellular invasion by pathogens and survivability of the cell (Esen *et al.*, 2001; Grassme *et al.*, 1997; Grassme *et al.*, 2017; Grassme *et al.*, 2003; Hauck *et al.*, 2000; Simonis *et al.*, 2014; Teichgraber *et al.*, 2008).

A prerequisite for the ASM to fulfill their task is translocation from membrane proximal lysosomes to the outer membrane, followed by activation. To date the exact mechanism of how pathogens trigger the initial steps of ceramide generation on the surface remains elusive.

In this study, the hypothesis was tested that the interaction between the meningococcal type 4 pili (T4P) and the host cell led to calcium release from intracellular storages; in turn, this promotes the delivery of ASM to the outer leaflet by mediating lysosomal fusion with the membrane. This work demonstrates that the highly pilated, Opa- and Opc-negative *N. meningitidis* strain 8013/12 effectively induced ceramide-enriched platform (CRP) formation on human brain microvascular endothelial cells (HBMEC). The same process was not observed by infection with an isogenic pilus-deficient mutant.

The increased ceramide surface levels relied on an increased ASM surface abundance and activity as shown by pharmacological ASM inhibition, immunofluorescence imaging and ASM activity assay. It was also evident that a pilus-enriched fraction (PeF) induced similar translocation and surface activity. Using microscopy approaches, we found evidence that live bacteria and PeF efficiently induced intracellular calcium release and lysosomal exocytosis, as detected by increased LAMP1 surface exposure. Finally, the importance of the intracellular calcium transients was demonstrated by inhibition of the IP₃ receptor localized in the endoplasmic reticulum (ER). Inhibition of the calcium transients from the ER abolished lysosomal fusion with the outer

membrane, ASM translocation and activity and CRP formation on HBMEC. This effect was observed on HBMEC either infected with *N. meningitidis* strain 8013/12 or treated with PeF.

Our group recently showed that the meningococcal outer membrane protein OpcA significantly contributed to the ASM translocation and ceramide platform formation. The results, however, also showed that between 70 % and 80 % of the ceramide increase remained after infection with an OpcA-deficient mutant compared to the wild type. This suggests that other bacterial factors must be involved (Simonis *et al.*, 2014). The meningococcal T4P is the initial mediator of adherence and is known to induce various signaling cascades, including cytoskeleton rearrangement and calcium transients in epithelial cells and monocytes (Ayala *et al.*, 2001; Ayala *et al.*, 2005; Hoffmann *et al.*, 2001; Kallstrom *et al.*, 1998). In this study, a real time microscopy approach was used to investigate the T4P induced calcium release in HBMEC during the course of infection with live pilated bacteria. It was previously shown that infection of A31 (epidermis carcinoma cell line) and ME180 (cervical carcinoma cell line) cells with live bacteria showed a comparable ability to induce calcium fluxes as observed for purified proteins (Ayala *et al.*, 2001; Kallstrom *et al.*, 1998).

Another major pathogenicity factor, which contributes to changes in the intracellular calcium level, are meningococcal porins. As their name implies, porins are known to form pores in eukaryotic cell membranes leading to a rapid (within 2 min) calcium influx from the extracellular environment into the cell. Another resulting phenomenon is endosomal exocytosis (Ayala *et al.*, 2002; Ayala *et al.*, 2005; Muller *et al.*, 1999). Importantly for this study, the influence of porins on the observed calcium changes was excluded by performing all related measurements in calcium free media; additionally, porin contamination of the PeF was excluded by dot blot. Nevertheless, a possible additive role of porins in the natural calcium-rich cellular environment seems plausible. Calcium transients in cultures of epithelial cells have been thought to be transduced by the proposed pilus receptor, CD46 (Kallstrom *et al.*, 1998), as it could be blocked by α CD46 antibodies (Kallstrom *et al.*, 1998). However, recent research has highlighted the specific interaction between the meningococcal pilus components PilE and PilV and the cellular host receptor CD147 as being essential for meningococcal adhesion to human brain endothelial cells and the colonization of human blood vessels (Bernard *et al.*, 2014). CD147 (Basigin) is a widely expressed plasma membrane glycoprotein, also known as extracellular matrix metalloproteinase inducer (termed

EMMPRIN; (Biswas et al., 1995). Previous studies demonstrated that CD147 can influence intracellular calcium mobilization (Jiang et al., 2004). Here, we applied real-time microscopy imaging to examine calcium levels in HBMEC in the presence of the blocking antibody MEM-M6/6 and treatment with PeF. We found that pre-incubation of the cells with MEM-M6/6- which recognizes the C-terminal domain D2 and competes with the meningococcal binding site on CD147 - blocked pilus-induced cytosolic calcium concentrations. However, the antibody alone led to a strong rise in intracellular free calcium shortly after the addition. This finding might imply that the non-detectable calcium increase during PeF treatment was due to the exhaustion of intracellular calcium storages by the previous antibody treatment. Nevertheless, whether the observed calcium transients depend on CD147 signaling needs further investigation. In addition to its role in lysosomal fusion with the membrane, calcium is involved in a broad range of cellular functions. Hence, meningococcal-induced calcium transients might affect various pathways (Berridge et al., 2000; Carafoli et al., 2001). Indeed, studies on the closely related pathogen *N. gonorrhoeae* have shown a positive effect of calcium transients on bacterial survival within the host cell. Based on the calcium triggered lysosomal fusion, LAMP1 is translocated to the cell surface, and cleaved by the neisserial secreted IgA protease. LAMP1 is thought to play an important role in maintaining the stability of the acidic lysosomal compartment; its degradation promotes bacterial survival within the cell (Ayala et al., 2001; Ayala et al., 2002; Lin et al., 1997). The current study shows the importance of T4P induced calcium transients in the formation of CRPs, including the calcium-driven ASM translocation to the outer leaflet of the plasma membrane. Because translocation is necessarily associated with ASM activation, the precise mechanism of T4P-mediated activation needs requires further experimental research.

In non-secretory cells, such as those in our endothelial model, calcium primarily effects and promotes the exocytosis of membrane proximal lysosomes. Calcium is thus more involved in the step of lysosomal fusion rather than in recruitment to the membrane (Jaiswal et al., 2002). An important task of the membrane proximal lysosomes is the maintenance and repair of membrane integrity, which is necessary to prevent apoptosis and necrosis (Andrews et al., 2014; Jaiswal et al., 2002; Reddy et al., 2001; Rodriguez et al., 1997). The membrane repair pathway can also be utilized by various pathogens, such as adenoviruses and *Trypanosoma cruzi*. When membrane damage is induced, a calcium influx occurs and the calcium-dependent ASM translocation and

further CRP formation are triggered. Afterwards the membrane lesion is internalized together with the pathogen (Fernandes *et al.*, 2011; Luisoni *et al.*, 2015). In the case of *N. meningitidis* infection, the mechanism does not rely on cell wounding and extracellular calcium influx, as shown for *T. cruzi* and the adenovirus. Instead *N. meningitidis* interaction leads to an intracellular calcium efflux from the ER in the cytosol. Importantly, as already mentioned, the ability of porin to enhance calcium influx cannot be denied and seems plausible.

Various other factors besides pathogen infections promote ASM translocation to the cell surface. General membrane damage, oxidative stress, UV irradiation and CD95 or DR5 ligation are all known to increase the ASM exposure (Avota *et al.*, 2011; Charruyer *et al.*, 2005; Dumitru *et al.*, 2007; Grassme *et al.*, 2001; Grassme *et al.*, 2005; Li *et al.*, 2012). Oxidative stress triggered by hydrogen peroxide was noted to induce ASM translocation; it also relied on calcium-dependent lysosomal exocytosis. By contrast, the CD95 or DR5 induces reactive oxygen species (ROS)-dependent translocation independently of calcium (Dumitru *et al.*, 2007; Li *et al.*, 2012). Calcium-independent ASM translocation is to date poorly understood and might depend on the phosphorylation of ASM by the protein kinase C δ (Zeidan and Hannun, 2007).

4.2 Cell-cycle-regulated gangliosides and meningococcal infection

Glycosphingolipids (GLSs) represent a group of sphingolipids with a vast number of different head motives. To date, over 400 different glycan structures have been found attached to ceramide, ranging from one to 20 sugar residues (D'Angelo *et al.*, 2013). Due to their great variety in appearance, it is not surprising that some glycosphingolipids represents important pathogen interaction partners (Nakayama *et al.*, 2018).

The GLS structure offers a unique footprint for cells that are recognized by the immune system. Hence, *Neisseria* and *Haemophilus* species are known to be able to hide by mimicking the glycan structure of GLS with their own lipopolysaccharides or lipooligosaccharides (Harvey *et al.*, 2001).

In-depth studies on the meningococcal glycointeractome have provided evidence for numerous general glycan-mediated interactions between *N. meningitidis* and the human host. Importantly, these include specific pathogen-glycosphingolipid

interactions (Hugosson *et al.*, 1998; Mubaiwa *et al.*, 2017). On the bacterial side, the interaction is mediated by different pathogenicity factors, such as the capsule, pili or OpcA, each interacting with a distinct subset of host GLS .

In this study, the importance of two representative cell-cycle-dependent expressed glycosphingolipids, GM1 and Gb3, were investigated regarding their influence on meningococcal pathogenesis. The results showed the cell-cycle-dependent expression of either GM1 (primarily G₁ phase) or Gb3 (primarily G₂ phase), as described in the literature (Majoul *et al.*, 2002). This was further demonstrated by partial synchronization of the cells by serum starvation. The cell population was shifted towards the G₁ phase, which correlates with an increase of GM1 on the cell surface. Interestingly, infection of either non-G₁ or G₁-synchronized cells led to a slightly stronger GM1 signal on the cells. It was previously shown that infection of either endothelial or epithelial cells with *N. meningitidis* causes cell-cycle arrest in the S or G₁ phase (Oosthuysen *et al.*, 2016; von Papen *et al.*, 2016). Importantly, both phases are positive for GM1/CtxB staining, indicating that *N. meningitidis* promote their own uptake by arresting the cells in a GM1 positive phase (Majoul *et al.*, 2002).

In the uninfected state, both GLSs display an even distribution of the lipids on the cell surface. During the course of infection, GM1 - but not Gb3 - strongly accumulates around the bacteria. This finding provides strong evidence of the importance of GM1 for infection with *N. meningitidis*. Additionally, blocking of GM1 with CtxB prior to infection in a gentamicin protection assay has been shown to strongly influence the ability of the bacteria to enter the host cell.

In the context of infection, GM1 is known to be an important binding target for several pathogens to colonize and infect the respiratory tract (e.g. *Pseudomonas aeruginosa*, *Haemophilus influenzae*, and *Staphylococcus aureus*; (Krivan *et al.*, 1988). It has been shown that *N. meningitidis* can bind to GM1 under specific circumstances. Whereas meningococcal wild-type strains (including MC58) fail to adhere, an un-capsulated mutant could do so as it is piliated (Hugosson *et al.*, 1998; Mubaiwa *et al.*, 2017). The meningococcal capsule is dismantled only after the initial attachment, in the further downstream colonization state; this could explain why blocking of GM1 with CtxB did not show any effect of bacterial adhesion that relies mainly on interaction with CD147 (Maïssa *et al.*, 2017). Nevertheless, the interaction between *N. meningitidis* and GM1 is crucial for the invasion, as shown by the gentamicin protection assay. Importantly,

CtxB is known to bind to other gangliosides as well as GM1 and it is possible that those gangliosides also play a role in meningococcal invasion (Kuziemko *et al.*, 1996). In general, the delivery of substances and particles into and through barrier forming cells, such as the endothelial cells forming the blood-brain barrier, is an important topic regarding drug delivery into tissues. A novel approach showed that coating nanoparticles with CtxB induced phagocytosis in various cells, including brain endothelial cells (Guan *et al.*, 2017; Walker *et al.*, 2016). Therefore, the endocytosis of CtxB, bound to GM1, occurs in either a clathrin- or caveolin- dependent manner (Walker *et al.*, 2016). With an approximate size of 0.13 μm , the CtxB-coated nanoparticles have roughly 1/10 the size of a single meningococci. Overall, CtxB-GM1-mediated endocytosis seems a promising pathway for further study regarding meningococcal invasion and the bacteria's ability to overcome the epithelial barrier of the nasopharyngeal region and the blood-brain barrier.

4.3 Antimicrobial activity of sphingolipids against *N. meningitidis*

Sphingolipids, including ceramides, form a diverse group of structurally related lipids. They are composed of a sphingosine backbone coupled to a fatty-acid side chain. A range of different head motives and complex glycosylation pattern achieves further variability (Hannun and Obeid, 2018). The burgeoning field of antibiotic-resistant pathogens and the attempt to identify other antimicrobial compounds proposes these host-derived lipids for possible antimicrobial treatment. For example, sphingosine is known as a host's innate first-line defense against airway infections by *P. aeruginosa*. By contrast, ceramide analogs – including the azido-functionalized ceramide used in this study – showed a growth-inhibitory effect against *Chlamydia trachomatis* and acted as a bactericidal compound against *N. meningitidis* and *N. gonorrhoeae*. (Becam *et al.*, 2017; Pewzner-Jung *et al.*, 2014; Saied *et al.*, 2015).

The antimicrobial activity of natural and synthetic sphingolipids against Gram-positive and -negative bacteria as well as fungi has been demonstrated in many studies (Becam *et al.*, 2017; Bibel *et al.*, 1992; Dongfack *et al.*, 2012; Drake *et al.*, 2008; El-Amraoui *et al.*, 2013; Fischer *et al.*, 2012; Fischer *et al.*, 2013; Possemiers *et al.*, 2005). Many host factors are known to induce ultrastructural damage to pathogens, including (for example) anionic peptides and defensins. It was also shown that sphingoid bases

cause ultrastructural damage to *E. coli* and *S. aureus*. (Brogden *et al.*, 1996; Fischer *et al.*, 2013; Harder *et al.*, 2001; Shimoda *et al.*, 1995). Although this effect on pathogen morphology is known, the mechanisms remain elusive. It is debated whether there is an interaction with the membranes or an accumulation in the cytosol that leads to interference with the bacterial metabolism (Fischer *et al.*, 2013).

In this study, together with Lena Kaiser, we report an improved correlative light and electron microscopy (CLEM) approach: We combined CLEM with the precision of click chemistry to explore the mechanisms behind the ultrastructural damage of azido-functionalized sphingosine and short-chain ceramide in combatting the human pathogen *N. meningitidis*.

First, the MIC/MBC values for the functionalized lipids to be used determined and confirmed. The results showed comparable effectiveness to the natural sphingosine, the best characterized sphingolipid with antimicrobial activity. Thereafter, morphological TEM studies revealed that the lipids we tested showed a similar picture as described for *E. coli* and *S. aureus* treated with various sphingoid bases (Fischer *et al.*, 2013). Low-concentration treatment (0.1 X MBC) of *N. meningitidis* with the functionalized lipids, led to a membrane elongation, but only in a subset of the bacteria. By contrast, high-concentration treatment (1 X MBC) with both compounds induced massive bacterial disintegration and lysis. Importantly, the observation of marked intracellular vesicle formation and the enrichment of electron dense material showed strong similarities to the data from Fischer *et al.* (2013), where they had treated *E. coli* and *S. aureus* with various sphingoid bases (Fischer *et al.*, 2013).

Interestingly, the functionalized ceramide had no effect on *E. coli* or *S. aureus* (data not shown). For *S. aureus*, this observation could be due to a primary effect of the lipids on the bacterial outer membrane, which is absent in the Gram-positive *S. aureus*. In the case of the Gram-negative *E. coli*, the hypothesis was tested that the lipopolysaccharide of *E. coli* protects against the lipids. In contrast to the resistant *E. coli*, the susceptible *N. meningitidis* expresses a lipooligosaccharide, that lacks the O-antigen of the classical lipopolysaccharide (Preston *et al.*, 1996). For this test, we used an *E. coli* K12 strain that lacked the O-antigen and tested this isolate in our MIC/MBC assay. The results showed that the bacteria remained resistant to the functionalized ceramide. Therefore, the mechanisms that render *N. meningitidis* susceptible and *E. coli* resistant remain elusive and need further investigation.

The determination of the minimal inhibitory and bactericidal concentration and description of ultrastructural alteration alone did not allow for firm conclusions about the mechanism. For initial insight, precise localization of the lipids is necessary. However, the small size and various forms of the sphingolipids mean that there is a lack of appropriate antibodies. Whereas a commercial antibody is available against ceramide (MID 15B4, which also recognizes sphingomyelin, for example), no antibodies are available against sphingosine. The lack of visualization possibilities led to the development of azido-functionalized sphingolipids (Collenburg *et al.*, 2016). Originally synthesized to track lipids in eukaryotic cell, these have become a powerful tool for a broad variety of applications (Becam *et al.*, 2017; Burgert *et al.*, 2017; Collenburg *et al.*, 2016; Walter *et al.*, 2017). We used the azido-functionalized sphingosine and ceramide in this study to obtain insight into the mechanisms of the antibacterial activity.

The improved CLEM approach (Click-CLEM), developed together with Lena Kaiser and Prof. Stigloher (Microscopy Core Unit, Wuerzburg), combines the strength of classical CLEM protocols with the advantages of click chemistry (Markert *et al.*, 2016; Ramil and Lin, 2013). The possibilities for epitope localization in the electron microscopic resolution range is greatly enhanced by the specificity of click chemistry reactions. In the classical antibody-based CLEM approach, post-fixation and embedding staining reduces the accessible epitopes and promotes the formation of fragments. Due to the pre-fixation and embedding staining used in the improved Click-CLEM protocol, the accessibility of all epitopes is achieved. This scenario results in an improved signal, obtained more rapidly (Hayat, 1989).

Treatment of the bacteria with a concentration corresponding to 1/10 the MBC of either ω -N₃-sphingosine or ω -N₃-C₆-ceramide resulted in minor changes in the bacterial appearance. Only a small proportion of the bacteria showed morphological changes, which manifested as outer membrane elongation. These results confirm the findings of morphological studies and show the incorporation of functional lipids into the outer membrane. In contrast, high-concentration treatment (1 X MBC) with the functionalized lipids had a devastating effect on the bacteria. All bacteria were in a state of lysis and a proportion appeared to be “bacterial-ghosts” with a single membranous envelope and complete loss of intracellular content. Most of the bacteria were characterized by strong vesicle formation in the cytosol, at least partial loss of membranes, and an

intracellular enrichment of electron dense material. This material was positive for lipid signal, as shown by the Click-CLEM approach.

We assumed that a low-concentration treatment was equal to - or mimicked - the early stage of high-concentration treatment (e.g. the first 30 to 60 min). The difference in lipid localization during high-concentration treatment was therefore most likely based on a previous disintegration of the outer membrane. This assumption was supported by the mass spectrometry results for the separated membrane fractions, which provided evidence of the primarily impact on the outer membrane.

A recent study indicated that the effect of sphingosine occurs because of interactions between the highly negatively charged bacterial lipid, cardiolipin, and the protonated form of the sphingosine NH_2 group (Verhaegh *et al.*, 2020). This would explain the antimicrobial effect of the functionalized sphingosine. However, it is not applicable to ceramide because this primary amine is reduced to secondary NH during the synthesis from sphinganine to dihydroceramide and the addition of a fatty-acid side chain. In addition, cardiolipin is known to be preferentially localized in the inner membrane of Gram-negative bacteria. This point is inconsistent with the results, which showed a primarily effect on the outer membrane (Lin and Weibel, 2016). Nevertheless, because cardiolipin seems not to exist only in the inner membrane, there might be a possible interaction.

Conclusion and future research

Sphingolipids, and the enzymes involved in their metabolism, are ubiquitous in and on human cells: They and influence host-pathogen interactions to varying degrees. .

In this study, the impact of sphingolipids on *N. meningitidis* was investigated to extend the understanding of the importance of host-derived lipids in meningococcal infections. Following earlier studies on the impact of ASM and ceramide on meningococcal pathogenesis, we first analyzed the contribution of T4P and intracellular calcium in CRP formation. Here, it was shown that the live highly piliated *N. meningitidis* strain 8013/12, and pili-enriched fractions from this strain, efficiently induced various steps in the CRP formation pathway. In addition, inhibition of this pathway strongly decreased the ability of *N. meningitidis* to invade cells. Our overall findings underline the importance of host-derived sphingolipids and add an active role in host cell invasion to the meningococcal T4P function.

Despite much work to examine the role of sphingolipids in pathogenesis, many facts remain unclear. Future experiments should focus on the proof of concept that the observed calcium release from the ER is directly mediated by the activation of the CD147 receptor. If this point is confirmed other factors involved downstream of T4P-CD147 interaction should be studied.

Apart from ASM translocation, this study also showed a strong increase in activity. It is known that activation of the ASM depends on the binding of zinc ions, but the exact mechanisms of how the activation is triggered and where it occurs remain elusive (Kornhuber *et al.*, 2015). In addition, the possible role of downstream enzymes and sphingolipid metabolites involved in ceramide degradation are the focus of current research. This pathway may be influenced by *N. meningitidis* towards a beneficial state of cellular sphingolipid equilibrium.

Another important sphingolipid in the context of meningococcal pathogenesis is the glycosphingolipid GM1. Our results clearly showed the enrichment of GM1 around the bacteria and the strong impact of bacterial invasion. GM1 has been characterized for its role in endocytotic mediation of nanoparticles; hence, it seems a promising candidate to reveal a possible candidate for meningococcal cellular entry into epithelial or endothelial cells. However, CtxB was used and not only bind only to GM1; hence, further research is needed regarding other possible candidates, such as GM2 and 3 (Kuziemko *et al.*, 1996).

Regarding the pathogen, more experiments are needed to identify the bacterial factors necessary for the interaction and accumulation of GM1. In the future, targeting GM1 or other glycosphingolipids, might be a strong possibility to block the ability of pathogens to invade and overcome cellular barriers in the human host.

The experiments were exclusively performed on endothelial cells that form the blood-cerebrospinal-fluid barrier. It would be of interest to investigate the impact of sphingolipids on epithelial cells from the nasopharyngeal region, which represents the first barrier encountered by *N. meningitidis*.

Sphingolipids not only have a positive effect on *N. meningitidis* and its interaction with the host cell. A disadvantage for the bacteria is the antimicrobial activity of some sphingolipids. Especially sphingoid bases, including sphingosine, are extensively studied against a broad range of pathogens, and with that seems to be a possible treatment approach for the future. Nevertheless, many questions remain unanswered at present and even the basic mechanism of how antimicrobial activity of sphingolipids is induced remains elusive. This study offers the first precise localization of antimicrobial sphingolipids in *N. meningitidis*, allowing conclusions to be drawn regarding the possible mechanism behind their activity against *N. meningitidis*.

Despite the evidence for the antimicrobial mechanism of sphingosine, the topic needs further investigation. Its effects on different pathogens and the mode of action of other sphingolipids with antimicrobial activity (e.g. short-chain ceramide) should also be further studied.

References

1. Airola, M.V., and Hannun, Y.A. (2013). Sphingolipid metabolism and neutral sphingomyelinases. *Handb Exp Pharmacol*, 57-76.
2. Alonso, A., and Goñi, F.M. (2018). The Physical Properties of Ceramides in Membranes. *Annual Review of Biophysics* 47, 633-654.
3. Andrews, N.W., Almeida, P.E., and Corrotte, M. (2014). Damage control: cellular mechanisms of plasma membrane repair. *Trends Cell Biol* 24, 734-742.
4. Andrieu-Abadie, N., and Levade, T. (2002). Sphingomyelin hydrolysis during apoptosis. *Biochim Biophys Acta* 1585, 126-134.
5. Arenas, J., Schipper, K., van Ulsen, P., van der Ende, A., and Tommassen, J. (2013). Domain exchange at the 3' end of the gene encoding the fratricide meningococcal two-partner secretion protein A. *BMC Genomics* 14, 622-622.
6. Asmat, T.M., Tenenbaum, T., Jonsson, A.B., Schwerk, C., and Schrotten, H. (2014). Impact of calcium signaling during infection of *Neisseria meningitidis* to human brain microvascular endothelial cells. *PLoS One* 9, e114474.
7. Avota, E., Gulbins, E., and Schneider-Schaulies, S. (2011). DC-SIGN mediated sphingomyelinase-activation and ceramide generation is essential for enhancement of viral uptake in dendritic cells. *PLoS Pathog* 7, e1001290.
8. Ayala, B.P., Vasquez, B., Clary, S., Tainer, J.A., Rodland, K., and So, M. (2001). The pilus-induced Ca²⁺ flux triggers lysosome exocytosis and increases the amount of Lamp1 accessible to *Neisseria* IgA1 protease. *Cell Microbiol* 3, 265-275.
9. Ayala, P., Vasquez, B., Wetzler, L., and So, M. (2002). *Neisseria gonorrhoeae* porin P1.B induces endosome exocytosis and a redistribution of Lamp1 to the plasma membrane. *Infect Immun* 70, 5965-5971.
10. Ayala, P., Wilbur, J.S., Wetzler, L.M., Tainer, J.A., Snyder, A., and So, M. (2005). The pilus and porin of *Neisseria gonorrhoeae* cooperatively induce Ca²⁺ transients in infected epithelial cells. *Cell Microbiol* 7, 1736-1748.
11. Bajwa H, A.W. (2020). Niemann-Pick Disease. StatPearls [Internet].
12. Baker, E.H., and Baines, D.L. (2018). Airway Glucose Homeostasis: A New Target in the Prevention and Treatment of Pulmonary Infection. *Chest* 153, 507-514.
13. Becam, J., Walter, T., Burgert, A., Schlegel, J., Sauer, M., Seibel, J., and Schubert-Unkmeir, A. (2017). Antibacterial activity of ceramide and ceramide analogs against pathogenic *Neisseria*. *Scientific Reports* 7, 17627.
14. Becker, K.A., Li, X., Seitz, A., Steinmann, J., Koch, A., Schuchman, E., Kamler, M., Edwards, M.J., Caldwell, C.C., and Gulbins, E. (2017). Neutrophils Kill Reactive Oxygen Species-Resistant *Pseudomonas aeruginosa* by Sphingosine. *Cellular Physiology and Biochemistry* 43, 1603-1616.

15. Bernard, S.C., Simpson, N., Join-Lambert, O., Federici, C., Laran-Chich, M.P., Maissa, N., Bouzinba-Segard, H., Morand, P.C., Chretien, F., Taouji, S., *et al.* (2014). Pathogenic *Neisseria meningitidis* utilizes CD147 for vascular colonization. *Nat Med* **20**, 725-731.
16. Berridge, M.J., Lipp, P., and Bootman, M.D. (2000). The versatility and universality of calcium signalling. *Nat Rev Mol Cell Biol* **1**, 11-21.
17. Bibel, D.J., Aly, R., and Shinefield, H.R. (1992). Antimicrobial activity of sphingosines. *J Invest Dermatol* **98**, 269-273.
18. Bille, E., Meyer, J., Jamet, A., Euphrasie, D., Barnier, J.-P., Brissac, T., Larsen, A., Pelissier, P., and Nassif, X. (2017). A virulence-associated filamentous bacteriophage of *Neisseria meningitidis* increases host-cell colonisation. *PLoS Pathog* **13**, e1006495-e1006495.
19. Birtles, A., Hardy, K., Gray, S.J., Handford, S., Kaczmarek, E.B., Edwards-Jones, V., and Fox, A.J. (2005). Multilocus sequence typing of *Neisseria meningitidis* directly from clinical samples and application of the method to the investigation of meningococcal disease case clusters. *J Clin Microbiol* **43**, 6007-6014.
20. Biswas, C., Zhang, Y., DeCastro, R., Guo, H., Nakamura, T., Kataoka, H., and Nabeshima, K. (1995). The human tumor cell-derived collagenase stimulatory factor (renamed EMMPRIN) is a member of the immunoglobulin superfamily. *Cancer Res* **55**, 434-439.
21. Brogden, K.A., De Lucca, A.J., Bland, J., and Elliott, S. (1996). Isolation of an ovine pulmonary surfactant-associated anionic peptide bactericidal for *Pasteurella haemolytica*. *Proc Natl Acad Sci U S A* **93**, 412-416.
22. Burgert, A., Schlegel, J., Becam, J., Doose, S., Bieberich, E., Schubert-Unkmeir, A., and Sauer, M. (2017). Characterization of Plasma Membrane Ceramides by Super-Resolution Microscopy. *Angew Chem Int Ed Engl* **56**, 6131-6135.
23. Capecchi, B., Adu-Bobie, J., Di Marcello, F., Ciucchi, L., Massignani, V., Taddei, A., Rappuoli, R., Pizza, M., and Arico, B. (2005). *Neisseria meningitidis* NadA is a new invasins which promotes bacterial adhesion to and penetration into human epithelial cells. *Mol Microbiol* **55**, 687-698.
24. Carafoli, E., Santella, L., Branca, D., and Brini, M. (2001). Generation, control, and processing of cellular calcium signals. *Crit Rev Biochem Mol Biol* **36**, 107-260.
25. Carbonnelle, E., Helaine, S., Nassif, X., and Pelicic, V. (2006). A systematic genetic analysis in *Neisseria meningitidis* defines the Pil proteins required for assembly, functionality, stabilization and export of type IV pili. *Mol Microbiol* **61**, 1510-1522.
26. CDC (2017). Centers for Disease Control and Prevention: Meningococcal Disease.

27. Chang, Q., Tzeng, Y.L., and Stephens, D.S. (2012). Meningococcal disease: changes in epidemiology and prevention. *Clin Epidemiol* 4, 237-245.
28. Charruyer, A., Grazide, S., Bezombes, C., Muller, S., Laurent, G., and Jaffrezou, J.P. (2005). UV-C light induces raft-associated acid sphingomyelinase and JNK activation and translocation independently on a nuclear signal. *J Biol Chem* 280, 19196-19204.
29. Chiricozzi, E., Lunghi, G., Di Biase, E., Fazzari, M., Sonnino, S., and Mauri, L. (2020). GM1 Ganglioside Is A Key Factor in Maintaining the Mammalian Neuronal Functions Avoiding Neurodegeneration. *Int J Mol Sci* 21, 868.
30. Christensen, H., May, M., Bowen, L., Hickman, M., and Trotter, C.L. (2010). Meningococcal carriage by age: a systematic review and meta-analysis. *The Lancet Infectious Diseases* 10, 853-861.
31. Christodoulides, M., Everson, J.S., Liu, B.L., Lambden, P.R., Watt, P.J., Thomas, E.J., and Heckels, J.E. (2000). Interaction of primary human endometrial cells with *Neisseria gonorrhoeae* expressing green fluorescent protein. *Mol Microbiol* 35, 32-43.
32. Claus, H., Maiden, M.C., Wilson, D.J., McCarthy, N.D., Jolley, K.A., Urwin, R., Hessler, F., Frosch, M., and Vogel, U. (2005). Genetic analysis of meningococci carried by children and young adults. *J Infect Dis* 191, 1263-1271.
33. Collenburg, L., Walter, T., Burgert, A., Muller, N., Seibel, J., Japtok, L., Kleuser, B., Sauer, M., and Schneider-Schaulies, S. (2016). A Functionalized Sphingolipid Analogue for Studying Redistribution during Activation in Living T Cells. *J Immunol* 196, 3951-3962.
34. Coureuil, M., Jamet, A., Bille, E., Lécuyer, H., Bourdoulous, S., and Nassif, X. (2019). Molecular interactions between *Neisseria meningitidis* and its human host. *Cell Microbiol* 21, e13063-e13063.
35. Crystal, R.G., Randell, S.H., Engelhardt, J.F., Voynow, J., and Sunday, M.E. (2008). Airway epithelial cells: current concepts and challenges. *Proc Am Thorac Soc* 5, 772-777.
36. Czarny, M., and Schnitzer, J.E. (2004). Neutral sphingomyelinase inhibitor scyphostatin prevents and ceramide mimics mechanotransduction in vascular endothelium. *Am J Physiol Heart Circ Physiol* 287, H1344-1352.
37. D'Angelo, G., Capasso, S., Sticco, L., and Russo, D. (2013). Glycosphingolipids: synthesis and functions. *the FEBS Journal*.
38. De Boeck, I., Wittouck, S., Wuyts, S., Oerlemans, E.F.M., van den Broek, M.F.L., Vandenheuvel, D., Vanderveken, O., and Lebeer, S. (2017). Comparing the Healthy Nose and Nasopharynx Microbiota Reveals Continuity As Well As Niche-Specificity. *Frontiers in microbiology* 8, 2372-2372.
39. de Boer, P., Hoogenboom, J.P., and Giepmans, B.N.G. (2015). Correlated light and electron microscopy: ultrastructure lights up! *Nature Methods* 12, 503-513.

40. De Gregorio, E., Zarrilli, R., and Di Nocera, P.P. (2019). Contact-dependent growth inhibition systems in *Acinetobacter*. *Scientific Reports* 9, 154.
41. De Rose, V., Molloy, K., Gohy, S., Pilette, C., and Greene, C.M. (2018). Airway Epithelium Dysfunction in Cystic Fibrosis and COPD. *Mediators Inflamm* 2018, 1309746-1309746.
42. Debets, M.F., van Berkel, S.S., Dommerholt, J., Dirks, A.J., Rutjes, F.P.J.T., and van Delft, F.L. (2011). Bioconjugation with Strained Alkenes and Alkynes. *Accounts of Chemical Research* 44, 805-815.
43. Deng, Y., Rivera-Molina, F.E., Toomre, D.K., and Burd, C.G. (2016). Sphingomyelin is sorted at the trans Golgi network into a distinct class of secretory vesicle. *Proc Natl Acad Sci U S A* 113, 6677-6682.
44. Desselle, A., Chaumette, T., Gaugler, M.-H., Cochonneau, D., Fleurence, J., Dubois, N., Hulin, P., Aubry, J., Birklé, S., and Paris, F. (2012). Anti-Gb3 Monoclonal Antibody Inhibits Angiogenesis and Tumor Development. *PLOS ONE* 7, e45423.
45. Dommerholt, J., Rutjes, F.P.J.T., and van Delft, F.L. (2016). Strain-Promoted 1,3-Dipolar Cycloaddition of Cycloalkynes and Organic Azides. *Topics in Current Chemistry* 374, 16.
46. Dongfack, M.D., Lallemand, M.C., Kuete, V., Mbazoa, C.D., Wansi, J.D., Trinh-van-Dufat, H., Michel, S., and Wandji, J. (2012). A new sphingolipid and furanocoumarins with antimicrobial activity from *Ficus exasperata*. *Chem Pharm Bull (Tokyo)* 60, 1072-1075.
47. dos Santos Souza, I., Maïssa, N., Ziveri, J., Morand, P.C., Coureuil, M., Nassif, X., and Bourdoulous, S. (2020). Meningococcal disease: A paradigm of type-IV pilus dependent pathogenesis. *Cell Microbiol* 22, e13185.
48. Drake, D.R., Brogden, K.A., Dawson, D.V., and Wertz, P.W. (2008). Thematic review series: skin lipids. Antimicrobial lipids at the skin surface. *J Lipid Res* 49, 4-11.
49. Dumitru, C.A., Carpinteiro, A., Trarbach, T., Hengge, U.R., and Gulbins, E. (2007). Doxorubicin enhances TRAIL-induced cell death via ceramide-enriched membrane platforms. *Apoptosis* 12, 1533-1541.
50. Edwards, M.S., and Baker, C.J. (1981). Complications and sequelae of meningococcal infections in children. *J Pediatr* 99, 540-545.
51. El-Amraoui, B., Biard, J.F., and Fassouane, A. (2013). Haliscosamine: a new antifungal sphingosine derivative from the Moroccan marine sponge *Haliclona viscosa*. *Springerplus* 2, 252.
52. Esen, M., Schreiner, B., Jendrossek, V., Lang, F., Fassbender, K., Grassme, H., and Gulbins, E. (2001). Mechanisms of *Staphylococcus aureus* induced apoptosis of human endothelial cells. *Apoptosis* 6, 431-439.

53. Exley, R.M., Shaw, J., Mowe, E., Sun, Y.-H., West, N.P., Williamson, M., Botto, M., Smith, H., and Tang, C.M. (2005). Available carbon source influences the resistance of *Neisseria meningitidis* against complement. *J Exp Med* *201*, 1637-1645.
54. Fernandes, M.C., Cortez, M., Flannery, A.R., Tam, C., Mortara, R.A., and Andrews, N.W. (2011). *Trypanosoma cruzi* subverts the sphingomyelinase-mediated plasma membrane repair pathway for cell invasion. *J Exp Med* *208*, 909-921.
55. Fischer, C.L., Drake, D.R., Dawson, D.V., Blanchette, D.R., Brogden, K.A., and Wertz, P.W. (2012). Antibacterial activity of sphingoid bases and fatty acids against Gram-positive and Gram-negative bacteria. *Antimicrob Agents Chemother* *56*, 1157-1161.
56. Fischer, C.L., Walters, K.S., Drake, D.R., Blanchette, D.R., Dawson, D.V., Brogden, K.A., and Wertz, P.W. (2013). Sphingoid bases are taken up by *Escherichia coli* and *Staphylococcus aureus* and induce ultrastructural damage. *Skin Pharmacol Physiol* *26*, 36-44.
57. Fussenegger, M., Rudel, T., Barten, R., Ryll, R., and Meyer, T.F. (1997). Transformation competence and type-4 pilus biogenesis in *Neisseria gonorrhoeae*--a review. *Gene* *192*, 125-134.
58. Futerman, A.H., and Hannun, Y.A. (2004). The complex life of simple sphingolipids. *EMBO Rep* *5*, 777-782.
59. Gault, C.R., Obeid, L.M., and Hannun, Y.A. (2010). An overview of sphingolipid metabolism: from synthesis to breakdown. *Adv Exp Med Biol* *688*, 1-23.
60. Gault, J., Ferber, M., Machata, S., Imhaus, A.-F., Malosse, C., Charles-Orszag, A., Millien, C., Bouvier, G., Bardiaux, B., Péhau-Arnaudet, G., *et al.* (2015). *Neisseria meningitidis* Type IV Pili Composed of Sequence Invariable Pilins Are Masked by Multisite Glycosylation. *PLoS Pathog* *11*, e1005162.
61. Goryunova, M. (2020). Does nonspecific protein labeling exist in Click Chemistry reactions?
62. Grassme, H., Gulbins, E., Brenner, B., Ferlinz, K., Sandhoff, K., Harzer, K., Lang, F., and Meyer, T.F. (1997). Acidic sphingomyelinase mediates entry of *N. gonorrhoeae* into nonphagocytic cells. *Cell* *91*, 605-615.
63. Grassme, H., Henry, B., Ziobro, R., Becker, K.A., Riethmuller, J., Gardner, A., Seitz, A.P., Steinmann, J., Lang, S., Ward, C., *et al.* (2017). beta1-Integrin Accumulates in Cystic Fibrosis Luminal Airway Epithelial Membranes and Decreases Sphingosine, Promoting Bacterial Infections. *Cell Host Microbe* *21*, 707-718
64. Grassme, H., Jekle, A., Riehle, A., Schwarz, H., Berger, J., Sandhoff, K., Kolesnick, R., and Gulbins, E. (2001). CD95 signaling via ceramide-rich membrane rafts. *J Biol Chem* *276*, 20589-20596.
65. Grassme, H., Jendrossek, V., Riehle, A., von Kurthy, G., Berger, J., Schwarz, H., Weller, M., Kolesnick, R., and Gulbins, E. (2003). Host defense against

- Pseudomonas aeruginosa* requires ceramide-rich membrane rafts. *Nat Med* 9, 322-330.
66. Grassme, H., Riehle, A., Wilker, B., and Gulbins, E. (2005). Rhinoviruses infect human epithelial cells via ceramide-enriched membrane platforms. *J Biol Chem* 280, 26256-26262.
67. Grimwood, K., Anderson, P., Anderson, V., Tan, L., and Nolan, T. (2000). Twelve year outcomes following bacterial meningitis: further evidence for persisting effects. *Arch Dis Child* 83, 111-116.
68. Grösch, S., Schiffmann, S., and Geisslinger, G. (2012). Chain length-specific properties of ceramides. *Progress in Lipid Research* 51, 50-62.
69. Guan, J., Zhang, Z., Hu, X., Yang, Y., Chai, Z., Liu, X., Liu, J., Gao, B., Lu, W., Qian, J., *et al.* (2017). Cholera Toxin Subunit B Enabled Multifunctional Glioma-Targeted Drug Delivery. *Advanced Healthcare Materials* 6, 1700709.
70. Hannun, Y.A., and Obeid, L.M. (2018). Sphingolipids and their metabolism in physiology and disease. *Nature Reviews Molecular Cell Biology* 19, 175-191.
71. Harder, J., Bartels, J., Christophers, E., and Schroder, J.M. (2001). Isolation and characterization of human beta -defensin-3, a novel human inducible peptide antibiotic. *J Biol Chem* 276, 5707-5713.
72. Harvey, H.A., Swords, W.E., and Apicella, M.A. (2001). The Mimicry of Human Glycolipids and Glycosphingolipids by the Lipooligosaccharides of Pathogenic *Neisseria* and *Haemophilus*. *Journal of Autoimmunity* 16, 257-262.
73. Hauck, C.R., Grassme, H., Bock, J., Jendrossek, V., Ferlinz, K., Meyer, T.F., and Gulbins, E. (2000). Acid sphingomyelinase is involved in CEACAM receptor-mediated phagocytosis of *Neisseria gonorrhoeae*. *FEBS Lett* 478, 260-266.
74. Hayat, M.A. (1989). *Colloidal gold : principles, methods, and applications*, Vol 3 (San Diego: Academic Press).
75. Helaine, S., Carbonnelle, E., Prouvensier, L., Beretti, J.L., Nassif, X., and Pelicic, V. (2005). PilX, a pilus-associated protein essential for bacterial aggregation, is a key to pilus-facilitated attachment of *Neisseria meningitidis* to human cells. *Mol Microbiol* 55, 65-77.
76. Hoffmann, I., Eugene, E., Nassif, X., Couraud, P.O., and Bourdoulous, S. (2001). Activation of ErbB2 receptor tyrosine kinase supports invasion of endothelial cells by *Neisseria meningitidis*. *J Cell Biol* 155, 133-143.
77. Hubert, B., Watier, L., Garnerin, P., and Richardson, S. (1992). Meningococcal disease and influenza-like syndrome: a new approach to an old question. *J Infect Dis* 166, 542-545.
78. Hugosson, S., Ångström, J., Olsson, B.-M., Bergström, J., Fredlund, H., Olcén, P., and Tenaberg, A. (1998). Glycosphingolipid Binding Specificities of *Neisseria*

- meningitidis and *Haemophilus influenzae*: Detection, Isolation, and Characterization of a Binding-Active Glycosphingolipid from Human Oropharyngeal Epithelium¹. *The Journal of Biochemistry* 124, 1138-1152.
79. Jaiswal, J.K., Andrews, N.W., and Simon, S.M. (2002). Membrane proximal lysosomes are the major vesicles responsible for calcium-dependent exocytosis in nonsecretory cells. *J Cell Biol* 159, 625-635.
80. Jamet, A., and Nassif, X. (2015a). Characterization of the Maf family of polymorphic toxins in pathogenic *Neisseria* species. *Microb Cell* 2, 88-90.
81. Jamet, A., and Nassif, X. (2015b). New Players in the Toxin Field: Polymorphic Toxin Systems in Bacteria. *mBio* 6, e00285-00215.
82. Jewett, J.C., and Bertozzi, C.R. (2010). Cu-free click cycloaddition reactions in chemical biology. *Chem Soc Rev* 39, 1272-1279.
83. Jiang, J.L., Chan, H.C., Zhou, Q., Yu, M.K., Yao, X.Y., Lam, S.Y., Zhu, H., Ho, L.S., Leung, K.M., and Chen, Z.N. (2004). HAb18G/CD147-mediated calcium mobilization and hepatoma metastasis require both C-terminal and N-terminal domains. *Cell Mol Life Sci* 61, 2083-2091.
84. Johswich - Homepage: Institute for hygiene and microbiology, K. Institute for Hygiene and Microbiology: *N. meningitidis* nasal colonization and disease.
85. Join-Lambert, O., Lecuyer, H., Miller, F., Lelievre, L., Jamet, A., Furio, L., Schmitt, A., Pelissier, P., Fraitag, S., Coureuil, M., *et al.* (2013). Meningococcal interaction to microvasculature triggers the tissular lesions of purpura fulminans. *J Infect Dis* 208, 1590-1597.
86. Kallstrom, H., Islam, M.S., Berggren, P.O., and Jonsson, A.B. (1998). Cell signaling by the type IV pili of pathogenic *Neisseria*. *J Biol Chem* 273, 21777-21782.
87. Kia'i N., B.T. (2019). *Histology, Respiratory Epithelium*. (StatPearls Publishing).
88. Kolb, H.C., Finn, M.G., and Sharpless, K.B. (2001). Click Chemistry: Diverse Chemical Function from a Few Good Reactions. *Angewandte Chemie International Edition* 40, 2004-2021.
89. Kornhuber, J., Rhein, C., Muller, C.P., and Muhle, C. (2015). Secretory sphingomyelinase in health and disease. *Biol Chem* 396, 707-736.
90. Krivan, H.C., Roberts, D.D., and Ginsburg, V. (1988). Many pulmonary pathogenic bacteria bind specifically to the carbohydrate sequence GalNAc beta 1-4Gal found in some glycolipids. *Proceedings of the National Academy of Sciences* 85, 6157.
91. Kunz, T.C., and Kozjak-Pavlovic, V. (2019). Diverse Facets of Sphingolipid Involvement in Bacterial Infections. *Frontiers in Cell and Developmental Biology* 7.

92. Kuziemko, G.M., Stroh, M., and Stevens, R.C. (1996). Cholera Toxin Binding Affinity and Specificity for Gangliosides Determined by Surface Plasmon Resonance. *Biochemistry* *35*, 6375-6384.
93. Lang, J., Bohn, P., Bhat, H., Jastrow, H., Walkenfort, B., Cansiz, F., Fink, J., Bauer, M., Olszewski, D., Ramos-Nascimento, A., *et al.* (2020). Acid ceramidase of macrophages traps herpes simplex virus in multivesicular bodies and protects from severe disease. *Nature Communications* *11*, 1338.
94. Li, L., Tang, W., Wu, X., Karnak, D., Meng, X., Thompson, R., Hao, X., Li, Y., Qiao, X.T., Lin, J., *et al.* (2013). HAb18G/CD147 Promotes pSTAT3-Mediated Pancreatic Cancer Development via CD44s. *Clinical Cancer Research* *19*, 6703.
95. Li, X., Gulbins, E., and Zhang, Y. (2012). Oxidative stress triggers Ca-dependent lysosome trafficking and activation of acid sphingomyelinase. *Cell Physiol Biochem* *30*, 815-826.
96. Lin, L., Ayala, P., Larson, J., Mulks, M., Fukuda, M., Carlsson, S.R., Enns, C., and So, M. (1997). The Neisseria type 2 IgA1 protease cleaves LAMP1 and promotes survival of bacteria within epithelial cells. *Mol Microbiol* *24*, 1083-1094.
97. Lin, T.-Y., and Weibel, D.B. (2016). Organization and function of anionic phospholipids in bacteria. *Applied Microbiology and Biotechnology* *100*, 4255-4267.
98. Luisoni, S., Suomalainen, M., Boucke, K., Tanner, L.B., Wenk, M.R., Guan, X.L., Grzybek, M., Coskun, U., and Greber, U.F. (2015). Co-option of Membrane Wounding Enables Virus Penetration into Cells. *Cell Host Microbe* *18*, 75-85.
99. Maiden, M.C., Bygraves, J.A., Feil, E., Morelli, G., Russell, J.E., Urwin, R., Zhang, Q., Zhou, J., Zurth, K., Caugant, D.A., *et al.* (1998). Multilocus sequence typing: a portable approach to the identification of clones within populations of pathogenic microorganisms. *Proc Natl Acad Sci U S A* *95*, 3140-3145.
100. Maïssa, N., Covarelli, V., Janel, S., Durel, B., Simpson, N., Bernard, S.C., Pardo-Lopez, L., Bouzinba-Ségard, H., Faure, C., Scott, M.G.H., *et al.* (2017). Strength of *Neisseria meningitidis* binding to endothelial cells requires highly-ordered CD147/ β (2)-adrenoceptor clusters assembled by alpha-actinin-4. *Nat Commun* *8*, 15764.
101. Majoul, I., Schmidt, T., Pomasanova, M., Boutkevich, E., Kozlov, Y., and Söling, H.-D. (2002). Differential expression of receptors for Shiga and Cholera toxin is regulated by the cell cycle. *Journal of Cell Science* *115*, 817.
102. Mangeney, M., Richard, Y., Coulaud, D., Tursz, T., and Wiels, J. (1991). CD77: an antigen of germinal center B cells entering apoptosis. *European Journal of Immunology* *21*, 1131-1140.
103. Markert, S.M., Bauer, V., Muenz, T.S., Jones, N.G., Helmprobst, F., Britz, S., Sauer, M., Rössler, W., Engstler, M., and Stigloher, C. (2017). 3D subcellular localization with superresolution array tomography on ultrathin sections of various species. *Methods Cell Biol* *140*, 21-47.

104. Markert, S.M., Britz, S., Proppert, S., Lang, M., Witvliet, D., Mulcahy, B., Sauer, M., Zhen, M., Bessereau, J.-L., and Stigloher, C. (2016). Filling the gap: adding super-resolution to array tomography for correlated ultrastructural and molecular identification of electrical synapses at the *C. elegans* connectome. *Neurophotonics* 3, 041802.
105. McGuinness, B.T., Clarke, I.N., Lambden, P.R., Barlow, A.K., Poolman, J.T., Jones, D.M., and Heckels, J.E. (1991). Point mutation in meningococcal por A gene associated with increased endemic disease. *Lancet* 337, 514-517.
106. Merrill, A.H., Jr. (2002). De novo sphingolipid biosynthesis: a necessary, but dangerous, pathway. *J Biol Chem* 277, 25843-25846.
107. Merrill, A.H., Jr. (2011). Sphingolipid and glycosphingolipid metabolic pathways in the era of sphingolipidomics. *Chem Rev* 111, 6387-6422.
108. Merz, A.J., So, M., and Sheetz, M.P. (2000). Pilus retraction powers bacterial twitching motility. *Nature* 407, 98-102.
109. Meyer, J., Brissac, T., Frapy, E., Omer, H., Euphrasie, D., Bonavita, A., Nassif, X., and Bille, E. (2016). Characterization of MDAΦ, a temperate filamentous bacteriophage of *Neisseria meningitidis*. *Microbiology* 162, 268-282.
110. Mikaty, G., Soyer, M., Mairey, E., Henry, N., Dyer, D., Forest, K.T., Morand, P., Guadagnini, S., Prevost, M.C., Nassif, X., *et al.* (2009). Extracellular bacterial pathogen induces host cell surface reorganization to resist shear stress. *PLoS Pathog* 5, e1000314.
111. Morand, P.C., Drab, M., Rajalingam, K., Nassif, X., and Meyer, T.F. (2009). *Neisseria meningitidis* differentially controls host cell motility through PilC1 and PilC2 components of type IV Pili. *PLoS One* 4, e6834.
112. Mubaiwa, T.D., Hartley-Tassell, L.E., Semchenko, E.A., Jen, F.E.C., Srikhanta, Y.N., Day, C.J., Jennings, M.P., and Seib, K.L. (2017). The glycointeractome of serogroup B *Neisseria meningitidis* strain MC58. *Scientific Reports* 7, 5693.
113. Muller, A., Gunther, D., Dux, F., Naumann, M., Meyer, T.F., and Rudel, T. (1999). Neisserial porin (PorB) causes rapid calcium influx in target cells and induces apoptosis by the activation of cysteine proteases. *Embo J* 18, 339-352.
114. Mumtaz, S., Burdyga, G., Borisova, L., Wray, S., and Burdyga, T. (2011). The mechanism of agonist induced Ca²⁺ signalling in intact endothelial cells studied confocally in in situ arteries. *Cell Calcium* 49, 66-77.
115. Nakayama, H., Nagafuku, M., Suzuki, A., Iwabuchi, K., and Inokuchi, J.-I. (2018). The regulatory roles of glycosphingolipid-enriched lipid rafts in immune systems. *FEBS Letters* 592, 3921-3942.

116. Nassif, X., Beretti, J.L., Lowy, J., Stenberg, P., O'Gaora, P., Pfeifer, J., Normark, S., and So, M. (1994). Roles of pilin and PilC in adhesion of *Neisseria meningitidis* to human epithelial and endothelial cells. *Proc Natl Acad Sci U S A* *91*, 3769-3773.
117. Obrig, T.G., Louise, C.B., Lingwood, C.A., Boyd, B., Barley-Maloney, L., and Daniel, T.O. (1993). Endothelial heterogeneity in Shiga toxin receptors and responses. *Journal of Biological Chemistry* *268*, 15484-15488.
118. Odile, B.H., Heike, C., Ying, J., Julia, S.B., Holly, B.B., Keith, A.J., Craig, C., Rory, C., Jan, T.P., Wendell, D.Z., *et al.* (2013). Description and Nomenclature of *Neisseria meningitidis* Capsule Locus. *Emerging Infectious Disease journal* *19*, 566.
119. Oosthuysen, W.F., Mueller, T., Dittrich, M.T., and Schubert-Unkmeir, A. (2016). *Neisseria meningitidis* causes cell cycle arrest of human brain microvascular endothelial cells at S phase via p21 and cyclin G2. *Cell Microbiol* *18*, 46-65.
120. Osborn, M.J., Gander, J.E., Parisi, E., and Carson, J. (1972). Mechanism of assembly of the outer membrane of *Salmonella typhimurium*. Isolation and characterization of cytoplasmic and outer membrane. *The Journal of biological chemistry* *247*, 3962-3972.
121. Pavoine, C., and Pecker, F. (2009). Sphingomyelinases: their regulation and roles in cardiovascular pathophysiology. *Cardiovasc Res* *82*, 175-183.
122. Pelton, S.I. (2016). The Global Evolution of Meningococcal Epidemiology Following the Introduction of Meningococcal Vaccines. *Journal of Adolescent Health* *59*, S3-S11.
123. Perkins-Balding, D., Ratliff-Griffin, M., and Stojiljkovic, I. (2004). Iron transport systems in *Neisseria meningitidis*. *Microbiol Mol Biol Rev* *68*, 154-171.
124. Peters, S., Schlegel, J., Becam, J., Avota, E., Sauer, M., and Schubert-Unkmeir, A. (2019). *Neisseria meningitidis* type IV pili trigger Ca²⁺-dependent lysosomal trafficking of the acid sphingomyelinase to enhance surface ceramide levels. *Infection and Immunity*, IAI.00410-00419.
125. Pewzner-Jung, Y., Tavakoli Tabazavareh, S., Grassme, H., Becker, K.A., Japtok, L., Steinmann, J., Joseph, T., Lang, S., Tuemmler, B., Schuchman, E.H., *et al.* (2014). Sphingoid long chain bases prevent lung infection by *Pseudomonas aeruginosa*. *EMBO Mol Med* *6*, 1205-1214.
126. Possemiers, S., Van Camp, J., Bolca, S., and Verstraete, W. (2005). Characterization of the bactericidal effect of dietary sphingosine and its activity under intestinal conditions. *Int J Food Microbiol* *105*, 59-70.
127. Preston, A., Mandrell, R.E., Gibson, B.W., and Apicella, M.A. (1996). The lipooligosaccharides of pathogenic gram-negative bacteria. *Crit Rev Microbiol* *22*, 139-180.

128. Ramil, C.P., and Lin, Q. (2013). Bioorthogonal chemistry: strategies and recent developments. *Chem Commun (Camb)* *49*, 11007-11022.
129. Reddy, A., Caler, E.V., and Andrews, N.W. (2001). Plasma membrane repair is mediated by Ca(2+)-regulated exocytosis of lysosomes. *Cell* *106*, 157-169.
130. Rodriguez, A., Webster, P., Ortego, J., and Andrews, N.W. (1997). Lysosomes behave as Ca²⁺-regulated exocytic vesicles in fibroblasts and epithelial cells. *J Cell Biol* *137*, 93-104.
131. Rouquette-Loughlin, C.E., Balthazar, J.T., Hill, S.A., and Shafer, W.M. (2004). Modulation of the mtrCDE-encoded efflux pump gene complex of *Neisseria meningitidis* due to a *Correia* element insertion sequence. *Mol Microbiol* *54*, 731-741.
132. Rusniok, C., Vallenet, D., Floquet, S., Ewles, H., Mouze-Soulama, C., Brown, D., Lajus, A., Buchrieser, C., Medigue, C., Glaser, P., *et al.* (2009). NeMeSys: a biological resource for narrowing the gap between sequence and function in the human pathogen *Neisseria meningitidis*. *Genome Biol* *10*, R110.
133. Saied, E.M., Banhart, S., Burkle, S.E., Heuer, D., and Arenz, C. (2015). A series of ceramide analogs modified at the 1-position with potent activity against the intracellular growth of *Chlamydia trachomatis*. *Future Med Chem* *7*, 1971-1980.
134. Sandhoff, R. (2010). Very long chain sphingolipids: Tissue expression, function and synthesis. *FEBS Letters* *584*, 1907-1913.
135. Schissel, S.L., Schuchman, E.H., Williams, K.J., and Tabas, I. (1996). Zn²⁺-stimulated sphingomyelinase is secreted by many cell types and is a product of the acid sphingomyelinase gene. *J Biol Chem* *271*, 18431-18436.
136. Schlegel, J., Peters, S., Doose, S., Schubert-Unkmeir, A., and Sauer, M. (2019). Super-Resolution Microscopy Reveals Local Accumulation of Plasma Membrane Gangliosides at *Neisseria meningitidis* Invasion Sites. *Frontiers in Cell and Developmental Biology* *7*.
137. Schneider-Schaulies, J., and Schneider-Schaulies, S. (2015). Sphingolipids in viral infection. *Biological Chemistry* *396*, 585-595.
138. Seib, K.L., Serruto, D., Oriente, F., Delany, I., Adu-Bobie, J., Veggi, D., Arico, B., Rappuoli, R., and Pizza, M. (2009). Factor H-binding protein is important for meningococcal survival in human whole blood and serum and in the presence of the antimicrobial peptide LL-37. *Infect Immun* *77*, 292-299.
139. Serruto, D., Adu-Bobie, J., Scarselli, M., Veggi, D., Pizza, M., Rappuoli, R., and Arico, B. (2003). *Neisseria meningitidis* App, a new adhesin with autocatalytic serine protease activity. *Mol Microbiol* *48*, 323-334.
140. Shimoda, M., Ohki, K., Shimamoto, Y., and Kohashi, O. (1995). Morphology of defensin-treated *Staphylococcus aureus*. *Infect Immun* *63*, 2886-2891.

141. Sidorenko, S., Zakharenko, S., Lobzin, Y., Zhdanov, K., Martens, E., Gostev, V., Mokhov, A., Volkova, M., Kalinogorskaya, O., Gelezova, L., *et al.* (2019). Observational study of nasopharyngeal carriage of *Neisseria meningitidis* in applicants to a military academy in the Russian Federation. *International Journal of Infectious Diseases* *81*, 12-16.
142. Simonis, A., Hebling, S., Gulbins, E., Schneider-Schaulies, S., and Schubert-Unkmeir, A. (2014). Differential activation of acid sphingomyelinase and ceramide release determines invasiveness of *Neisseria meningitidis* into brain endothelial cells. *PLoS Pathog* *10*, e1004160.
143. Smith, D.J., Lamont, I.L., Anderson, G.J., and Reid, D.W. (2013). Targeting iron uptake to control *Pseudomonas aeruginosa* infections in cystic fibrosis. *European Respiratory Journal* *42*, 1723.
144. Steeghs, L., de Cock, H., Evers, E., Zomer, B., Tommassen, J., and van der Ley, P. (2001). Outer membrane composition of a lipopolysaccharide-deficient *Neisseria meningitidis* mutant. *Embo j* *20*, 6937-6945.
145. Stephens, D.S. (2012). 306 - *Neisseria Meningitidis* Infections. In Goldman's Cecil Medicine (Twenty Fourth Edition), L. Goldman, and A.I. Schafer, eds. (Philadelphia: W.B. Saunders), pp. 1851-1855.
146. Stins, M.F., Gilles, F., and Kim, K.S. (1997). Selective expression of adhesion molecules on human brain microvascular endothelial cells. *J Neuroimmunol* *76*, 81-90.
147. Sultan, B., Labadi, K., Guégan, J.F., and Janicot, S. (2005). Climate drives the meningitis epidemics onset in west Africa. *PLoS Med* *2*, e6.
148. Teichgraber, V., Ulrich, M., Endlich, N., Riethmuller, J., Wilker, B., De Oliveira-Munding, C.C., van Heeckeren, A.M., Barr, M.L., von Kurthy, G., Schmid, K.W., *et al.* (2008). Ceramide accumulation mediates inflammation, cell death and infection susceptibility in cystic fibrosis. *Nat Med* *14*, 382-391.
149. Till, A., Rosenstiel, P., Bräutigam, K., Sina, C., Jacobs, G., Oberg, H.H., Seegert, D., Chakraborty, T., and Schreiber, S. (2008). A role for membrane-bound CD147 in NOD2-mediated recognition of bacterial cytoinvasion. *J Cell Sci* *121*, 487-495.
150. Tonjum, T., Freitag, N.E., Namork, E., and Koomey, M. (1995). Identification and characterization of pilG, a highly conserved pilus-assembly gene in pathogenic *Neisseria*. *Mol Microbiol* *16*, 451-464.
151. Torgersen, M.L., Skretting, G., van Deurs, B., and Sandvig, K. (2001). Internalization of cholera toxin by different endocytic mechanisms. *Journal of Cell Science* *114*, 3737.
152. Tzeng, Y.L., and Stephens, D.S. (2000). Epidemiology and pathogenesis of *Neisseria meningitidis*. *Microbes Infect* *2*, 687-700.

153. van Geel, R., Pruijn, G.J.M., van Delft, F.L., and Boelens, W.C. (2012). Preventing Thiol-Yne Addition Improves the Specificity of Strain-Promoted Azide-Alkyne Cycloaddition. *Bioconjugate Chemistry* 23, 392-398.
154. Verhaegh, R., Becker, K.A., Edwards, M.J., and Gulbins, E. (2020). Sphingosine kills bacteria by binding to cardiolipin. *Journal of Biological Chemistry*.
155. Virji, M., and Heckels, J.E. (1983). Antigenic cross-reactivity of *Neisseria pili*: investigations with type- and species-specific monoclonal antibodies. *J Gen Microbiol* 129, 2761-2768.
156. Virji, M., Makepeace, K., Ferguson, D.J., Achtman, M., and Moxon, E.R. (1993a). Meningococcal Opa and Opc proteins: their role in colonization and invasion of human epithelial and endothelial cells. *Mol Microbiol* 10, 499-510.
157. Virji, M., Makepeace, K., Peak, I.R., Ferguson, D.J., Jennings, M.P., and Moxon, E.R. (1995). Opc- and pilus-dependent interactions of meningococci with human endothelial cells: molecular mechanisms and modulation by surface polysaccharides. *Mol Microbiol* 18, 741-754.
158. Virji, M., Saunders, J.R., Sims, G., Makepeace, K., Maskell, D., and Ferguson, D.J. (1993b). Pilus-facilitated adherence of *Neisseria meningitidis* to human epithelial and endothelial cells: modulation of adherence phenotype occurs concurrently with changes in primary amino acid sequence and the glycosylation status of pilin. *Mol Microbiol* 10, 1013-1028.
159. von Papen, M., Oosthuysen, W.F., Becam, J., Claus, H., and Schubert-Unkmeir, A. (2016). Disease and Carrier Isolates of *Neisseria meningitidis* Cause G1 Cell Cycle Arrest in Human Epithelial Cells. *Infect Immun* 84, 2758-2770.
160. Walker, W.A., Tarannum, M., and Vivero-Escoto, J.L. (2016). Cellular endocytosis and trafficking of cholera toxin B-modified mesoporous silica nanoparticles. *Journal of Materials Chemistry B* 4, 1254-1262.
161. Walter, T., Schlegel, J., Burgert, A., Kurz, A., Seibel, J., and Sauer, M. (2017). Incorporation studies of clickable ceramides in Jurkat cell plasma membranes. *Chem Commun (Camb)* 53, 6836-6839.
162. Wang, H., Dai, W., Feng, X., Zhou, Q., Wang, H., Yang, Y., Li, S., and Zheng, Y. (2018). Microbiota Composition in Upper Respiratory Tracts of Healthy Children in Shenzhen, China, Differed with Respiratory Sites and Ages. *Biomed Res Int* 2018, 6515670-6515670.
163. Wang, S.S., Tang, Y.L., Pang, X., Zheng, M., Tang, Y.J., and Liang, X.H. (2019). The maintenance of an oral epithelial barrier. *Life Sci* 227, 129-136.
164. Weichselbaum, A. (1887). Über die Ätiologie der akuten Meningitis cerebrospinalis. *Fortschr Med* 5, 573-583, 620-626.

165. Wigger, D., Gulbins, E., Kleuser, B., and Schumacher, F. (2019). Monitoring the Sphingolipid de novo Synthesis by Stable-Isotope Labeling and Liquid Chromatography-Mass Spectrometry. *Frontiers in Cell and Developmental Biology* 7.
166. Wu, B., Cui, J., Yang, X.-M., Liu, Z.-Y., Song, F., Li, L., Jiang, J.-L., and Chen, Z.-N. (2017). Cytoplasmic fragment of CD147 generated by regulated intramembrane proteolysis contributes to HCC by promoting autophagy. *Cell Death & Disease* 8, e2925-e2925.
167. Xiong, L., Edwards, C.K., 3rd, and Zhou, L. (2014). The biological function and clinical utilization of CD147 in human diseases: a review of the current scientific literature. *Int J Mol Sci* 15, 17411-17441.
168. Xu, M., Xia, M., Li, X.X., Han, W.Q., Boini, K.M., Zhang, F., Zhang, Y., Ritter, J.K., and Li, P.L. (2012). Requirement of translocated lysosomal V1 H(+)-ATPase for activation of membrane acid sphingomyelinase and raft clustering in coronary endothelial cells. *Mol Biol Cell* 23, 1546-1557.
169. Yu, Q.-J., Tao, H., Wang, X., and Li, M.-C. (2015). Targeting brain microvascular endothelial cells: a therapeutic approach to neuroprotection against stroke. *Neural Regen Res* 10, 1882-1891.
170. Zeidan, Y.H., and Hannun, Y.A. (2007). Activation of acid sphingomyelinase by protein kinase Cdelta-mediated phosphorylation. *J Biol Chem* 282, 11549-11561.

Appendix

Acknowledgment

In the last three years, I have met many people whom I would like to thank.

First, I would like to thank the directors of the Institute of Hygiene and Microbiology, Prof. Frosch and Prof. Kurzai, for their competent leadership, which gave me optimal conditions for working on my dissertation here at the Institute.

My special thanks go to my supervisor, Prof. Schubert-Unkmeir, for her guidance, trust and encouragement from the first day until the end of my dissertation (and beyond). I would also like to thank the rest of my dissertation committee, Prof. Sauer and Dr. Johswich, for the useful discussions during our meetings and the help whenever needed.

Such work would not be possible without a good environment, for which I am grateful to all past and present members of the group, with special thanks to Jeromé and Sabrina, who gave me a hard but good start.

In addition to the "internal" environment, I was very lucky to be part of FOR2123 (and partly of GRK2581), which offers an excellent consortium with great PhD students and PIs. To list all this would be too much, but I would especially like to thank Jan Schlegel for a really good time, useful discussions and an overall smooth collaboration.

Finally yet importantly, I am grateful for the support from my family. Especially my wife always had my back and believed in me. A special thanks goes to my little daughter, who teaches me to be patient, especially in difficult times, and never to give up.

Publications and presentations

Publications:

- Peters, S., Schlegel, J., Becam, J., Avota, E., Sauer, M., Schubert-Unkmeir, A.: *Neisseria meningitidis* Type IV Pili Trigger Ca²⁺-Dependent Lysosomal Trafficking of the Acid Sphingomyelinase To Enhance Surface Ceramide Levels. *Infection and Immunity* Jul 2019, 87 (8) e00410-19; DOI: 10.1128/IAI.00410-19
- Schlegel, J., Peters, S., Doose, S., Schubert-Unkmeir, A., Sauer, M.: Super-Resolution Microscopy Reveals Local Accumulation of Plasma Membrane Gangliosides at *Neisseria meningitidis* Invasion Sites. *Frontiers in Cell and Developmental Biology* 7, Sep 2019, DOI=10.3389/fcell.2019.00194
- Peters, S., Kaiser, L., Fink, J., Schumacher, F., Perschin, V., Schlegel, J., Sauer, M., Stigloher, C., Kleuser, B., Seibel, J. and Schubert-Unkmeir, A.: Click-correlative light electron microscopy (Click-CLEM) for imaging and tracking azido-functionalized sphingolipids. (Under review by Scientific Reports)

Presentations:

| Date, Place | Meeting Title, Presentation Title |
|---------------------------------|--|
| 28 - 30.6.2018, Würzburg | Sphingolipids – from basic science to novel therapeutic concepts Oral Presentation: Calcium-dependent ceramide release in response to <i>N. meningitidis</i> infection |
| 10 - 11.10.2018, Würzburg | Eureka! 13 th International Student Symposium Poster Presentation: Calcium-dependent ceramide release in response to <i>N. meningitidis</i> infection |
| 25 - 27.2.2019, Göttingen | 71. Jahrestagung der DGHM Oral Presentation: <i>Neisseria meningitidis</i> type IV pili trigger Ca ²⁺ -dependent lysosomal trafficking of the acid sphingomyelinase to enhance surface ceramide levels |
| 11 - 1.9.2019, Würzburg | 22 nd International Symposium on Signal Transduction at the Blood-Brain Barrier Oral Presentation: <i>Neisseria meningitidis</i> Type IV Pili Induce Ca ²⁺ -Dependent ASM Translocation |
| 9 - 10.10.2019, Würzburg | Eureka! 14 th International Student Symposium Oral Presentation: Mechanism of the bactericidal effect of azido modified ceramide against <i>N. meningitidis</i> |
| 8 - 11.3.2020, Leipzig | 6th Joint Conference of the DGHM & VAAM Oral Presentation: Using Click-CLEM to reveal the mechanism of the bactericidal effect of azido modified ceramides against <i>Neisseria meningitidis</i> |

Affidavit/ Eidesstattliche Erklärung

Affidavit

I hereby declare that my thesis entitled: “The impact of sphingolipids on *Neisseria meningitidis* and their role in meningococcal pathogenicity” is the result of my own work. I did not receive any help or support from commercial consultants. All sources and/or materials applied are listed and specified in the thesis.

Furthermore I verify that the thesis has not been submitted as part of another examination process neither in identical nor in similar form.

Würzburg,

Signature

Eidesstattliche Erklärung

Hiermit erkläre ich an Eides statt, die Dissertation: “ Einfluss von Sphingolipiden auf *Neisseria meningitidis* und deren Bedeutung für die Pathogenität”, eigenständig, d. h. insbesondere selbständig und ohne Hilfe eines kommerziellen Promotionsberaters angefertigt und keine anderen, als die von mir angegebenen Quellen und Hilfsmittel verwendet zu haben.

Ich erkläre außerdem, dass die Dissertation weder in gleicher noch in ähnlicher Form bereits in einem anderen Prüfungsverfahren vorgelegen hat.

Würzburg,

Unterschrift